OUKA
The University of Osaka
Institutional Knowledge Archive

Title	Configuration-conformation Relationship of Polystyrenes in Various Aggregation States, Including Crystal, Gel and Glass
Author(s)	中沖, 隆彦
Citation	大阪大学, 1992, 博士論文
Version Type	VoR
URL	https://doi.org/10.11501/3060135
rights	
Note	

The University of Osaka Institutional Knowledge Archive : OUKA

https://ir.library.osaka-u.ac.jp/

The University of Osaka

CONFIGURATION-CONFORMATION RELATIONSHIP OF POLYSTYRENES IN VARIOUS AGGREGATION STATES, INCLUDING CRYSTAL, GEL AND GLASS

A Doctoral Thesis

by

Takahiko Nakaoki

Submitted to the Faculty
of Science, Osaka University

February, 1992

CONFORMATION AND CONFIGURATION OF POLYSTYRENES IN VARIOUS AGGREGATION STATES, INCLUDING CRYSTAL, GEL AND GLASS

A Doctoral Thesis

by

Takahiko Nakaoki

Submitted to the Faculty

of Science, Osaka University

February, 1992

Approvals

February, 1992

This thesis is approved as to

style and content by

小林雅通

Member-in-chief

寺本明夫

Member

勝部幸輝

Member

Acknowledgements

This research work has been performed under the direction of Professor Masamichi Kobayashi, Department of Macromolecular Science, Faculty of Science, Osaka University. The author would like to express his sincere to Professor Masamichi Kobayashi for his instructive suggestion and cordial discussion throughout the investigation. He also wishes his sincere thanks to Drs. Kohji Tashiro and Fumitoshi Kaneko for their continuing discussions and encouragements.

The author is deeply indebted to Idemitsu Kosan Co. Ltd., for kindly supplying syndiotactic polystyrene samples. He is also grateful to Assistant professor Hirotaro Mori of Research Center for Ultra High Voltage Electron Microscopy, Osaka University for kind suggestion and direction to measure electron microscope and Professor Yoshinobu Izumi of Yamagata University and Dr. Satoru Funahashi of Tokai Research Establishment, Japan Atomic Energy Research Institute for their kind direction to carry out neutron scattering measurement.

The author wishes to thanks Takehito Kozasa and Masaaki Izuchi of Kobayashi's laboratory for their kind assistances. Thanks are also due to all the members of Kobayashi's laboratory for their friendship. Finally the author would like to express his cordial appreciation to his parents.

中沖隆彦

Takahiko Nakaoki

February, 1992

CONTENTS

CHAPTER 1. General Introduction 1

References 5

CHAPTER 2. Molecular Conformations of Syndiotactic Polystyrene 8

2-1. Introduction 8

2-2. Experimental 9

2-2-1. Samples 9

2-2-2. Measurements 11

2-3. Results and Discussion 11

2-3-1. Conformational stability in crystalline state 11

2-3-2. Crystallization from the glass and solid-state phase transition 21

2-3-3. Normal modes analysis 25

References 42

CHAPTER 3. Crystal Modifications and Molecular Structures of Syndiotactic Polystyrene 44

3-1. Introduction 44

3-2. Experimental 44

3-2-1. Samples 44

3-2-2. Measurements 45

3-3. Results and Discussion 45

3-3-1. Polymorphism 45

3-3-2. Phase transition 54

References 60

CHAPTER 4. Gelation Mechanism and Structure in Gels of Syndiotactic Polystyrene 61

4-1. Introduction 61

4-2. Experimental 62

4-2-1. Samples 62

4-2-2. Measurements 62

4-3. Results and Discussion 63

4-3-1. Molecular conformation formed in SPS gels 63

4-3-2. Phase diagram of SPS/o-dichlorobenzene 67

4-3-3. Gelation rate of SPS/o-dichlorobenzene 73

4-3-4. Small angle neutron scattering of SPS/ o-dichlorobenzene 75

4-3-4. Crystallization from SPS/decalin solution 78

References 83

CHAPTER 5. Gelation Mechanism and Structure in Gels of Isotactic Polystyrene 87

5-1. Introduction 87

5-2. Experimental 88

5-2-1. Samples 88

5-2-2. Measurements 89

5-3. Results and Discussion 89

5-3-1. Molecular structure of IPS formed in gel 89

5-3-2. Critical sequence length of conformation-sensitive bands 104

References 111

CHAPTER 6. Gelation Mechanism and Structure in Gels of Atactic Polystyrene 113
6-1. Introduction 113
6-2. Experimental 114
6-2-1. Samples 114
6-2-2. Measurements 115
6-3. Results and Discussion 115
6-3-1. Gel structure of APS 115
6-3-2. The relationship between gel structure and stereoregularity 122
References 127
CHAPTER 7. Glassy State of Various Stereoregular Polystyrenes 129
7-1. Introduction 129
7-2. Experimental 129
7-2-1. Samples 129
7-2-2. Measurements 130
7-3. Results and Discussion 130
7-3-1. Preferred conformation in the glassy state 130
7-3-2. CP/MAS ^{13}C-NMR spectra 134
7-3-3. Long-range conformational structure and stiffness of polymer molecules in glassy state 139
References 145
CHAPTER 8. Concluding Remarks 147
List of Publications 152

CHAPTER 1

General Introduction

The success in the synthesis of stereoregular polymers by Natta and his coworkers in 1955[1] made an epoch in the field of polymer science. The "stereoregularity" or "tacticity" of polymer molecules is the fundamentally important concept to be taken into account in considering structures and properties of various series of polymeric materials. Isotactic polystyrene (abbreviated as IPS) is one of the typical stereoregular polymers synthesized by Natta et al. in the earliest stage of their works,[2] and many studies have been made on the structures and physical properties of IPS in crystalline and non-crystalline states in comparison with stereo-irregular atactic polystyrene (APS) in order to elucidate the role of the regular isotactic configuration in various characteristic behaviors of IPS. Among the various phenomena that stereoregular polymers exhibit, the structural ordering processes occurring in various phases, such as crystallization, gelation and various types of phase transition are very fascinating problems to be clarified from the viewpoint of molecular level.

As for the crystallization of IPS, it has been established that the molecule forms a (3/1) helix with a regular repetition of trans (T) and gauche (G) conformations of the skeletal C-C bonds.[2,3] The crystallization kinetics of IPS from the amorphous glass and from solutions were studied by many investigations.

Conformational ordering process of IPS occurring in carbon disulfide (CS_2) solutions was investigated by Kobayashi et al.[4]

by means of infrared spectroscopy. They indicated that on cooling an IPS/CS_2 solution down to -100°C long regular sequences (long as 12 or more monomeric units) of the TG conformation were formed in the polymer chains. For non-crystalline APS, such a conformational ordering in solution could not be detected. In order to clarify the ability of forming such an ordered conformation as well as the thermodynamic stability of the resultant structure in relation to the stereoregularity of polystyrene (PS), we need various PS samples having different tacticities ranging from highly isotactic to highly syndiotactic. Thus, preparation of syndiotactic polystyrene (SPS), the other counterpart of stereoregular polystyrene, has been eagerly awaited for a long time. However, it was not successful until Ishihara et al. obtained quite recently a series of highly crystalline SPS samples by using a Kaminsky type catalyst composed of titanium compounds and methylaluminoxane.[5,6] With these samples together with the previously prepared IPS, APS and also non-crystalline PS samples derived from IPS by an epimerization reaction, we started a series of works on the molecular-level structures of polystyrenes formed in various aggregation states, including both crystalline and non-crystalline phases, the polymorphism, the phase transition behavior, the molecular vibrations, structural ordering process like crystallization and gelation, and so on. The author's attention has been focused to the role of the stereoregularity in the mechanism of the structural organization and the resultant structures.

In addition to the structure and properties of the bulk

polystyrenes, gels of various PS/solvent systems give us very fascinating subjects. It was demonstrated first by Keller and his coworkers[7] that decalin solutions of IPS formed a clear gel at sufficiently high supercoolings. Since then many studies have been done on IPS[8-19] and APS[20-31] gels in order to elucidate the structure and properties of the gels and the gelation mechanism. The gel-forming behavior was found to be strongly influenced by the tacticity of PS and also by the solvent. However, details of the effect of stereoregularity still remain unclarified. For getting the full scope of the gelation of PS/solvent systems, investigation of the SPS gels is inevitable. From this standpoint, a comprehensive work on the structure of SPS gels and the gel-formation was attempted by using various techniques, including the vibrational spectroscopy, the small angle neutron scattering, the thermal analysis and so on.

This doctoral thesis consists of the following eight chapters.

In Chapter 2, the stable conformation of SPS molecules in crystalline states are investigated by means of X-ray diffraction and vibrational spectroscopy along with the normal mode calculations. The infrared and Raman spectral data for the bands characteristic of the particular regular conformations are summarized. They are to be used as basic data for considering the conformations in the non-crystalline phases. The solid-state phase transition of SPS accompanied with conformational change is also investigated.

Chapter 3 is concerned with the polymorphism in SPS. Various crystal modifications different in the molecular conformation as well as in the packing mode of molecules are considered by X-ray

diffraction, infrared spectroscopy and electron microscopy. Possibility of the formation of polymer-solvent complexes is also discussed. The change in the conformational order during the annealing process is another subject.

Chapters 4-6 deal with the gels formed in various PS/solvent systems. In Chapter 4, we are concerned with the gelation mechanism and the molecular structures in gels of SPS/o-dichlorobenzene system. The phase diagram of the gels is obtained by DSC, and the ordered molecular conformation as well as the polymer-solvent interactions are discussed with the aid of the infrared spectroscopic method. The size of the cross-linking coagurates is investigated by small angle neutron scattering.

Chapter 5 deals with the IPS/CS_2 gels. The process of conformation ordering during the gelation is followed by infrared spectroscopy. The stable conformation formed in gels is discussed in comparison with the results reported by previous workers.

Chapter 6 is described about the gelation of APS/CS_2 system by using infrared spectroscopy. The most important subject is to clarify what type of cross-linking structure is formed in non-crystalline APS gel. By using epimerized IPS, the tacticity dependence of gel structure is also investigated.

In Chapter 7, glassy states of SPS, IPS and APS is dealt by means of vibrational spectroscopy. The formation of preferred ordered conformation in relation to the stereoregularity is investigated. The result is to be connected to the dimension of chain in glass.

In Chapter 8, concluding remarks on this thesis is summarized.

References

1) G. Natta, J. Polym. Sci., 16, 143 (1955).

2) G. Natta, P. Pino, P. Corradini, F. Danusso, E. Mantica, J. Am. Chem. Soc., 77, 1700 (1955).

3) G. Natta, P. Corradini, I. W. Bassi, Nuovo Cimento, Suppl., 15, 68 (1960).

4) M. Kobayashi, K. Tsumura, H. Tadokoro, J. Polym. Sci., Polym. Phys. Ed., 6, 1493 (1968).

5) N. Ishihara, T. Seimiya, M. Kuramoto, M. Uoi, Macromolecules, 19, 2464 (1986).

6) N. Ishihara, M. Kuramoto, M. Uoi, Macromolecules, 21, 3356 (1988).

7) M. Girolamo, A. Keller, K. Miyasaka, N. Overbergh, J. Polym. Sci., Polym. Phys. Ed., 14, 39 (1976).

8) E. D. T. Atkins, D. H. Isaac, A. Keller, K. Miyasaka, J. Polym. Sci., Polym. Phys. Ed., 15, 211 (1977).

9) E. D T. Atkins, D. H. Isaac, A. Keller, J. Polym. Sci., Polym. Phys. Ed., 18, 71 (1980).

10) E. D. T. Atkins, A. Keller, J. S. Shapiro, P. J. Lemstra, Polymer, 22, 1161 (1981).

11) E. D. T. Atkins, M. J. Hill, D. A. Jarvis, A. Keller, E. Sarhene, J. S. Shapiro, Colloid & Polymer Sci., 232, 22 (1984).

12) P. R. Sundararajan, Macromolecules, 12, 575 (1979).

13) P. R. Sundararajan, N. J. Tyrer, Macromolecules, 15, 1004 (1982).

14) N. J. Tyrer, T. L. Bluhm, P. R. Sundararajan, Macromolecules, 17, 2296 (1984).

15) J. -M. Guenet, Macomolecules, **19**, 1961 (1986).

16) J. -M. Guenet, G. B. McKenna, Macromolecules, **21**, 1752 (1988).

17) M. Klein, J. -M. Guenet, Macromolecules, **22**, 3716 (1989).

18) M. Klein, A. Brulet, J. -M. Guenet, Macromolecules, **23**, 540 (1990).

19) M. Klein, A. Mathis, A. Menelle, J. -M. Guenet, Macromolecules, **23**, 4591 (1990).

20) S. J. Wellinghoff, J. Shaw, E. Baer, Macromolecules, **12**, 932 (1979).

21) H. Tan, A. Hiltner, E. Moet, E. Baer, Macromolecules, **16**, 28 (1983).

22) J. Francois, J. Y. S. Gan, J. -M. Guenet, Macromolecules, **19**, 2755 (1986).

23) X. -M. Xie, A. Tanioka, K. Miyasaka, Polymer, **31**, 281 (1990).

24) X. -M. Xie, A. Tanioka, K. Miyasaka, Polymer, **32**, 479 (1991).

25) Y. Izumi, Y. Miyake, K. Inoue, S. Katano, M. Iizumi, Rep. Prog. Polym. Phys. Jpn., **27**, 9 (1984).

26) Y. Izumi, Y. Miyake, M. Iizumi, N. Minakawa, S. Katano, Rep. Prog. Polym. Phys. Jpn., **28**, 5 (1985).

27) Y. Izumi, Y. Miyake, S. Katano, N. Minakawa, M. Iizumi, Rep. Prog. Polym. Phys. Jpn., **29**, 7 (1986).

28) Y. Izumi, Y. Miyake, K. Inoue, Rep. Prog. Polym. Phys. Jpn., **29**, 9 (1986).

29) Y. Izumi, Y. Miyake, K. Inoue, Rep. Prog. Polym. Phys. Jpn., **30**, 3 (1987).

30) Y. Izumi, Y. Miyake, S. Katano, N. Minakawa, M. Iizumi, M. Furusaka, H. Kumano, K. Kurita, Rep. Prog. Polym. Phys. Jpn., **30**, 5 (1987).

31) Y. Izumi, T. Matsuo, Y. Miyake, S. Katano, N. Minakawa, M. Iizumi, S. Funahashi, M. Arai, M. Furusaka, S. Hirota, K. Kurita, Rep. Prog. Polym. Phys. Jpn., **31**, 5 (1988).

CHAPTER 2

Molecular Structures of Syndiotactic Polystyrene

2-1. Introduction

Isotactic polystyrene (abbreviated as IPS) is a candidate of stereoregular polymers. Since the first invention by Natta et al. in 1955,[1] many studies have been reported on the structure of IPS and related low molecular weight compounds in crystalline and non-crystalline states. It is well-known that in the crystalline state the IPS molecule assumes a (3/1) helical form with a regular repetition of trans (T) and gauche (G) conformations of the skeletal C-C bonds.[2,3] Molecular vibrations of IPS having the regular TG conformation have been investigated by means of infrared[4-8] and Raman[9] spectroscopies as well as by normal modes analysis.[10-12]

Preparation of syndiotactic polystyrene (abbreviated as SPS), the other counterpart of stereoregular polystyrene, has been eagerly waited for a long time as a key material to be used for the elucidation of the effects of the stereochemical structure on various physical and chemical properties of stereoregular polymers. However, it was not succeeded until Ishihara et al. obtained recently a series of highly crystalline SPS samples by using a specific catalytic system.[13,14]

With these samples, we studied the molecular level structures of SPS in crystalline and noncrystalline states, i. e., the polymorphism, phase transitions and the molecular vibrations. The results are to be compared with those of IPS and isotactic

(IPP) and syndiotactic polypropylenes (SPP). In particular, SPP crystallizes in two modifications which are different in the molecular conformation : one being the TTGG form[15,16] and the other the all trans (TT) form.[17] The TTGG form is stable in ambient conditions and TT form is obtained when the melt-quenched sample is highly stretched in iced water.[18] The presence of the two stable conformers in the crystalline phase is inferred from the potential energy calculation.[19] In the case of SPS, Ishihara et al. suggested that it assumed the all-trans (TT) planar structure. It is of importance to elucidate the conformational stability of the SPS molecule and compare it with the case of SPP.

In this chapter, we deal with the molecular conformations of SPS revealed by X-ray diffraction, vibrational spectroscopy and the normal mode analysis.

2-2. Experimental

2-2-1. Samples

SPS : The SPS samples used were supplied from Idemitsu Petrochemical Co. Ltd. The weight-average molecular weights were measured as 7×10^4, 16×10^4, 35×10^4, and 114×10^4 by GPC. The pentad syndiotacticity was evaluated as 96% or more by ^{13}C-NMR. The samples were first dissolved in chloroform, and film specimens were cast from the solution. The cast films held between two polished metal plates were heated in a Wood's alloy bath kept at 270^{o}C and then quenched in iced water, giving noncrystalline glassy films.

According to the crystallization condition, two types of

molecular conformation were obtained. We refer them to α and β forms as described in the following.

α-SPS : Unoriented films of α form were obtained by annealing the quenched glassy films at 200°C for 30 min. When a quenched film was drawn about 5 times the original length in boiling water and then annealed in a fixed-end state at 200°C for 30 min, a uniaxially oriented film of α form was obtained.

β-SPS : Film samples cast from a chloroform solution were dried by keeping them in an evacuated desiccator for several days, and thereafter they were put in boiling water for several hours in order to remove contaminating solvent. Thus, we obtain unoriented films of β form. These samples showed infrared spectrum typical of this particular crystalline phase as described below. The removal of solvent was checked by elimination of the infrared absorptions due to the solvent. Uniaxially oriented films of the β form were prepared by holding stretched melt-quenched glassy films in a vapor of chloroform or benzene. The vapor exposure was continued until the infrared pattern changed to the β-type. For this process, a few days or a week were needed depending on the film thickness. For thicker filaments used for the X-ray diffraction experiment, the oriented filaments (poorly crystallized in the α form) were immersed in benzene until the reflection due to the α form almost disappeared.

IPS : IPS samples used were obtained by polymerization with a Ziegler-Natta catalyst ($TiCl_3$-$(C_2H_5)_3Al$) in n-heptane at 70°C. The unoriented and uniaxially oriented film specimens in the glassy and crystalline states were prepared through the procedures

similar to the case of α-SPS.

2-2-2. Measurements

Infrared spectra (with the 1 cm^{-1} resolution) were taken by using JASCO FT-IR 5MP and 8000 spectrometers equipped with a DTGS detector. The number of accumulation cycles was in the range of 50-100. Polarized spectra were measured with a wire-grid polarizer. Far-infrared spectra (with 2cm^{-1} resolution) were taken by using a Perkin-Elmer 1800 FT-IR spectrometer equipped with a DTGS detector. Raman spectra were taken with a JASCO R-500 double monochromator with the 514.5-nm excitation light from an Ar^{+} laser. Fiber diffraction patterns of uniaxially oriented specimens were taken with a cylindrical camera of 57.3 mm diameter with the CuKα line monochromatized by a Ni filter.

2-3. Results and Discussion

2-3-1. Conformational stability in crystalline state

The fiber identity periods of α and β phases were measured from the fiber diagram photographs (Figure 2-1) as 0.5 and 0.75 nm, respectively. This suggests, by analogy of SPP, that the α phase takes an all-trans planar zigzag (TT) skeletal conformation and the β phase a TTGG-type conformation forming presumably a twofold helical structure, as depicted in Figure 2-2.

The molecular conformations of the two crystalline phases of SPS derived from the X-ray fiber patterns are supported by the infrared and Raman spectra (Figures 2-3, 2-4 and 2-5). The number

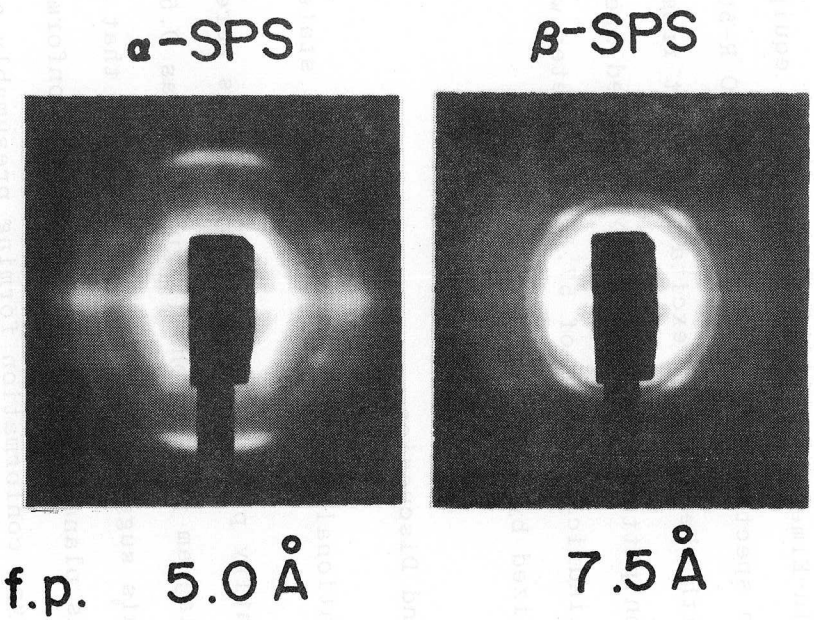

Figure 2-1. X-ray fiber photograph of (a) α-SPS and (b) β-SPS.

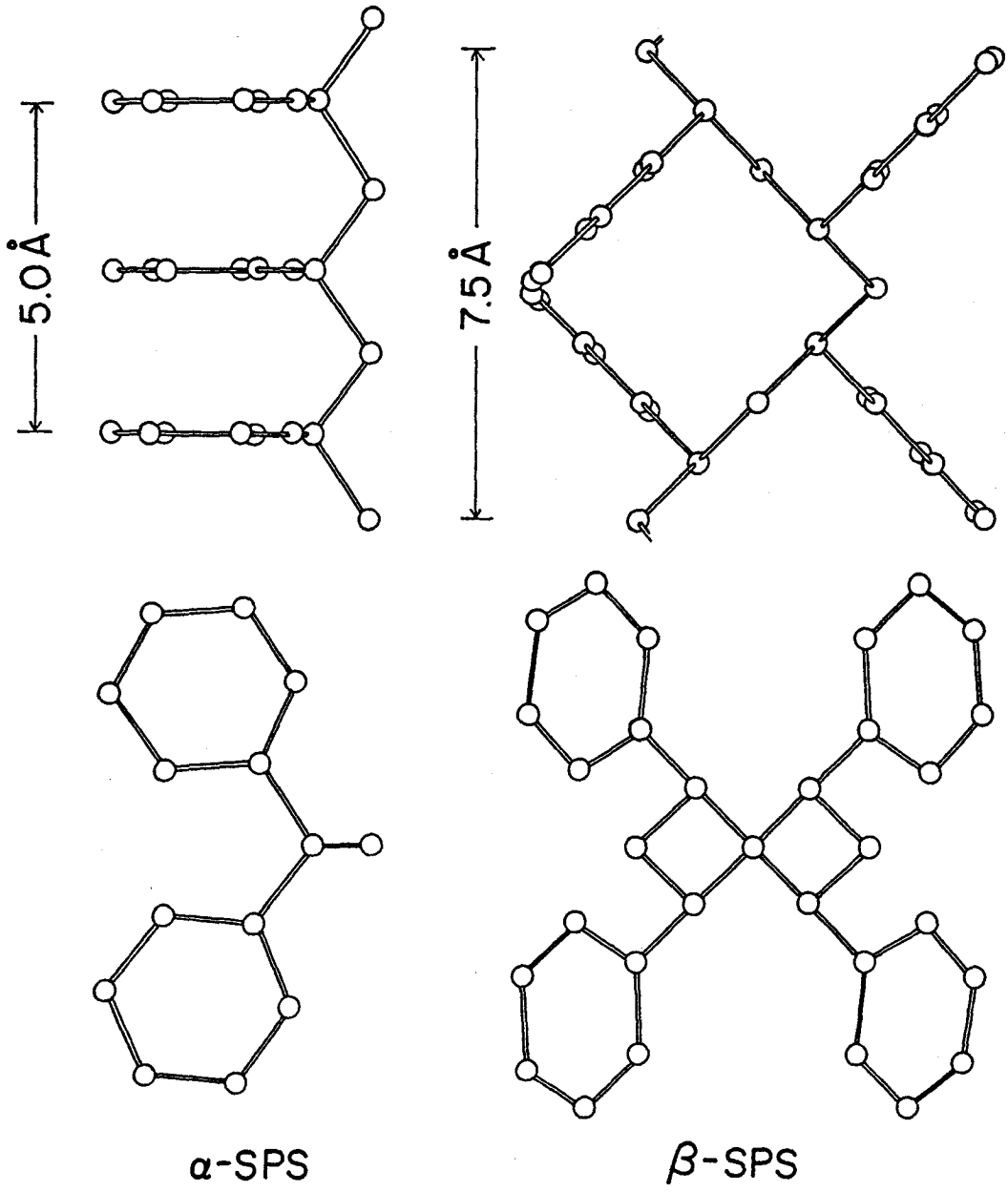

Figure 2-2. Schematic representation of molecular structures of α-SPS and β-SPS.

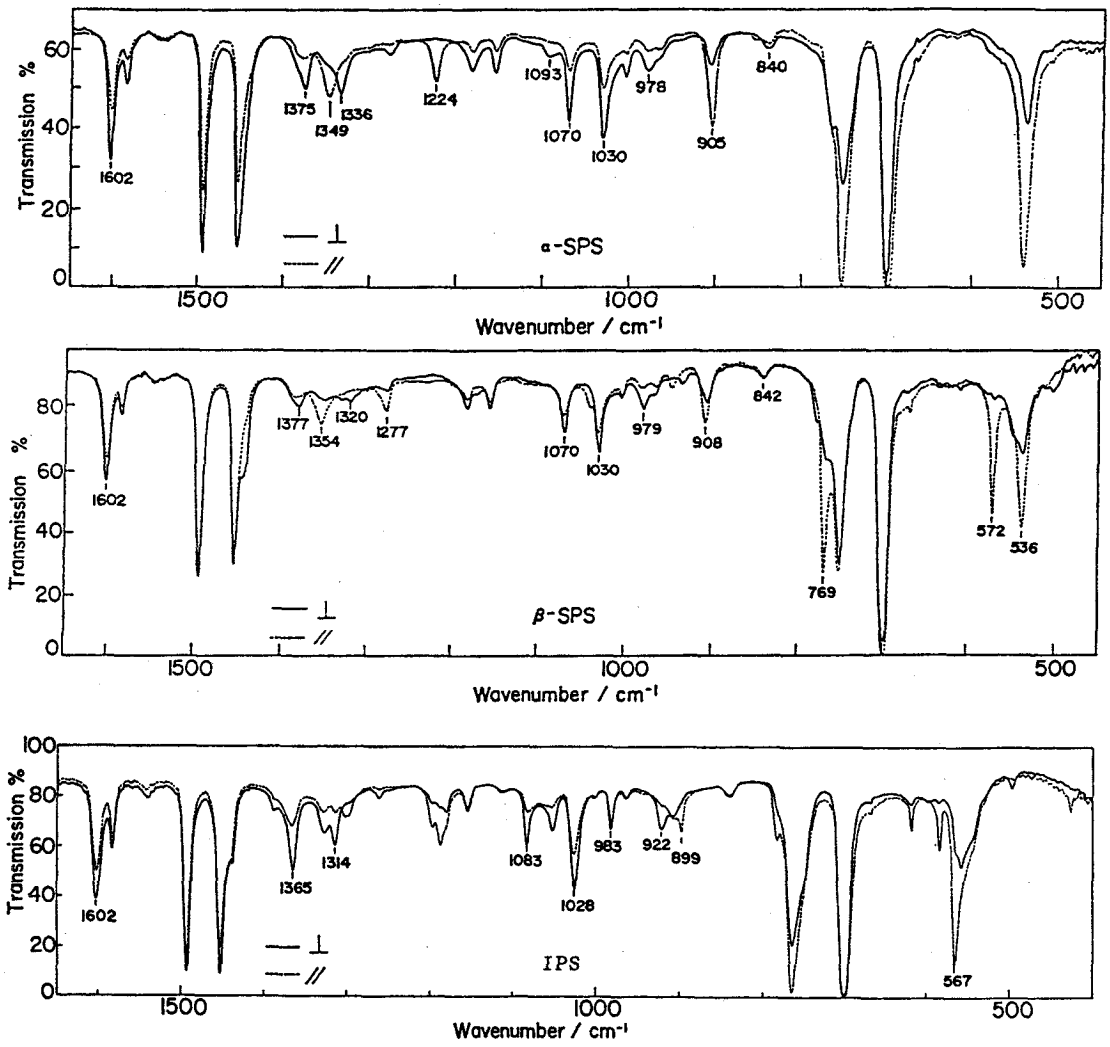

Figure 2-3. Polarized infrared spectra of uniaxially oriented films of α and β forms of SPS and IPS (crystalline).

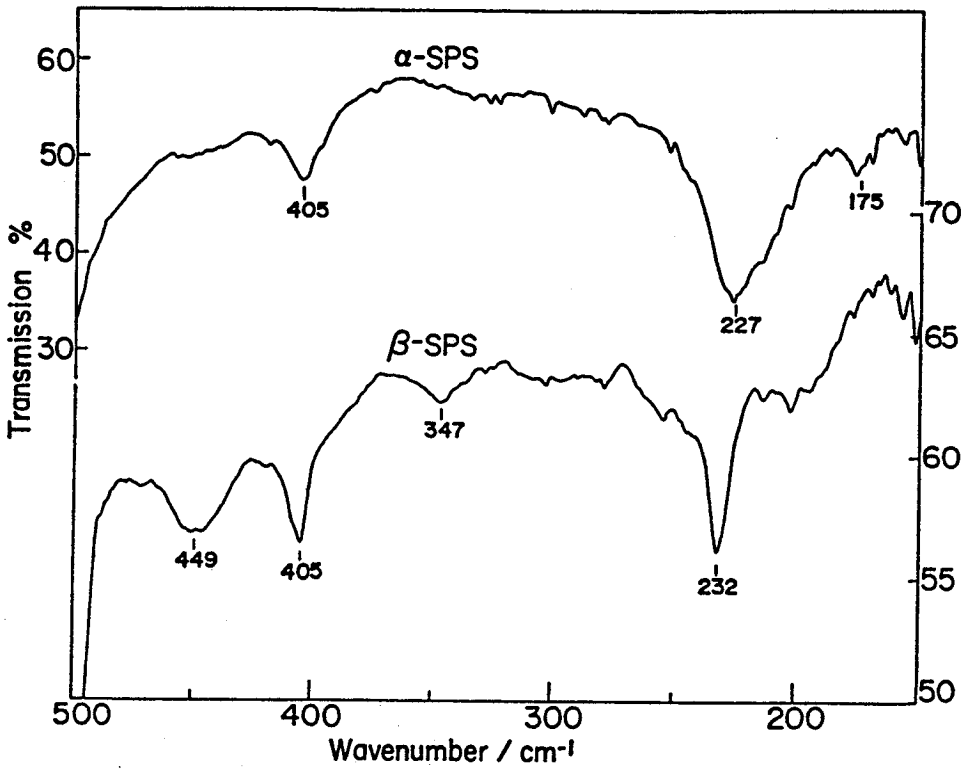

Figure 2-4. Far-infrared spectra of α-SPS and β-SPS.

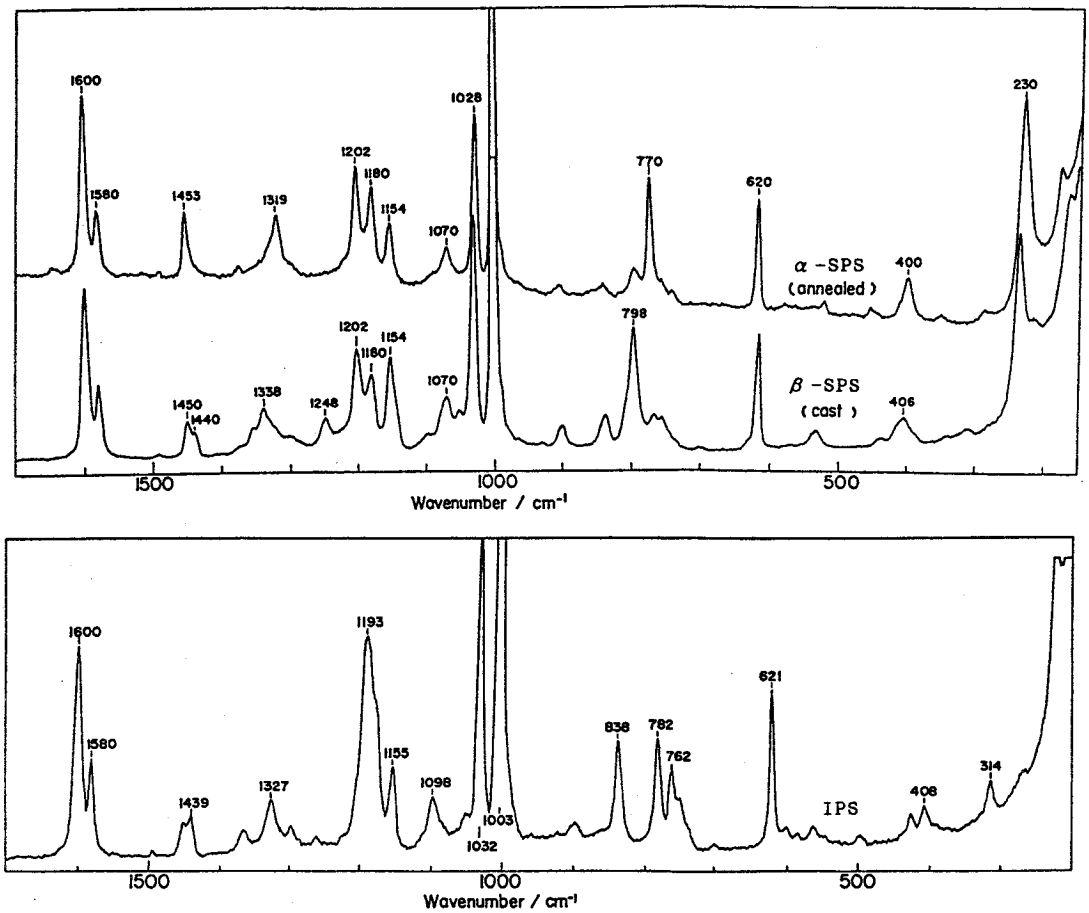

Figure 2-5. Raman spectra of α-SPS, β-SPS and IPS (crystalline).

of the normal modes and the infrared and Raman selection rules of the optically active symmetry species for the (TT) and (TTGG) molecules of SPS are given in Table 2-1, in comparison with those of the threefold helical (TG) molecule of IPS. Here, we assume that in the TT SPS molecule the plane of the phenyl ring is located perpendicular to the zigzag skeletal plane (having the C_{2v} factor group symmetry) and that the TTGG molecule has the twofold screw axis along the chain axis and two twofold rotation axes that pass through the methylene carbon atoms and cross perpendicularly the twofold screw axis (the D_2 factor group symmetry).

Table 2-1 tells us the following things:

(1) The number n of infrared bands of the TT-SPS molecule is far small compared with the case of the TTGG-SPS and TG-IPS molecules, because of the smaller number of monomeric units per fiber period and presence of the infrared-inactive A_2 species (TT-SPS, two units with C_{2v} symmetry; TTGG-SPS, four units with D_2 symmetry; TG-IPS, three units with C_3 symmetry). The difference in the number of the detected infrared-active bands between the two modifications of SPS is quite obvious in the region 1100-500 cm^{-1} (see Figure 2-3). The number of Raman-active bands is, however, not so different (Figure 2-5), because most of the Raman bands observed are due to the modes localized to the phenyl ring which are scarcely separated by the difference in the phase between the neighboring rings (i. e., in the symmetry species).

(2) The difference in molecular conformation is reflected in the infrared polarization of the ring modes. In the TTGG-SPS molecule, one ring mode splits into four different symmetry species, three of

Table 2-1. Number of normal modes and selection rules for α-SPS, β-SPS and IPS molecules.

α-SPS

C_{2v}	E	$C_2(x)$	$\sigma_v(xy)$	$\sigma_g(xz)$	n_i	T,R	n	IR*	Raman*
A_1	1	1	1	1	30	T_x	29	A($\perp$)	A
A_2	1	1	-1	-1	17	—	17	F	A
B_1	1	-1	1	-1	31	T_y,R_z	29	A($\perp$)	A
B_2	1	-1	-1	1	18	T_z	17	A($\parallel$)	A

β-SPS

D_2	E	$C_2(x)$	$C_2(y)$	$C_2(z)$	n_i	T,R	n	IR*	Raman*
A	1	1	1	1	47	—	47	F	A
B_1	1	1	-1	-1	48	T_x	47	A($\perp$)	A
B_2	1	-1	1	-1	48	T_y	47	A($\perp$)	A
B_3	1	-1	-1	1	49	T_z	47	A($\parallel$)	A

IPS

C_3	E	C^1_3	C^2_3	n_i	T,R	n	IR*	Raman*
A	1	1	1	48	T_z,R_z	46	A($\parallel$)	A
E	1	ε	ε^2	48	(T_x,T_y)	47	A($\perp$)	A
	1	ε^{-1}	ε^{-2}	48				

$\varepsilon = \exp i(2\pi/3)$.

* A:active, F:forbidden

which being infrared-active. Therefore, a triplet of IR absorption is expected to be observed. However, for most of the ring modes, the components due to different species are located very close to each other and, hence, actually overlap at the same frequency because of comparatively weak intrachain coupling between neighboring phenyl rings. Therefore, the parallel (B_3) and perpendicular (B_1 and B_2) infrared-active components of a particular ring mode overlap each other, resulting in a single peak having dichroic ratio determined by the orientation of the local transition dipole moment of the mode with respect to the fiber axis. In case of ring C-H stretch modes, the dichroic ratios are expected to be close to unity since the phenyl rings are inclined to the fiber axis by about 45°. On the contrary, in the TT-SPS molecule the out-of-plane ring modes belong to B_2 (with infrared polarization parallel to the fiber axis), and the in-plane ring modes belong to A_1 or B_1 (with infrared polarization perpendicular to the fiber axis). Therefore, all the ring modes might exhibit well-defined polarization. The observed infrared bands of the α-form due to the ring C-H stretch modes (the in-plane modes) and the skeletal C-H stretch modes as well exhibit clear perpendicular polarization, compared with those of the β form (Figure 2-6). This also supports our conclusion about the molecular conformation of the two modifications of SPS.

As for the relationship between the vibrational spectra and the molecular conformation of SPS, Jasse et al. investigated Raman spectra of the racemo-racemo-type stereoisomer of 2,4,6-triphenylheptane (a trimer of SPS).[9] This compound gives rise to two bands

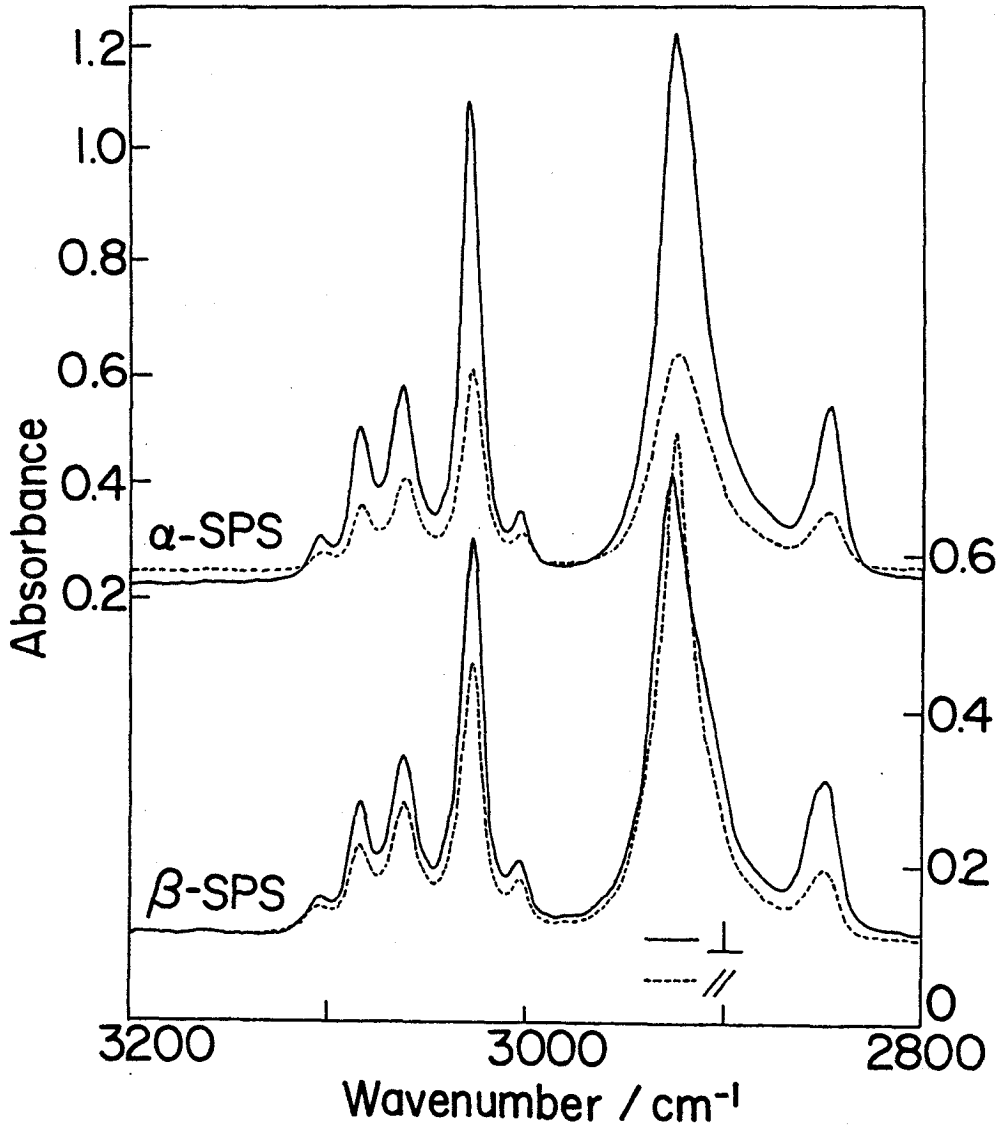

Figure 2-6. Polarized infrared spectra (in the C-H stretch region) of uniaxially oriented films of α-SPS and β-SPS.

at 763 and 623 cm^{-1} in a crystalline state, while in a liquid state additional bands appear at 789 and 737 cm^{-1} (Figure 2-7), indicating that there exist at least two conformers in the liquid state. If we compare the Raman spectra of α- and β-SPS in the same frequency region (Figure 2-7b with Figure 2-7a), it is evident that the crystalline trimers and the α-form take the same TTTT conformation. This is consistent with the fact that the most stable conformation of syndiotactic dimers and trimers so far investigated is the all-trans form. The 789-cm^{-1} band appearing in the liquid trimer corresponds to the 798-cm^{-1} band of β-SPS. This suggests that the additional conformer present in the liquid trimer should contain gauche C-C bonds like in β-SPS.

2-3-2. Crystallization from the glass and solid-state phase transition

DSC of the heating process of glassy SPS shows that crystallization occurs at about 140°C, and melting at about 270°C (Figure 2-8). Crystallization and melting enthalpies measured on various samples with different molecular weights are summarized in Table 2-2. The temperature Tc at which the crystallization starts and the magnitude of the accompanying exotherm varied somewhat depending on the molecular weight as well as on the heating rates. During this heating process, the infrared spectrum changes as shown in Figure 2-9. The appearance of the 1335 and 1224 cm^{-1} bands on crystallization indicates that the resultant crystalline phase is the α modification. As a β-SPS film is heated, it transforms to the α modification at about 180°C as followed by

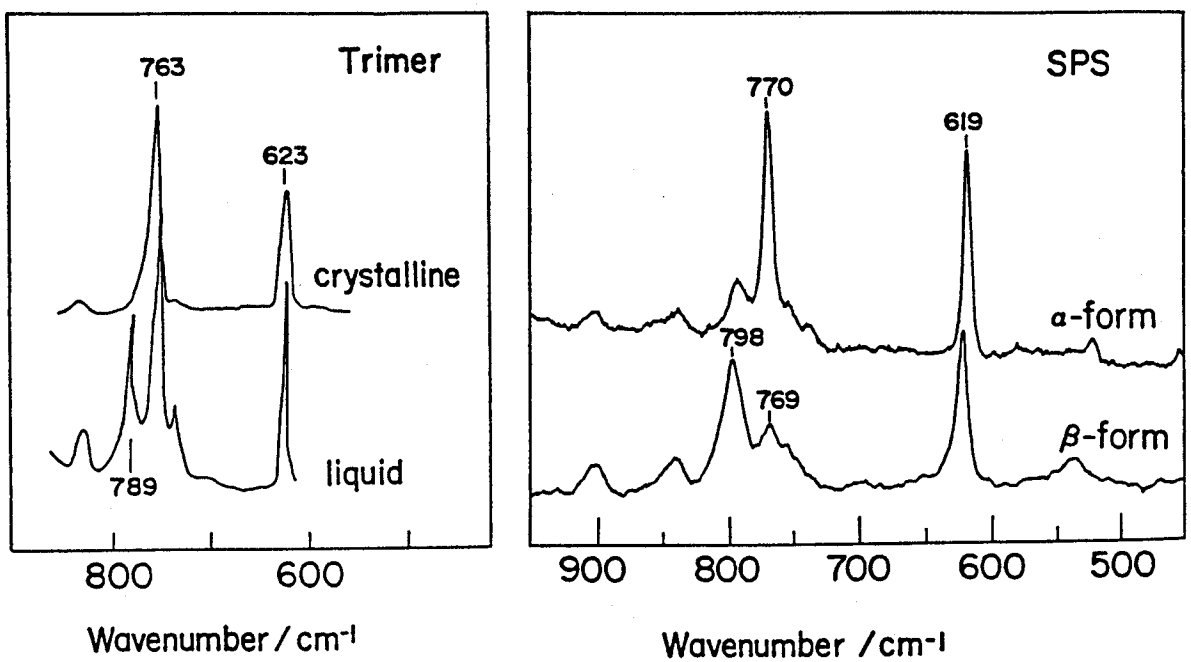

Figure 2-7. Comparison of Raman spectra of (a) racemo-racemo 2,4,6-triphenylheptane and (b) two crystal modifications of SPS.

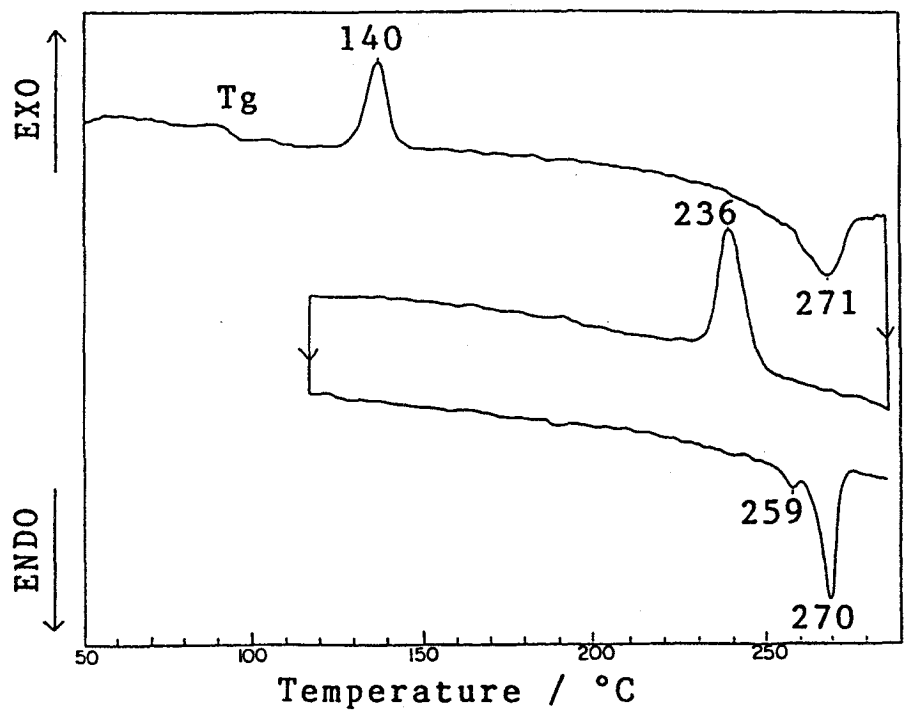

Figure 2-8. DSC thermogram on a crystallization process of SPS from a glassy state.

Table 2-2. Enthalpies (Δ Hc and Δ Hm) and temperatures (Tc and Tm) corresponding to crystallization and melt.

Mw	Tc/^{o}C	Δ Hc/Jg^{-1}	Tm/^{o}C	Δ Hm/Jg^{-1}
70000	147	-18	259	28
160000	137	-16	268	28
350000	139	-14	270	28
1135000	140	-14	271	28

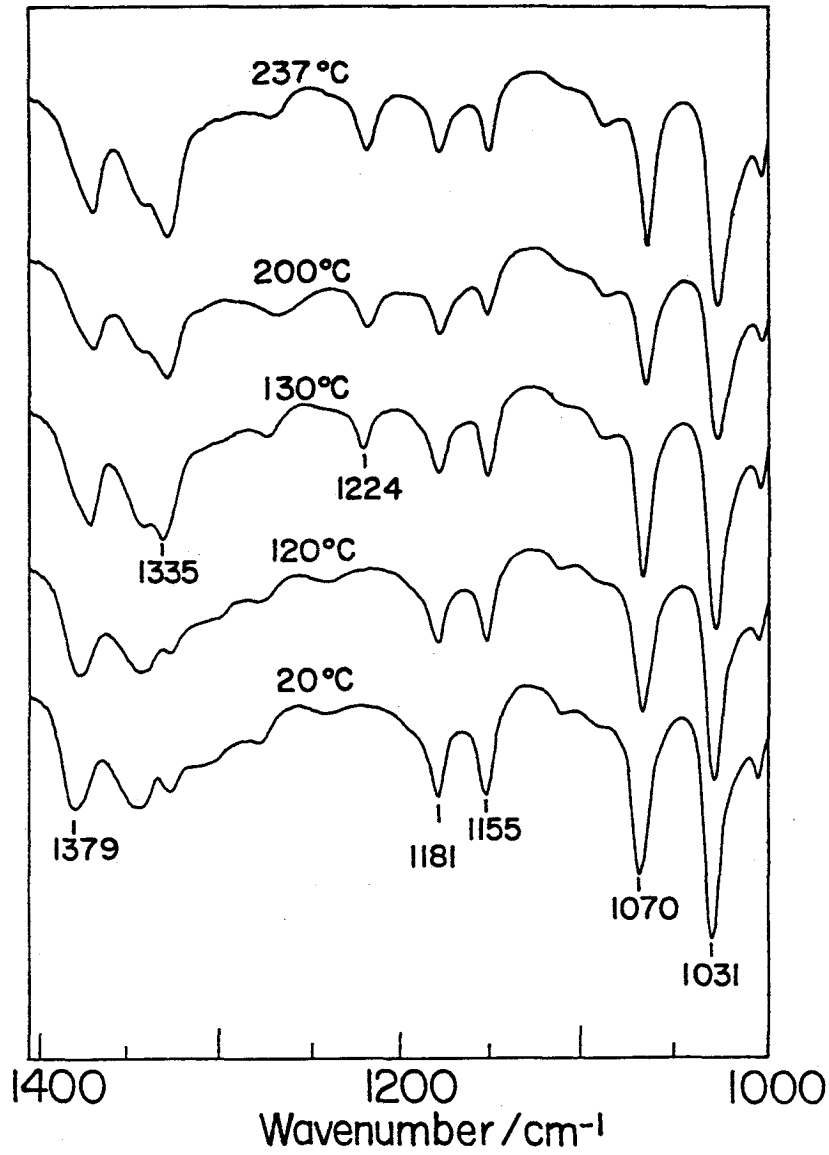

Figure 2-9. Infrared spectral change on a heating process of a glassy film of SPS. Appearance of the 1335 and 1224 cm^{-1} bands above 130°C indicates that the resultant crystalline phase is α.

the infrared spectral change shown in Figure 2-10. The transformation is clearly detected by the appearance of the 1224 cm^{-1} band (α) and the disappearance of the 935 cm^{-1} band (β). In the DSC thermogram, we could detect a weak exotherm peak at 180°C, although it was too weak to evaluate its magnitude. Thus, in the dried state, the α phase consisting of the all-trans skeletal conformation is thermodynamically more stable than the β phase consisting of the TTGG conformation. In the construction of the TTGG conformation, presence of solvent molecules seems to play an important role. The reverse is true in syndiotactic polypropylene (SPP), where the TTGG form is always obtained through the ordinary crystallization process from the melt and from solution, while the TT form is obtained by stretching a melt-quenched sample on iced water. The difference in conformational stability between SPS and SPP may be ascribed to the difference in the shape and bulkiness of the pendant group.

2-3-3. Normal modes analysis

In previous works on molecular vibrations of polystyrene, it has been revealed that most of the infrared and Raman bands characteristic of IPS are due to some specific intramolecular interactions in regular sequences of the TG skeletal conformation. For the well-established (3/1) helix of IPS, the normal mode analysis was performed by Painter et al. in order to elucidate the origin of the conformation-sensitive character of some infrared and Raman bands.[10-12] In the case of SPS, the bands characteristic of the TT or TTGG conformation are found in the spectra of α-

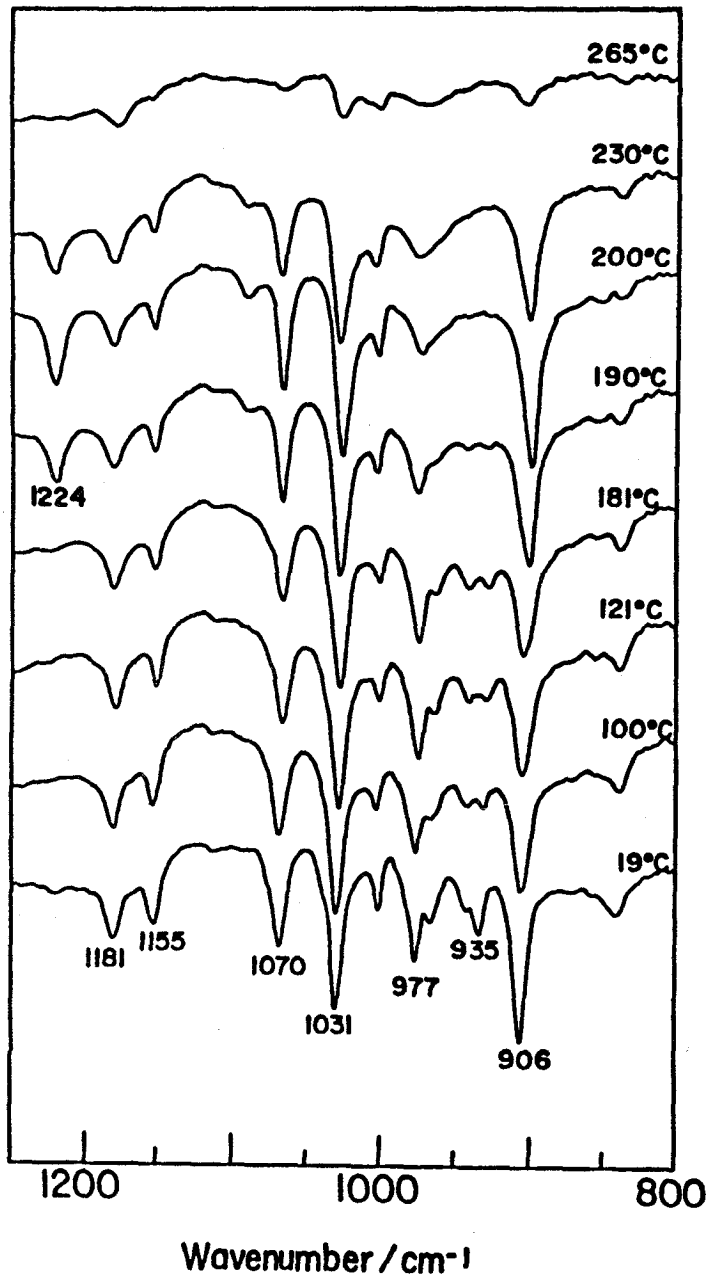

Figure 2-10. Infrared spectral change on a heating process of β-SPS. Appearance of the 1224 cm^{-1} band and disappearance of the 935 cm^{-1} band above 190°C indicates that β transforms to α.

or β-SPS by comparing them with the spectra of glassy SPS. They are used as the key bands for the identification of crystal modification or of particular local conformation present in noncrystalline phases.

The vibrational modes of SPS were calculated by the use of the Wilson's GF-matrix method. In the present calculation, we assume the following molecular parameters ; the bond lengths (in nm) : C_{ring}-C_{ring}=0.14, C_{ring}-C_{chain}=0.151, C_{chain}-H_{chain}=0.109, C_{ring}-H_{ring}=0.1084; the valence angles : 109.5^{o} for the main chain, 120^{o} for the ring. The internal coordinates were defined as shown in Figure 2-11. The symmetry coordinates of the both forms were generated from the group coordinates of the monomeric unit. These group coordinates were formed linear combination of the internal coordinates (Table 2-3). Starting from the initial force constant set directly transferred from that of the (3/1) helix of IPS, the values of the force constants were refined by a trial-and-error method so as to obtain a good agreement between the observed and calculated frequencies (Table 2-4). The final results are summarized in Tables 2-5 and 2-6, where the potential energy distributions (PED's) are also listed. Vibrational modes of several characteristic band in 1200-1300 and 500-600 cm^{-1} region are depicted in Figures 2-12 and 2-13. The 1224 cm^{-1} band characteristic of α-form was assigned to the coupling mode of CH_2 wagging and CH bending. ($\nu_{calc.}$=1224 cm^{-1}) The bands in 500-600 cm^{-1} region are the most sensitive to the conformational change, and associated with the coupling of the phenyl out-of-plane mode and main chain mode.

In this calculation, origin of all bands were clarified.

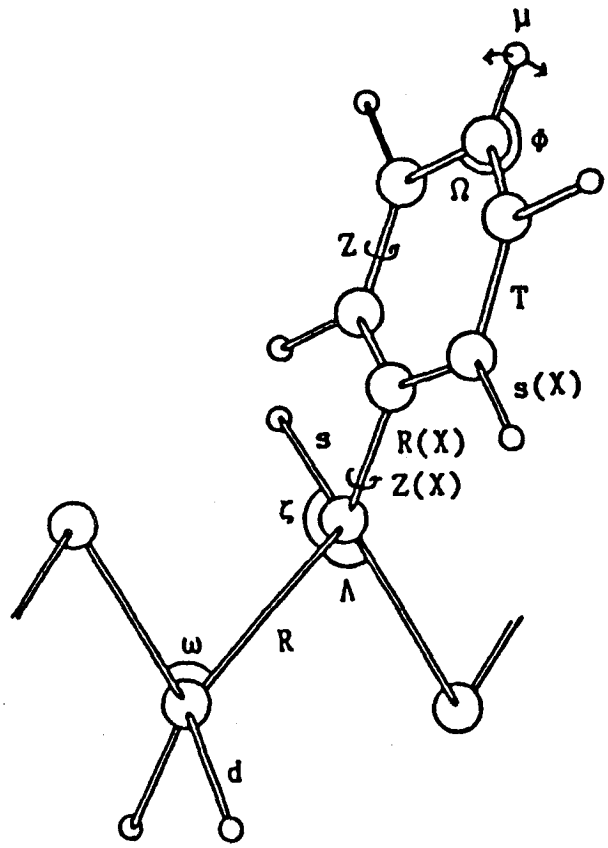

Figure 2-11. Internal coordinates for SPS molecules.

Table 2-3. Intermediate symmetry coordinates.

	Coordinate	Description of force constant
1	R_1+R_2	CC skeletal stretching
2	R_1-R_2	CC skeletal stretching
3	$R_1(X)$	CC strtching
4	$T_1+T_2+T_3+T_4+T_5+T_6$	CC ring stretching
5	$T_1-T_2+T_3-T_4+T_5-T_6$	CC ring stretching
6	$T_1+2T_2+T_3-T_4-2T_5-T_6$	CC ring stretching
7	$T_1-T_3+T_4-T_6$	CC ring stretching
8	$T_1-2T_2+T_3+T_4-2T_5+T_6$	CC ring streching
9	$T_1-T_3+T_4-T_6$	CC ring streching
10	d_1+d_2	CH_2 sym. stretching
11	d_1-d_2	CH_2 antisym. strtching
12	s_1	CH stretching
13	$s_3(X)$	CH ring stretching
14	$s_1(X)+s_2(X)+s_4(X)+s_5(X)$	CH ring stretching
15	$s_1(X)+s_2(X)-s_4(X)-s_5(X)$	CH ring stretching
16	$s_1(X)-s_2(X)+s_4(X)-s_5(X)$	CH ring stretching
17	$s_1(X)-s_2(X)-s_4(X)+s_5(X)$	CH ring stretching
18	$4\delta-\gamma_3-\gamma_4-\gamma_5-\gamma_6$	CH_2 bending
19	$5\omega_2-\delta_2-\gamma_3-\gamma_4-\gamma_5-\gamma_6$	CCC skeletal bending
20	$\gamma_3+\gamma_4-\gamma_5-\gamma_6$	CH_2 rocking
21	$\gamma_3-\gamma_4+\gamma_5-\gamma_6$	CH_2 wagging
22	$\gamma_3-\gamma_4-\gamma_5+\gamma_6$	CH_2 twisting
23	$\omega_2+\delta_2+\gamma_3+\gamma_4+\gamma_5+\gamma_6$	redundancy
24	$2\zeta_1-\zeta_2-\zeta_3$	CH bending
25	$\zeta_2-\zeta_3$	CH bending
26	$\zeta_1+\zeta_2+\zeta_3$	CH bending
27	$2\Lambda_1-\Lambda_2-\Lambda_3$	CCC skeletal bending
28	$\Lambda_2-\Lambda_3$	CCC skeletal bending
29	$\Lambda_1+\Lambda_2+\Lambda_3$	CCC skeletal bending
30	$2\Omega_1-\Phi_1(X)-\Phi_2(X)$	CCC ring bending
31	$2\Omega_2-\phi_1-\phi_2$	CCC ring bending
32	$2\Omega_3-\phi_3-\phi_4$	CCC ring bending

Table 2-3. Continued from previous page

	Coordinate	Description of force constant
33	$2\Omega_4-\phi_5-\phi_6$	CCC ring bending
34	$2\Omega_5-\phi_7-\phi_8$	CCC ring bending
35	$2\Omega_6-\phi_9-\phi_{10}$	CCC ring bending
36	$\Phi_1(X)-\Phi_2(X)$	CCC ring bending
37	$\phi_1-\phi_2$	CCC ring bending
38	$\phi_3-\phi_4$	CCC ring bending
39	$\phi_5-\phi_6$	CCC ring bending
40	$\phi_7-\phi_8$	CCC ring bending
41	$\phi_9-\phi_{10}$	CCC ring bending
42	$\Omega_1+\Phi_1(X)+\Phi_2(X)$	redundancy
43	$\Omega_2+\phi_1+\phi_2$	redundancy
44	$\Omega_2+\phi_1+\phi_2$	redundancy
45	$\Omega_2+\phi_1+\phi_2$	redundancy
46	$\Omega_2+\phi_1+\phi_2$	redundancy
47	$\Omega_2+\phi_1+\phi_2$	redundancy
48	$\tau+\tau$	skeletal torsion
49	$\tau-\tau$	skeletal torsion
50	$Z_1+Z_2+Z_3+Z_4+Z_5+Z_6$	ring torsion
51	$Z_1-Z_2+Z_3-Z_4+Z_5-Z_6$	ring torsion
52	$Z_1+2Z_2+Z_3-Z_4-2Z_5-Z_6$	ring torsion
53	$Z_1-Z_3+Z_4-Z_6$	ring torsion
54	$Z_1-2Z_2+Z_3+Z_4-2Z_5+Z_6$	ring torsion
55	$Z_1-Z_3+Z_4-Z_6$	ring torsion
56	$Z_1(X)+Z_2(X)+Z_3(X)+Z_4(X)$	torsion
57	$Z_1(X)+Z_2(X)-Z_3(X)-Z_4(X)$	torsion
58	$Z_1(X)-Z_2(X)+Z_3(X)-Z_4(X)$	torsion
59	$Z_1(X)-Z_2(X)-Z_3(X)+Z_4(X)$	torsion
60	M	CC out-of-plane
61	μ_3	CH out-of-plane
62	$\mu_1+\mu_2+\mu_4+\mu_5$	CH out-of-plane
63	$\mu_1+\mu_2-\mu_4-\mu_5$	CH out-of-plane
64	$\mu_1-\mu_2+\mu_4-\mu_5$	CH out-of-plane
65	$\mu_1-\mu_2-\mu_4+\mu_5$	CH out-of-plane

Table 2-4. Force constants for SPS

Force constant	Internal coordinate	values*
Phenyl group		
K_T	T	7.090
K_s	s	5.022
H_Ω	$R_i(\Omega)$	1.461
H_ϕ	$R_i(\phi)$	0.496
$F^o{}_T$	T_i, T_{i+1}	0.693
$F^m{}_T$	T_i, T_{i+2}	-0.510
$F^p{}_T$	T_i, T_{i+2}	0.604
$F^o{}_{T\phi}$	$T_i, R_i(\phi)$	-0.272
$F'^o{}_{T\phi}$	$T_i, R_{i+1}(\phi)$	0.272
$F^m{}_{T\phi}$	$T_i, R_{i-1}(\phi)$	-0.057
$F'^m{}_{T\phi}$	$T_i, R_{i+2}(\phi)$	0.057
$F^p{}_{T\phi}$	$T_i, R_{i-2}(\phi)$	0.102
$F'^p{}_{T\phi}$	$T_i, R_{i+3}(\phi)$	-0.102
$F_{T\Omega}$	$T_i, R_{i,i+1}(\Omega)$	0.573
F_{Ts}	$T_i, s_{i,i+1}$	-0.115
$F^o{}_s$	s_i, s_{i+1}	0.013
F_Ω	$R_i(\Omega), R_{i+1}(\Omega)$	0.085
$F^o{}_{\Omega\phi}$	$R_i(\Omega), R_{i-1}(\phi)$	-0.128
$F'^o{}_{\Omega\phi}$	$R_i(\Omega), R_{i+1}(\phi)$	0.128
$F^o{}_\phi$	$R_i(\phi), R_{i+1}(\phi)$	0.013
$F^m{}_\phi$	$R_i(\phi), R_{i+2}(\phi)$	-0.001
$F^p{}_\phi$	$R_i(\phi), R_{i+2}(\phi)$	-0.020
H_μ	μ	0.300
H_z	z	0.098
$F^o{}_\mu$	μ_i, μ_{i+1}	0.003
$F^m{}_\mu$	μ_i, μ_{i+2}	-0.005
$F^p{}_\mu$	μ_i, μ_{i+3}	-0.005
$F^o{}_z$	z_i, z_{i+1}	-0.030
$F_{z\mu}$	z_i, μ_i	0.032

Table 2-4. Cotinued from previous page

Force constant	Internal coodinate	Values
Phenyl group main chain interaction		
$K_{R(X)}$	R(X)	4.740
H_{Φ}	R(Φ(X))	0.700
$H_{Z(X)}$	Z(X)	0.025
H_{M}	M	0.080
$F_{TR(X)}$	T,R(X)	0.173
$F^{o}{}_{\Omega\Phi(X)}$	R_i(Ω),R(Φ(X))	0.076
$F'^{o}{}_{\Omega\Phi(X)}$	R_{i-2}(Ω),R(Φ(X))	-0.076
$F_{T\Phi(X)}$	T_{i-1},R(Φ(X))	-0.375
$F'_{T\Phi(X)}$	T_{i-2},R(Φ(X))	0.375
$F_{R(X)\Omega}$	R(X),R_{i-1}(Ω)	-0.588
$F^{o}{}_{R(X)\Omega}$	R(X),$R_{i,i-2}$(Ω)	0.171
Main chain		
$K_{s'}$	s'	4.588
K_{d}	d	4.538
K_{R}	R	4.532
H_{δ}	δ	0.540
H_{γ}	γ	0.660
H_{ζ}	ζ	0.660
H_{ω}	ω	0.045
H_{Λ}	Λ	1.010
H_{τ}	τ	0.024
F_{d}	d,d	0.006
F_{R}	R,R	0.101
$F_{RR(X)}$	R,R(X)	0.083
$F_{R\gamma}$	R, γ	0.355
$F'_{R\gamma}$	R, γ	0.079
$F_{R(X)\zeta}$	R(X), ζ	0.328
$F'_{R(X)\zeta}$	R(X), ζ	0.079
$F_{R\omega}$	R, ω	0.417

Table 2-4. Continued from previous page

Force constant	Internal coordinate	Values
F_{γ}	γ , γ	-0.021
F'_{γ}	γ , γ	0.012
$F_{\gamma\omega}$	γ , ω	-0.031
$f^{t}_{\gamma\xi}$	γ , ξ	0.127
$f^{g}_{\gamma\xi}$	γ , ξ	-0.005
$f'^{t}_{\gamma\xi}$	γ , ξ	0.002
$f'^{g}_{\gamma\xi}$	γ , ξ	0.009
$f''^{t}_{\gamma\xi}$	γ , ξ	-0.014
$f''^{g}_{\gamma\xi}$	γ , ξ	-0.025
$f^{t}_{\gamma\omega}$	γ , ω	0.049
$f^{g}_{\gamma\omega}$	γ , ω	-0.040
f^{t}_{ω}	ω , ω	-0.011
f^{g}_{ω}	ω , ω	-0.011
F_{Λ}	Λ , Λ	0.308
$F_{\Lambda R}$	R, Λ	0.313
F'_{ζ}	ζ , ζ	0.012

* Stretching constants are in mdyn/A, bending constants are in mdyn A/rad^2 and stretch-bend interactions are in mdyn/rad.

Table 2-5. Observed and calculated frequences (cm-1) for TT form.

ν obs. IR	ν obs. Raman	ν calc.	Potential energy distribution
A_1 mode (IR $\perp$)			
3105		3061	Sx 99%
3084		3053	Sx 99%
3062	3052	3050	Sx 98%
3028	3037	3046	Sx 98%
3003	3000	3045	Sx 98%
2919	2898	2907	S 99%
2847	2845	2848	d 99%
1603	1601	1602	T 69%, Ω 18%
1584	1579	1592	T 73%, Ω 16%
1494		1513	ϕ 51%, T 36%
1453	1453	1455	δ 77%
		1444	ϕ 49%, T 30%, δ 14%
1376	1373	1368	t 44%, ζ , Rx 16%
1335		1335	ϕ 61%, T 37%
		1305	ϕ 42%, T 36%
1278		1256	Ω 63%, Rx 13%
	1203	1205	ϕ 67%, Ω 25%
1183	1180	1171	ϕ 63%, ζ 23%
1156	1154	1147	ζ 42%, t 17%, ϕ 18%, T 17%
		1130	T 32%, ϕ 19%, Rx 16%, Ω 11%
1070	1071	1044	T 50%, ϕ 23%
1030	1028	1008	T 74%, ϕ 16%
1005	1001	1004	R 46%, T 20%
	794	811	R 23%, T 22%, ϕ 16%, Ω 13%
697	700	740	Ω 72%, ϕ 19%
633		652	Ω 45%, ϕ 15%, Λ 10%
401	402	391	Φ 32%, R 14%, Λ 13%
175	175	152	Φ 55%, Λ 18%
		12	τ 93%
A_2 mode (IR inactive)			
	2845	2848	d 99%
	1453	1443	δ 97%
	1320	1326	ζ 63%, t 27%
		1137	t 56%, ζ 23%
		1041	R 75%, ζ 23%

Table 2-5. Continued from previous page

ν obs. IR	ν obs. Raman	ν calc.	Potential energy distribution
		994	μ 68%,Z 30%
	902	870	μ 92%
	840	835	μ 89%
	756	753	μ 99%
		699	μ 97%
		542	Z 39%, μ 26%, Λ 18%
	402	392	Z 48%, μ 29%
		389	Z 49%, ω 21%, Λ 12%
	285	278	Z 94%
	134	101	ω 43%,Z 16%, Λ 10%,M 10%
		41	Zx 85%
		21	M 27%, ω 26%, Λ 18%,Zx 11%
B_1 mode (IR $\perp$)			
3105		3062	Sx 99%
3084		3053	Sx 99%
3062	3052	3051	Sx 98%
3028	3037	3046	Sx 98%
3003	3000	3045	Sx 98%
2924		2926	d 86%,S 13%
2919	2898	2904	S 86%,d 14%
1603	1601	1602	T 69%, Ω 18%
1584	1579	1592	T 73%, Ω 16%
1494		1512	ϕ 52%,T 36%
		1446	ϕ 56%,T 35%
1376	1373	1364	ξ 34%,w 30%,R 12%
1335		1335	ϕ 63%,T 34%
		1314	w 40%,T 17%, ϕ 14%, ξ 11%
		1297	ϕ 28%,T 25%,Rx 19%, Ω 14%
1278		1246	Ω 57%, ξ 13%,w 10%
	1202	1203	ϕ 69%, Ω 20%
1183	1180	1166	ϕ 75%,T 21%
1156	1154	1136	T 23%,R 23%, ϕ 17%, Ω 14%
1112		1113	R 35%,r 14%, ϕ 13%,T 13%
1030	1028	1039	T 55%, ϕ 23%,R 11%
1005	1001	1008	T 75%, ϕ 17%
978	990	982	T 33%,r 24%, ξ 16%,R 11%
765	770	775	Ω 37%, ϕ 20%,Rx 18%,T 14%
	738	740	Ω 72%, ϕ 19%
621	620	584	Ω 36%,Rx 18%,r 12%,T 11%, ϕ 10%
		550	Λ 31%, Φ 14%, ξ 13%
227	231	227	Λ 57%, Φ 21%
		206	Φ 53%, Λ 32%

Table 2-5. Continued from previous page

ν obs. IR	ν obs. Raman	ν calc.	Potential energy distribution
B_2 mode (IR ‖)			
2919		2922	d 99%
1348		1363	R 34%, ζ 32%, w 32%
1224		1225	ζ 46%, w 45%
		1096	R 68%, w 20%
966		994	μ 68%, Z 30%
905	902	869	μ 92%
854		850	r 57%, μ 25%
840	840	830	μ 67%, r 23%
751	756	753	μ 99%
698		699	μ 97%
537		536	Z 44%, μ 26%, Λ 13%
332	352	377	Z 60%, Λ 26%
		279	Z 98%
		250	Λ 46%, Z 44%
		96	Λ 40%, M 21%, Z 16%, Zx 14%
		42	Zx 81%
		24	Λ 52%, M 22%

Table 2-6. Observed and calculated frequences (cm-1) for TTGG form.

ν obs. IR	ν obs. Raman	ν calc.	Potential energy distribution
A mode (IR inactive)			
		3062	Sx 99%
		3053	Sx 99%
	3056	3050	Sx 98%
	3039	3046	Sx 98%
	2905	2905	S 99%
	2850	2849	d 99%
		2847	d 99%
	1599	1602	T 69%, Ω 18%
	1579	1592	T 73%, Ω 16%
	1491	1512	ϕ 52%,T 36%
	1450	1455	δ 90%
		1448	δ 61%, ϕ 20%
	1440	1443	ϕ 37%, δ 34%,T 22%
	1354	1345	t 28%, ξ 23%,T 15%,Rx 10%
	1338	1334	ϕ 61%,T 29%
	1300	1306	ϕ 37%,T 32%
		1271	Ω 30%, ξ 23%,Rx 18%
	1248	1248	t 37%, Ω 31%
		1225	ξ 35%,t 30%, ϕ 11%
	1202	1203	ϕ 65%, Ω 20%
	1180	1166	ϕ 70%,T 20%
	1154	1138	ξ 31%,T 20%, ϕ 16%,t 13%
		1116	t 31%,T 23%, ξ 18%
	1052	1054	R 54%,T 15%
	1030	1038	T 42%,R 22%, ϕ 18%
	1001	1008	T 74%, ϕ 18%
	990	991	μ 67%,Z 30%
		887	R 49%,T 13%
	901	872	μ 92%
	838	836	μ 87%
	798	819	T 18%, Ω 17%,Rx 16%, Λ 12%
	756	751	μ 99%
	744	740	Ω 57%, ϕ 19%
	701	700	μ 97%
	620	666	Ω 52%, ϕ 18%
	534	535	Z 45%, μ 27%, Λ 12%
	406	400	Φ 28%, Λ 22%,R 21%
		375	Z 44%, Λ 29%
	310	308	Λ 32%,Z 30%
		279	Z 98%
	171	174	Λ 48%,Z 23%, Φ 17%
	151	143	Φ 38%, Λ 26%
		75	ω 51%,Zx 16%,M 13%
		41	Zx 80%
		20	ω 30%,M 27%, Λ 16%
		10	ω 37%, υ 26%, Λ 21%

Table 2-6. Continued from previous page

ν obs. IR	ν obs. Raman	ν calc.	Potential energy distribution
B_1 mode (IR $\perp$)			
3104	3056	3062	Sx 99%
3084	3039	3053	Sx 99%
3062		3050	Sx 98%
3028		3046	Sx 98%
3003	3003	3045	Sx 98%
2925		2922	d 93%
2908	2905	2904	S 93%
2849	2850	2847	d 99%
1602	1599	1602	T 69%, Ω 18%
1584	1579	1592	T 72%, Ω 16%
1494	1491	1512	ϕ 52%, T 36%
1453	1450	1450	δ 70%, ϕ 14%
1440	1440	1444	ϕ 44%, T 27%, δ 22%
1378	1374	1357	ξ 35%, t 31%, w 11%, Rx 11%
1330	1338	1335	ϕ 59%, T 39%
1320		1310	ϕ 38%, T 28%, ξ 24%
	1300	1296	ξ 28%, w 22%, R 21%
1278		1262	Ω 44%, w 28%, Rx 14%
	1248	1244	w 25%, Ω 22%, ξ 16%, t 11%
	1202	1204	ϕ 68%, Ω 23%
1182	1180	1169	ϕ 62%, T 11%
1155	1154	1148	ξ 35%, t 23%, ϕ 15%, T 15%
1114		1125	T 37%, ϕ 20%, Rx 15%, Ω 12%
1070	1070	1094	R 54%, ξ 24%
1029	1030	1044	T 50%, ξ 24%
1003	1001	1008	T 74%, ϕ 18%
978	990	992	μ 63%, Z 30%
967		985	r 33%, R 29%
908	901	872	μ 92%
		845	T 23%, Rx 20%, R 13%, Ω 11%
842	838	837	μ 85%
		762	R 33%, r 21%
750	756	751	μ 99%
	744	741	Ω 72%, ϕ 19%
698	701	701	μ 97%
634	632	651	Ω 40%, ϕ 14%, Λ 13%
548		557	Λ 27%, Z 25%, μ 23%
449	440	477	Z 23%, Λ 13%
405	406	386	Z 37%, Λ 19%
347	310	307	Z 41%, Φ 12%
		279	Z 98%
232	238	221	Λ 45%, Φ 18%, Z 14%
	151	137	Λ 49%, Φ 38%
		89	ω 38%, Z 16%, M 14%
		40	Zx 76%
		19	ω 30%, M 25%, Λ 17%, Zx 11%
		11	τ 82%

Table 2-6. Continued from previous page

ν obs. IR	ν obs. Raman	ν calc.	Potential energy distribution
B_2 mode (IR $\perp$)			
3104		3062	Sx 99%
3084		3053	Sx 99%
3062	3056	3050	Sx 98%
3028	3039	3046	Sx 98%
3003	3003	3045	Sx 98%
2925		2924	d 92%
2908	2905	2903	S 92%
2849	2850	2849	d 99%
1602	1599	1602	T 69%, Ω 18%
1584	1589	1592	T 72%, Ω 16%
1494	1491	1512	ϕ 52%,T 37%
1453	1450	1457	δ 88%
		1446	ϕ 56%,T 35%
1378	1374	1361	w 34%, ξ 25%,R 19%
1330	1338	1336	ϕ 59%,T 39%
1320		1316	ϕ 28%, ξ 24%,T 20%,w 12%
1278		1288	Rx 28%, Ω 23%, ϕ 16%,T 16%
		1252	t 57%,w 15%
	1248	1245	Ω 44%, ξ 22%
		1218	ξ 60%,t 14%
	1202	1203	ϕ 66%, Ω 20%
1182	1180	1165	ϕ 73%,T 23%
1155	1154	1133	T 33%, ϕ 23%,Rx 11%
1070	1070	1069	R 47%,t 15%
1029	1030	1049	T 47%, ϕ 25%
1003	1001	1008	T 74%, ϕ 18%
978	990	993	μ 63%,Z 28%
967		977	R 48%,T 10%
935	930	938	r 27%,T 25%,R 17%
908	901	872	μ 92%
842	838	836	μ 87%
778		782	Ω 30%,Rx 17%, ϕ 17%,T 14%,r 13%
750	756	751	μ 99%
	740	740	Ω 72%, ϕ 19%
698	701	700	μ 97%
621	620	631	Ω 41%, ϕ 13%,r 13%
548		542	Λ 28%,Z 23%, μ 15%
502		512	Λ 27%,Z 22%, Φ 12%
347	310	362	Z 68%, Λ 15%
		279	Z 98%
232	238	244	Λ 44%,Z 16%, Φ 16%
	217	200	Λ 38%, Φ 32%,R 16%
	151	149	Λ 41%,Z 25%, Φ 17%
		99	ω 33%, τ 20%
		41	Zx 83%
		26	M 28%, ω 23%,Zx 12%
		9	τ 57%, ω 22%

Table 2-6. Continued from previous page

ν obs. IR	ν obs. Raman	ν calc.	Potential energy distribution
B_3 mode	(IR ‖)		
3104	3056	3062	Sx 99%
3084	3039	3053	Sx 99%
3062		3050	Sx 98%
3028		3046	Sx 98%
3003	3003	3045	Sx 98%
2925	2905	2925	d 88%,S 11%
		2921	d 99%
2908		2903	S 88%
1602	1599	1602	T 69%, Ω 18%
1584	1579	1592	T 72%, Ω 16%
1494	1491	1512	ϕ 53%,T 36%
		1446	ϕ 55%,T 35%
1354	1354	1379	w 35%,R 24%, ξ 20%
		1336	ϕ 58%,T 41%
		1318	ξ 26%, ϕ 15%,w 13%,Rx 11%
		1305	ϕ 25%,w 25%,T 21%
1278		1263	Ω 28%, ξ 19%,w 18%
		1258	ξ 36%, Ω 22%,w 17%
		1234	ξ 31%,w 24%, Ω 16%, ϕ 10%
	1202	1203	ϕ 66%, Ω 21%
1182	1180	1165	ϕ 73%,T 22%
1155	1154	1138	R 30%,T 16%, ϕ 13%
1070	1070	1122	T 25%, ϕ 15%,R 14%, ξ 13%
1040	1052	1055	T 31%,R 22%, ϕ 18%
1030	1030	1020	R 38%,T 27%
1003	1001	1008	T 74%, ϕ 18%
978	990	992	μ 67%,Z 30%
947		959	R 29%,T 23%,r 16%
908	901	872	μ 92%
		862	r 74%
842	838	836	μ 87%
768	767	783	Ω 33%,Rx 19%, ϕ 18%,r 11%
750	756	751	μ 99%
	744	740	Ω 72%, ϕ 19%
698	701	701	μ 97%
621	620	612	Ω 35%, ϕ 16%,r 14%
572	534	546	Z 28%, μ 20%, Λ 17%
538		527	μ 22%, Φ 11%
405	406	390	Z 53%, Λ 34%
		280	Z 90%
		276	Z 50%, Λ 34%
232	238	223	Λ 44%, Φ 25%
		198	Λ 45%, Φ 34%
		64	Zx 35%,M 29%,Z 15%, τ 13%
		58	Zx 63%,M 15%
		22	τ 83%,Zx 13%
		14	τ 83%

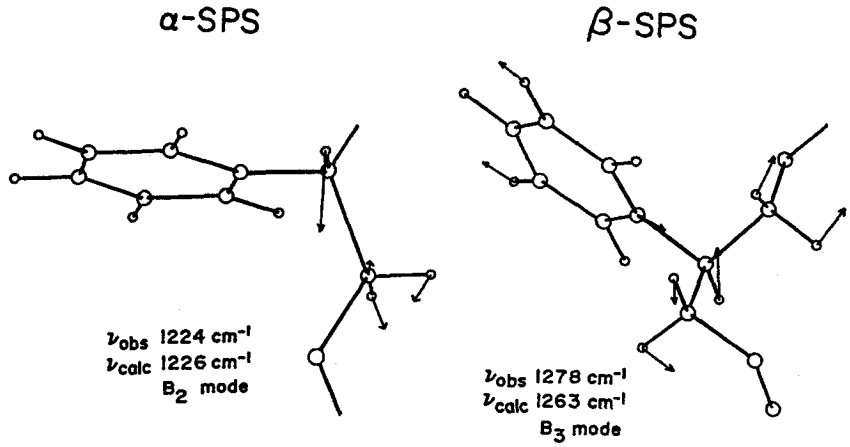

Figure 2-12. Cartesian displacement coordinates of α- and β-SPS (1200-1300 cm^{-1}).

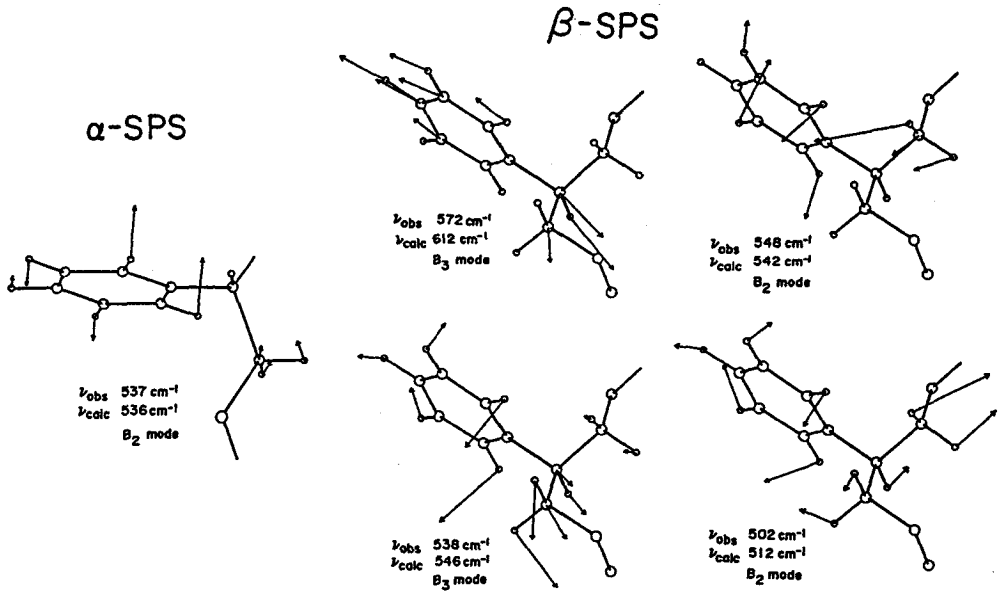

Figure 2-13. Cartesian displacement coordinates of α- and β-SPS (500-600 cm^{-1}).

This result will be used as a criterion to determine what the conformational structure of SPS is in various states.

References

1) G. Natta, P. Pino, P. Corradini, F. Danusso, E. Mantica, J. Am. Chem. Soc., 77, 1700 (1955).

2) G. Natta, F. Danusso, G. Moraglio, Makromol. Chem., 28, 166 (1958).

3) G. Natta, F. Danusso, I. W. Bassi, Nuovo Cimento, Suppl., 15, 68 (1960).

4) H. Tadokoro, S. Nozakura, T. Kitazawa, Y. Yasuhara, S. Murahashi, Bull. Chem. Soc. Jpn., 32, 313 (1959).

5) M. Kobayashi, Bull. Chem. Soc. Jpn., 33, 1416 (1960).

6) M. Kobayashi, Bull. Chem. Soc. Jpn., 34, 56 (1961).

7) M. Kobayashi, Bull. Chem. Soc. Jpn., 34, 1045 (1961).

8) T. Onishi, S. Krimm, J. Appl. Phys., 32, 2320 (1961).

9) B. Jasse, R. S. Chao, J. L. Koenig, J. Raman Spectrosc., 8, 244 (1979).

10) P. C. Painter, J. L. Koenig, J. Polym. Sci., Polym. Phys. Ed., 15, 1885 (1977).

11) R. W. Snyder, P. C. Painter, Polymer, 22, 1629 (1981).

12) R, W, Snyder, P. C. Painter, Polymer, 22, 1633 (1981).

13) N. Ishihara, T. Seimiya, M. Kuramoto, M. Uoi, Macromolecules, 19, 2464 (1986).

14) N. Ishihara, M. Kuramoto, M. Uoi, Macromolecules, 21, 3356 (1988).

15) G. Natta, I. Pasquon, P. Corradini, M. Peraldo, M. Pegoraro, A. Zambelli, Atti. Acad. Nazl. Lincei, Rend, **28**, 539 (1960).

16) G. Natta, P. Corradini, P. Gannis, P. A. Temmussi, J. Polym. Sci., Part C, **16**, 2477 (1967).

17) G. Natta, M. Peraldo, G. Allegra, Makromol. Chem., **75**, 215 (1964).

18) H. Tadokoro, M. Kobayashi, S. Kobayashi, K. Yasufuku, K. Mori, Rep. Prog. Polym. Phys. Jpn., **9**, 181 (1966).

19) G. Natta, P. Corradini, P. Ganis, Makromol. Chem., **39**, 238 (1960).

CHAPTER 3

Crystal modifications and molecular structures of Syndiotactic Polystyrene

3-1. Introduction

After the success in stereospecific polymerization of syndiotactic polystyrene (SPS) having extremely high degree of stereoregularity,[1] many investigators in the world started their studies for revealing structures, physical and chemical properties, and industrial functionalities of this interesting new material.[2-8]

As for the molecular structures of SPS, we have demonstrated that there are two stable skeletal conformations in the crystalline state ; the all trans (TT) and the trans-trans-gauche-gauche (TTGG) forms.[9] In addition to the molecular conformation, difference in the molecular packing causes a complicated polymorphism of SPS. At present at least five different crystal modifications are reported.

In this chapter, we are concerned with characterization of crystal modifications by means of X-ray diffraction and the change in crystal modification on solid-state phase transition.

3-2. Experimental

3-2-1. Samples

The SPS sample with the weight average molecular weight 15×10^4 was supplied by Idemitsu Petrochemical Co. Ltd.
The film specimens of various crystal modifications were obtained by the following procedures :

(1) α_1-form : Films cast from chloroform solution were annealed at 200°C.

(2) α_2-form : Melt-quenched glassy films were annealed at 200°C.

(3) β_1-form : Films cast from chloroform solution were dried at 150°C.

(4) β_2-form : Melt-quenched glassy films were exposed in chloroform vapor and then annealed at 150°C.

(5) γ-form : As-cast films were prepared from chloroform, toluene, o-xylene, or 1,2,4-trichlorobenzene solutions.

These samples were subjected to X-ray diffraction and FT-IR measurements.

The lamellar-shaped single-crystals of SPS for the electron microscope observation were grown from a 0.3 w/v% solution of n-tetradecane/decalin (2:1) kept at 180°C for a day.

3-2-2. Measurements

Infrared spectra (with 1 cm^{-1} resolution) were taken using a JASCO FT-IR 8000 spectrometer equipped with a DTGS detector.

X-ray diffraction powder patterns were obtained using a Rigaku RAD-ROC diffractometer with a graphite-monochromatized Cu-Kα radiation.

Electron microscope (EM) observation and electron diffraction measurement were made using a Hitachi HU-12A transmission EM apparatus operated at 100 kV.

3-3. Results and Discussion

3-3-1. Polymorphism

Among the five modifications mentioned above, the α_1 and α_2 forms consist of the molecules assuming the TT conformation. Both modifications give rise to the essentially the same infrared spectra. On the contrary, the X-ray diffraction patterns of α_1 and α_2 are quite different from each other as shown in Figure 3-1. Preliminary results of the crystal structures of α_1 and α_2 were reported by Chatani's group (by X-ray diffraction)[2] and Greis et al. (by electron diffraction),[5] respectively. The crystal systems and the unit cell dimensions are summarized in Table 3-1. The positions of the reflections shown in Figure 3-1 are consistent with the reported until cell dimensions. The fine precipitates deposited from dilute solution of n-tetradecane/decalin (2:1) at 180°C has a thin hexagon shape under the view of bright-field electron micrograph. (Figure 3-2). This is recognized as a single-crystal which gives rise to the electron diffraction pattern shown in Figure 3-3. The diffraction indicates that the crystal is the α_1 form with the a=28.8 A and b=9.0 A, both being located parallel to the lamellar surface.

Greis et al.[5] reported that single-crystals of the α_2 form were obtained by annealing a thin film cast from a dilute o-xylene solution at 200°C for 5 min onto hot orthophosphoric acid. We tried to prepare the α_2 single-crystal by the same way. Although similar electron diffraction pattern was obtained, the unit cell dimensions measured from it were quite different from the reported ones.

The β_1 and β_2 forms consist of the molecules of the TTGG conformation. There is no detectable difference in infrared and

Table 3-1. Crystallographic data of α_1 form[2] and α_2 form.[5]

	α_1	α_2
crystal system	orthorhombic	hexagonal
a /A	28.82	26.26
b /A	8.81	–
c /A	5.06	5.04

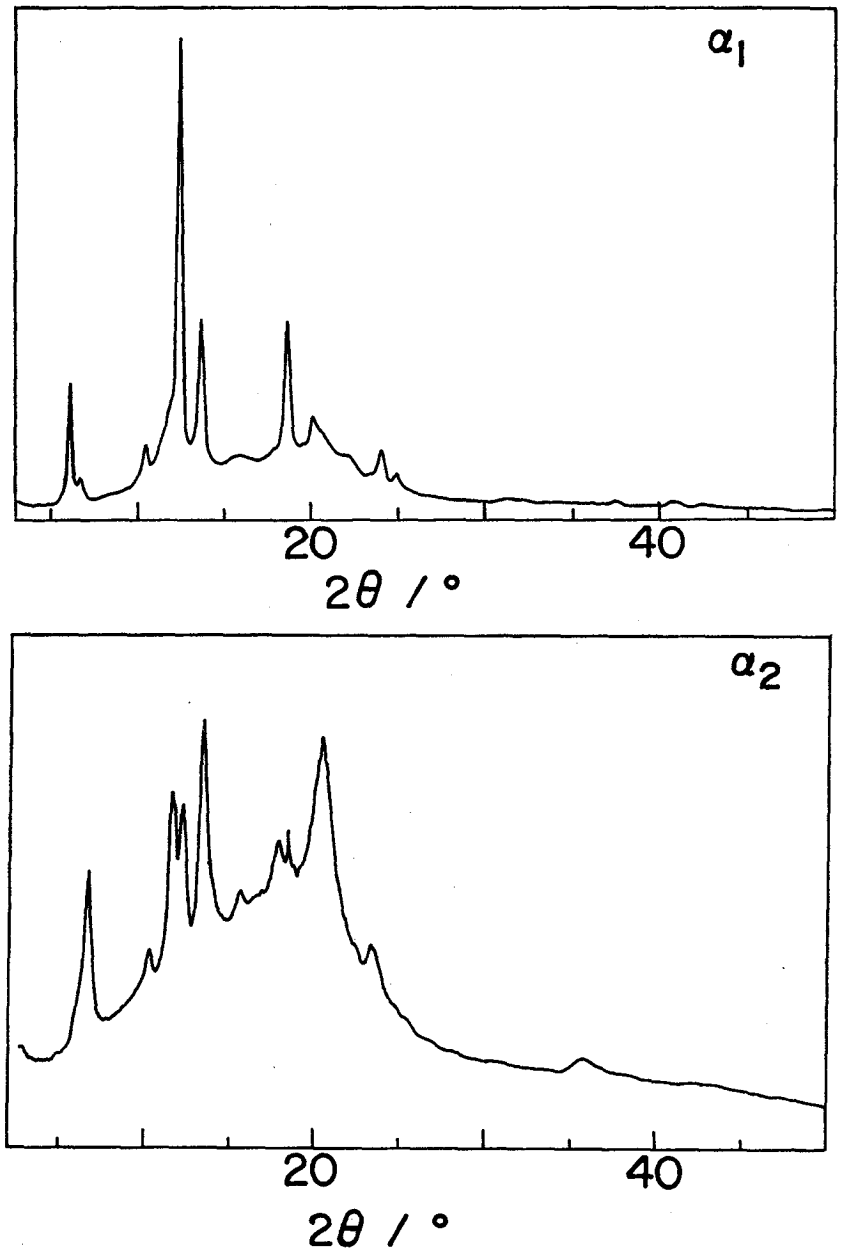

Figure 3-1. X-ray diffraction patterns of TT-SPS (unoriented).

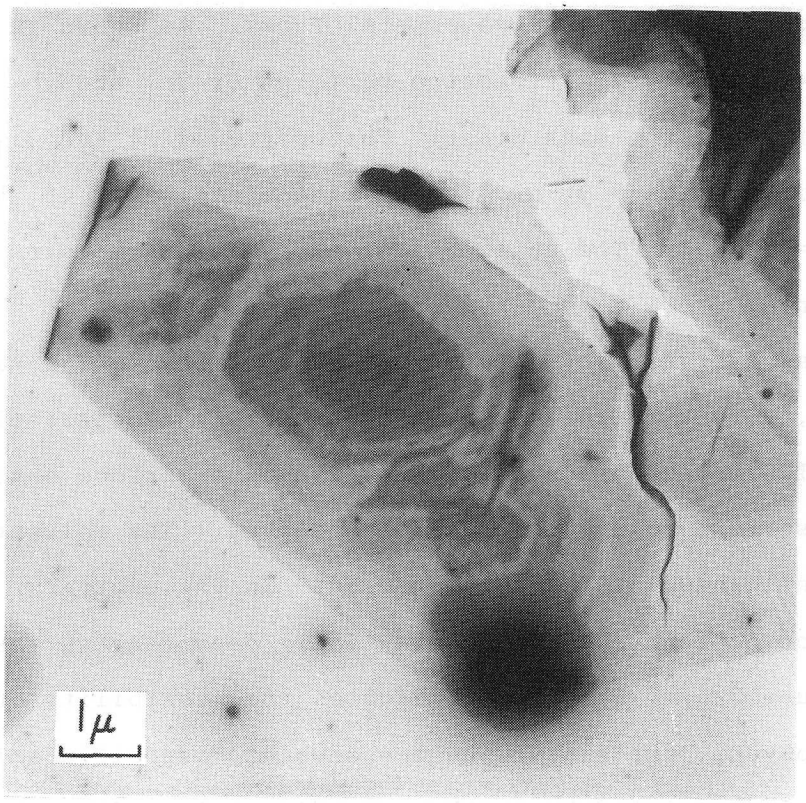

Figure 3-2. Electron micrograph of a single crystal of α_1-SPS grown at 180°C from decalin/n-tetradecane (1:2) solution.

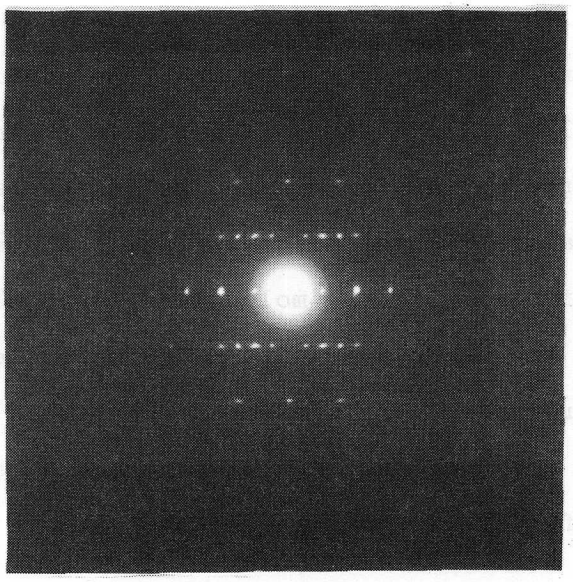

Figure 3-3. Electron diffraction pattern of α_1-SPS.

Raman spectra between the two crystal forms. As shown in Figure 3-4, the X-ray diffraction patterns of β_1 and β_2 are quite different from each other. The unit cell of the β_1 form was determined by Chatani et al.[8] to be monoclinic [a=17.48, b=13.27, c (f. a.)=7.71 A]. The unit cell of the β_2 form remains undetermined.

The as-cast films (γ-form) of SPS (obtained using various solvents), give rise to the infrared spectra characteristic of the regular TTGG molecular conformation. The absorptions associated with the solvent molecules are also observed. The polymer bands are not influenced by the solvent used. On the contrary, the X-ray diffraction pattern changes substantially depending on the solvent used (Figure 3-5). This fact indicates the possibility of forming polymer-solvent complexes. The presence of a specific solvated structure is supported by another experimental result. Figure 3-6 showed the polarized infrared spectra taken on an oriented SPS film moistened with benzene. The polymer bands at 572, 548 and 502 cm^{-1} which are characteristic of the TTGG conformation show clear parallel polarization. The 676 cm^{-1} band due to an out-of-plane CH deformation of the benzene molecule also exhibit definite parallel polarization. This indicates that the adsorbed benzene molecules are oriented with the molecular planes align nearly perpendicular to the chain axis of the SPS molecule. In electron micrograph, unfortunately the crystal morphologies of the β and γ forms are not decided, because of the very small crystallite size and the suffering of radiation damage.

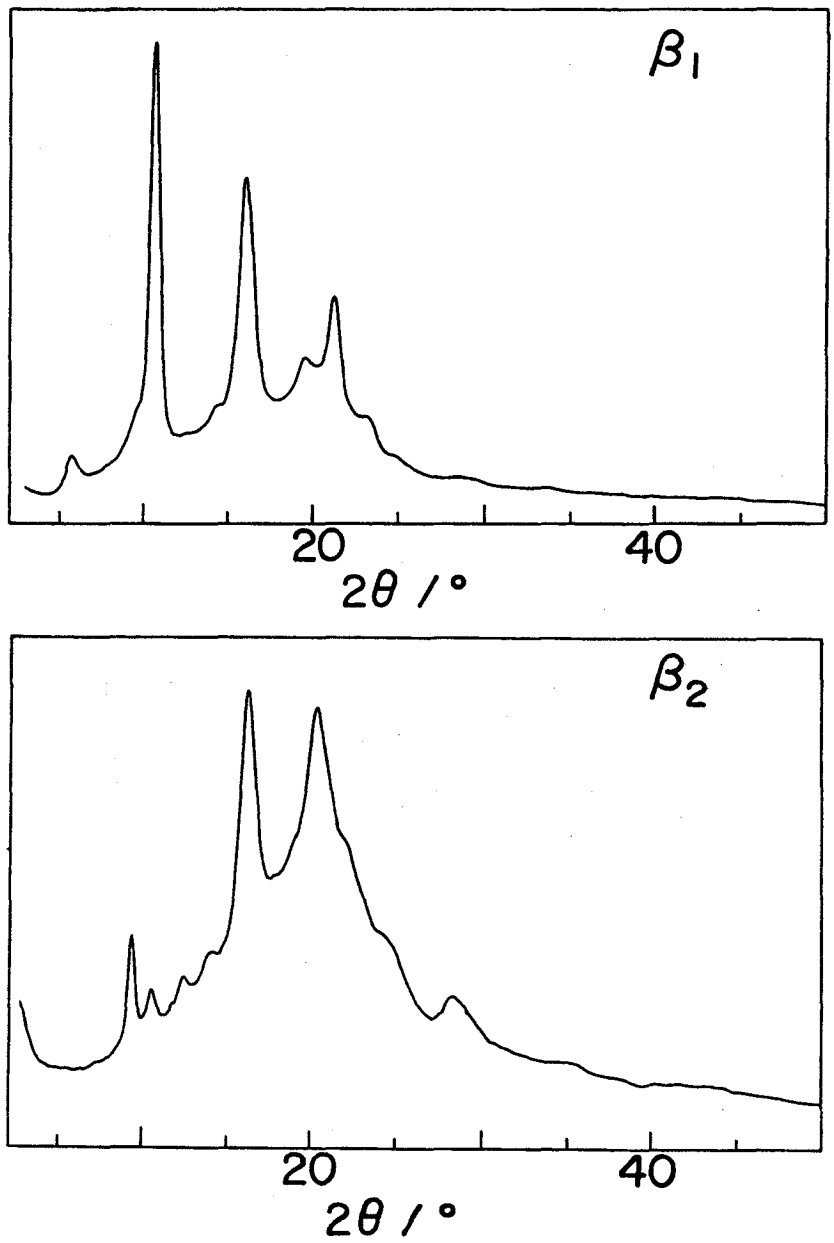

Figure 3-4. X-ray diffraction patterns of TTGG-SPS (unoriented).

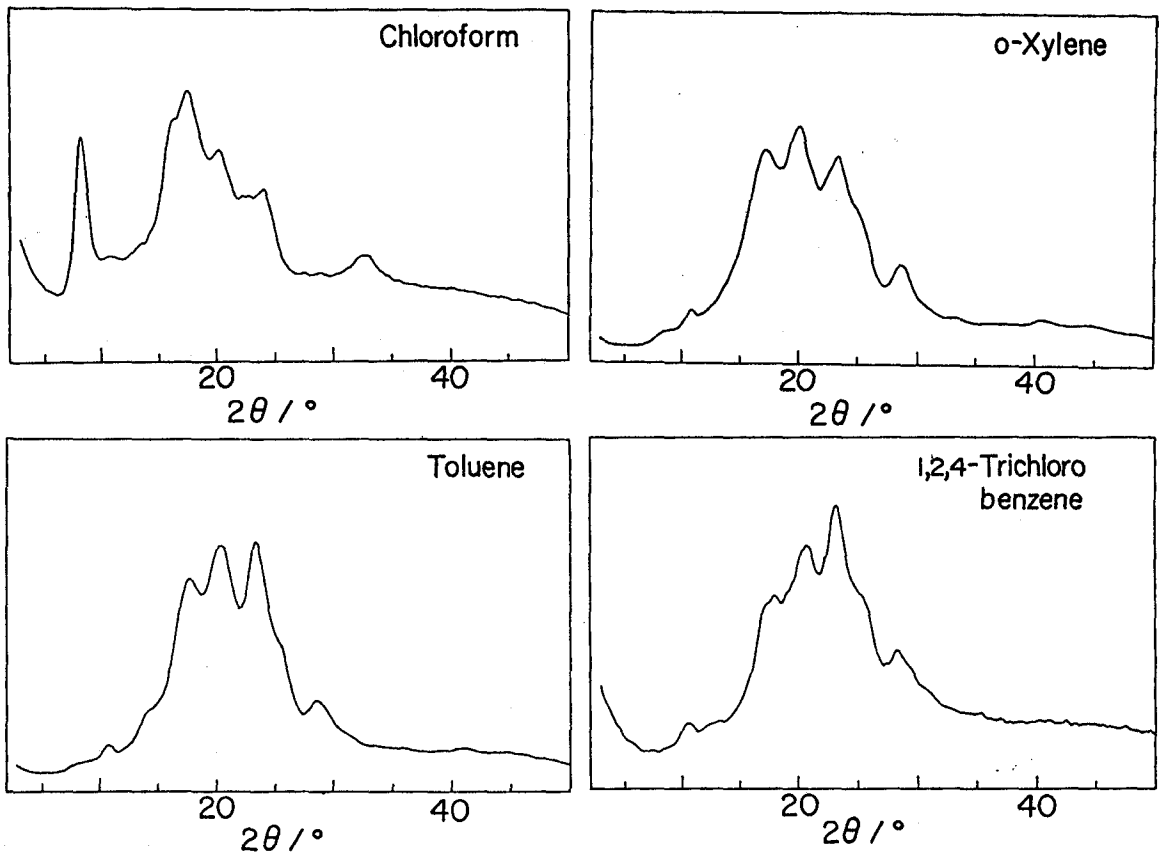

Figure 3-5. X-ray diffraction patterns of γ -SPS.

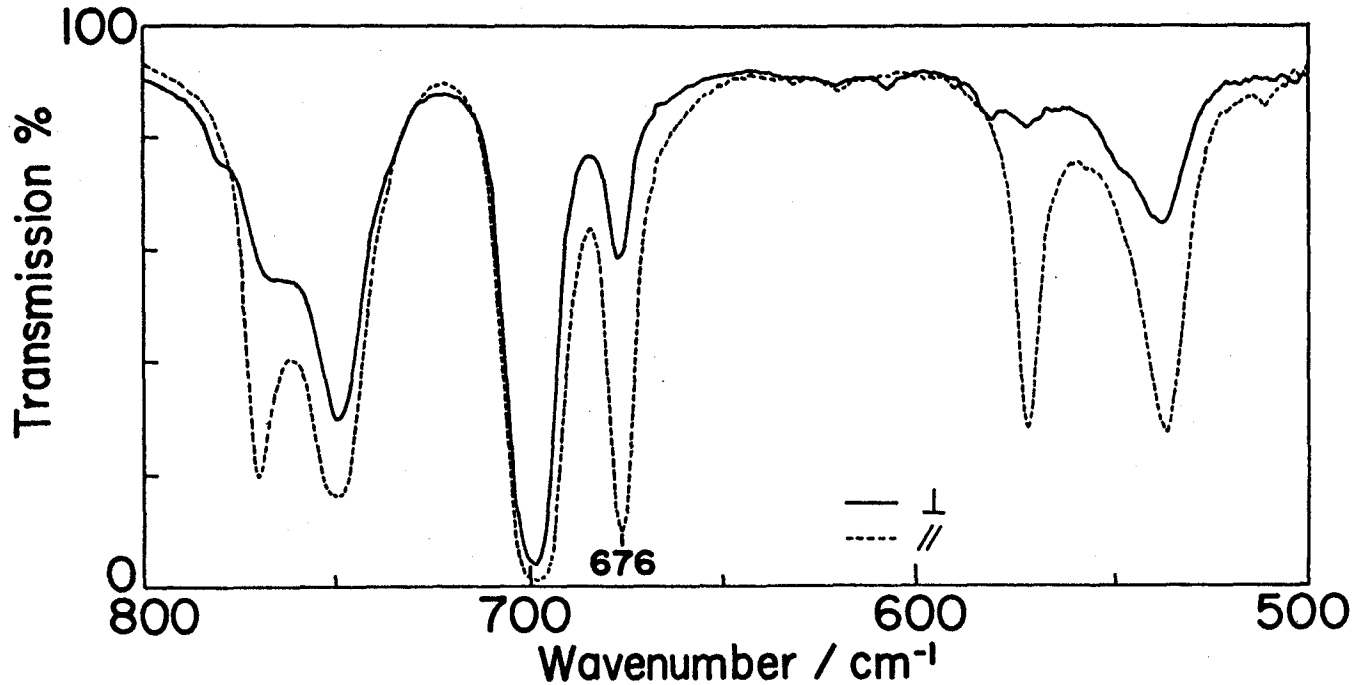

Figure 3-6. Polarized infrared spectra of uniaxially oriented film of γ-SPS moistened with benzene. The 676 cm^{-1} band due to benzene shows a definite parallel polarization.

3-3-2. Phase transition

Thermogram of an SPS/chloroform as-cast film on heating is shown in Figure 3-7. There appears a small endothermic peak at 121°C, followed by broad endotherms around 160°C, and finally a large melting peak at 246°C. The heating process was followed by infrared spectrum (Figure 3-8). With increasing temperature the 1220 cm^{-1} band due to chloroform decreases in intensity and disappears above 120°C. This corresponds to the first endothermic peak in the thermogram. It is noted that the solvent molecules are accommodated in the sample until the temperature 60°C higher than its boiling point (61.2°C). The stage until 120°C corresponds to the removal of the solvent molecule from γ-phase. The conformational change of the SPS molecules during this process is followed in more detail by the infrared spectral change in the 500-600 cm^{-1} range (Figure 3-9). The absorption profile in this region was separated into five Lorentzian components and the integrated intensity of each band was plotted against temperature (Figure 3-10). On heating, the 571 and 548 cm^{-1} bands characteristic of the TTGG conformation decreases in intensity up to 100°C. This indicates that the TTGG conformation stabilized by the solvent molecule, is partly disordered. The temperature dependence of X-ray diffraction is identical with the result of infrared and DSC measurements as shown in Figure 3-11. The γ phase at room temperature gives rise to a rather diffuse diffraction pattern. Below and above 120°C, the diffraction patterns are significantly different, indicating that the sample is converted to the β phase. Above 190°C, it transforms to α_2 form. When

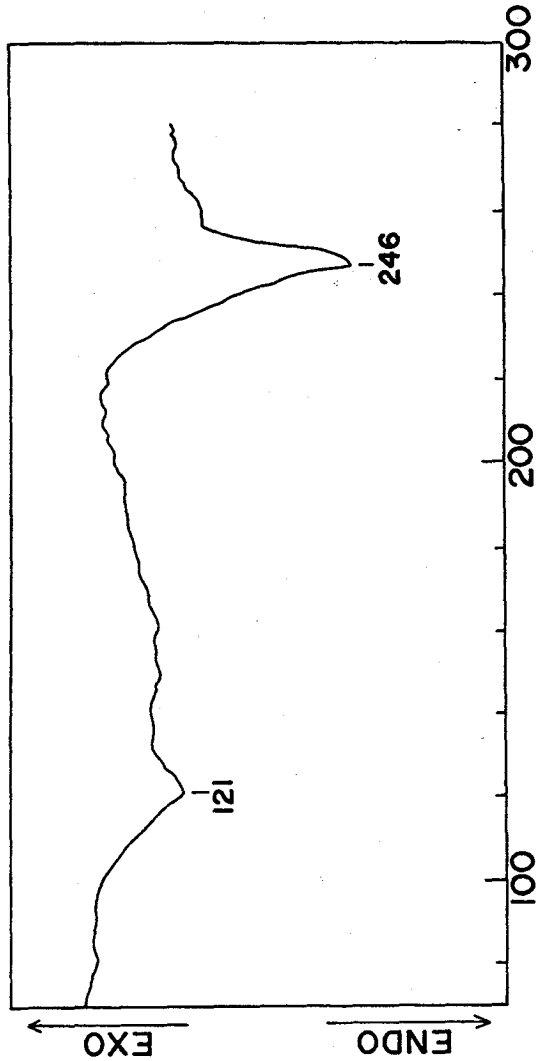

Figure 3-7. DSC thermogram of a SPS film cast from chloroform solution.

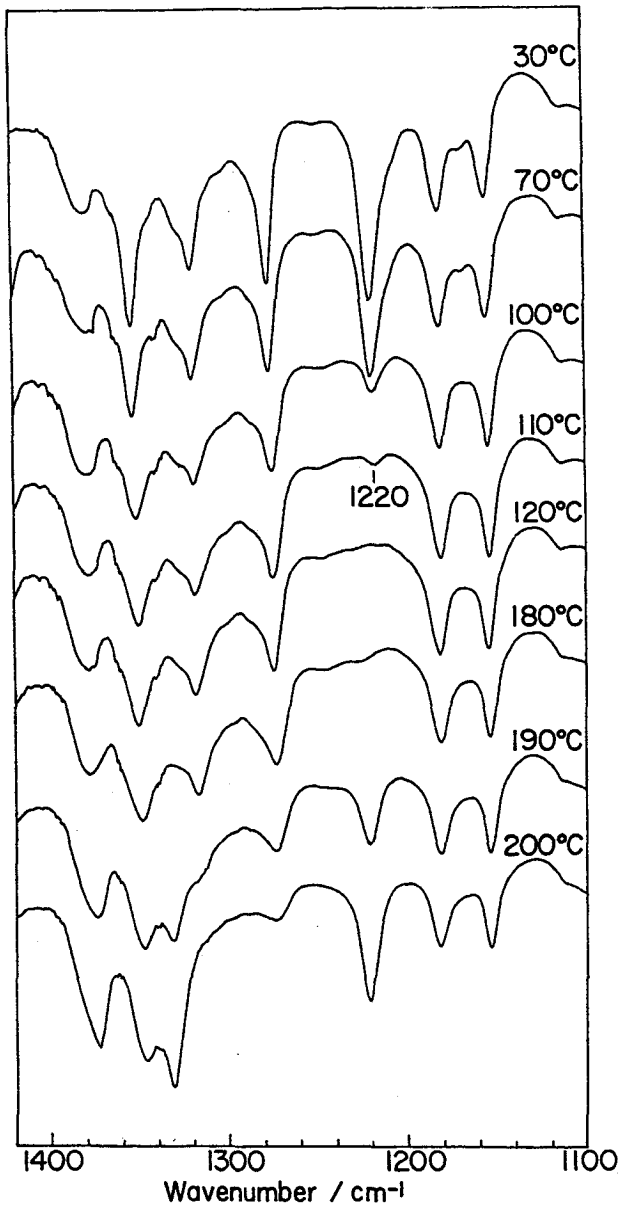

Figure 3-8. Infrared spectral change on a heating process of γ-SPS. The 1220 cm^{-1} band below 110°C is due to chloroform.

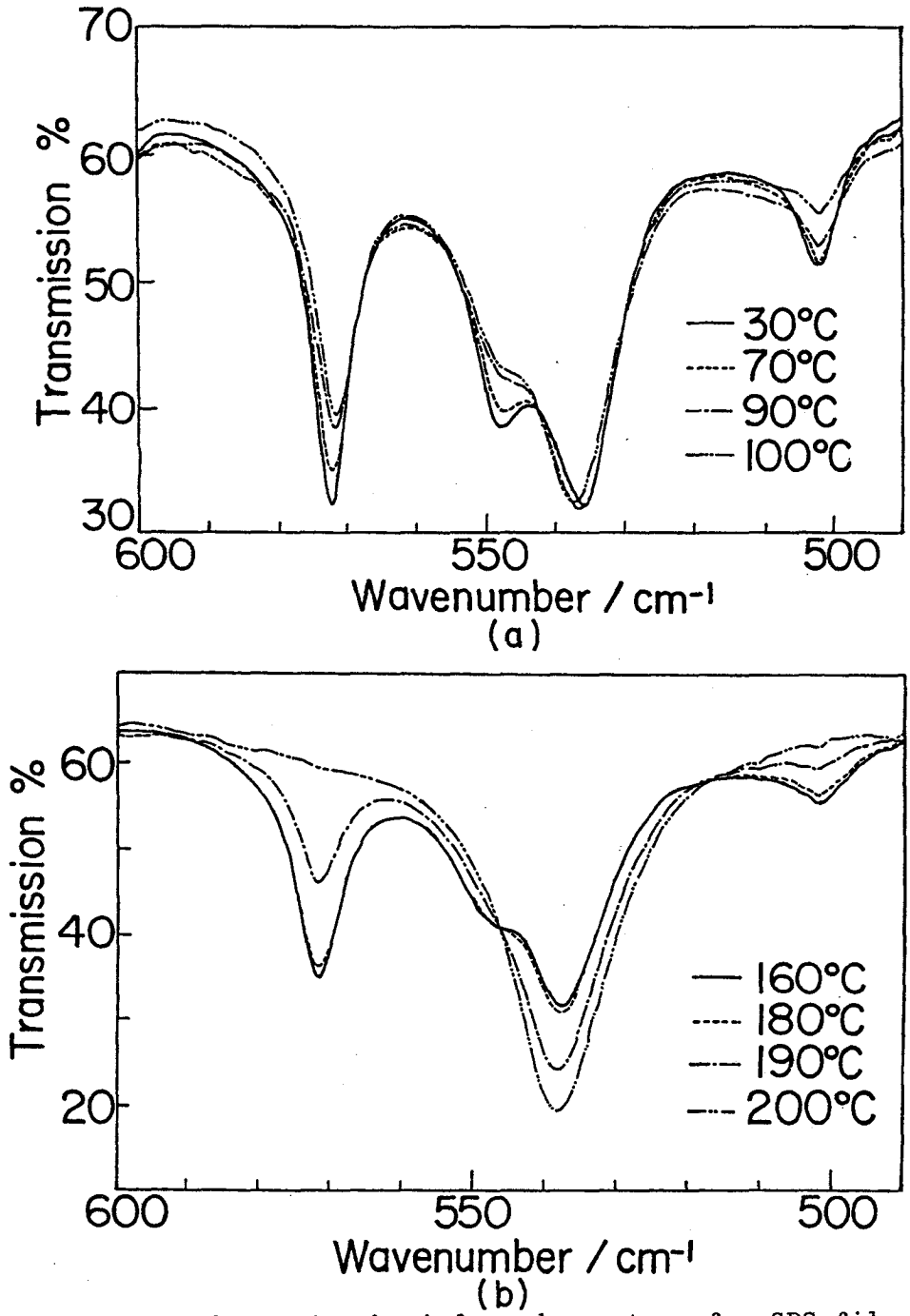

Figure 3-9. Change in the infrared spectra of a SPS film cast from chloroform solution during annealing ; (a) 30-100°C, transition from the γ to β phase; (b) 160-200°C, transition from the β to α phase.

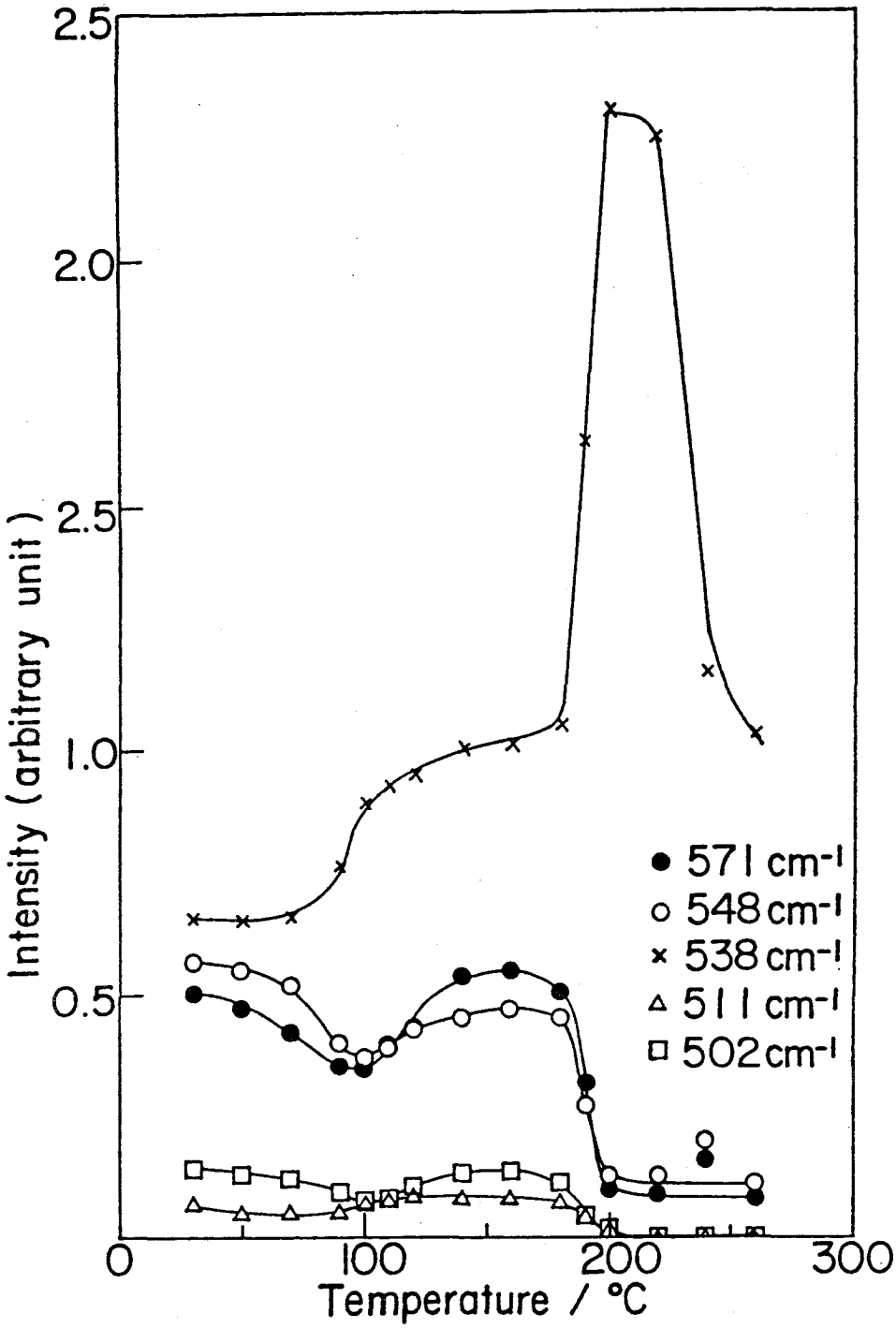

Figure 3-10. Changes in the integrated intensities of the bands characteristic of the local conformation during annealing of a SPS film cast from chloroform solution.

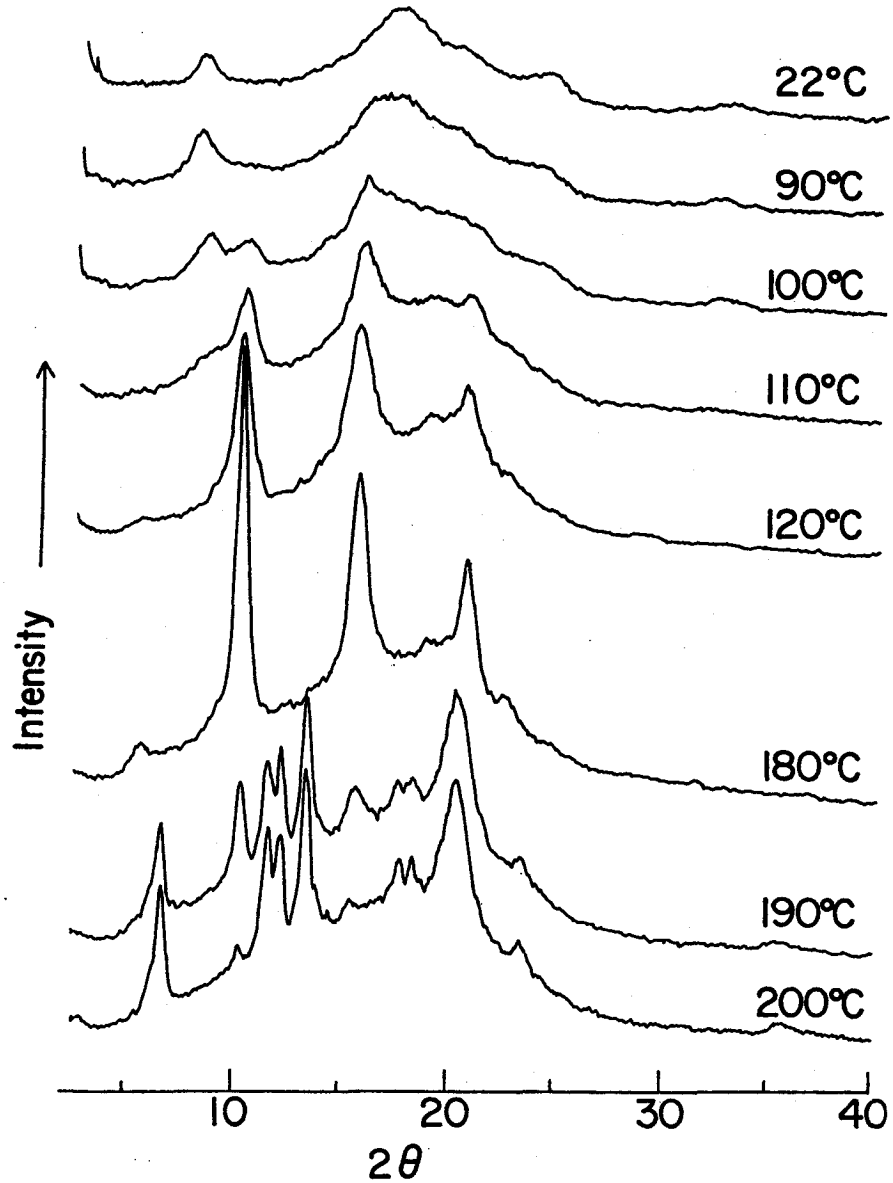

Figure 3-11. The change of X-ray diffraction pattern on a heating process of γ-SPS.

cast films are annealed at 200oC, the α_1 form is obtained in most cases, as described in Section 3-2-1. However in this heating process the α_2 form is produced. Therefore, the heating rate might take some part in the formation of different polymorphs of the α type.

References

1) N. Ishihara, T. Seimiya, M. Kuramoto, M. Uoi, Macromolecules, 19, 2464 (1986).
2) Y. Chatani, Y. Fujii, Y. Shimane, T. Ijitsu, Polym. Prep. Jpn. (Engl. Ed.), 37, E428 (1988).
3) A. Immirzi, F. de Candia, P. Ianneli, A. Zambelli, V. Vittoria, Makromol. Chem., Rapid Commun., 9, 761 (1988).
4) V. Vittoria, F. de Candia, P. Ianneli, A. Immirzi, Makromol. Chem. Rapid Commun., 9, 765 (1988).
5) O. Greis, Y. Xu, T. Asano, J. Petermann, Polymer, 30, 590 (1989).
6) G. Guerra, V. M. Vitagliano, C. De Rosa, V. Petraccone, P. Corradini, Macromolecules, 23, 1539 (1990).
7) P. Pradere, E. L. Thomas, Macromolecules, 23, 4954 (1990).
8) Y. Shimane, Y. Inoue, T. Inagaki, T. Ishioka, Y. Chatani, Polym. Prep. Jpn., 39, 3917 (1990).
9) M. Kobayashi, T. Nakaoki, N. Ishihara, Macromolrecules, 22, 4377 (1989).

CHAPTER 4

Gelation Mechanism and Structure in Gels of Syndiotactic Polystyrene

4-1. Introduction

During the recent decade interests in gels of synthetic polymers are growing from the scientific and industrial points of view. Systems of polystyrene dissolved in various organic solvents form thermoreversible physical gels. The most interesting point of the polystyrene gels is that kinetic behaviors of gelation as well as physical properties of the resultant gel are strongly influenced by the stereoregularity of the polystyrene sample and the solvent used. Therefore, elucidation of the role of the stereostructure of polystyrene in the gel-forming process is the fundamentally important task in order to clarify the whole scope of polystyrene gels. In chapters 4-6, we deal with the molecular mechanism of gelation and the structure formed in gels for syndiotactic, isotactic and atactic polystyrenes. In this chapter, the gelation process of SPS/o-dichlorobenzene systems are followed by FT-IR spectroscopy and differential scanning calorimetry (DSC). We will focus our attention mainly to the ordered molecular conformation formed on gelation and to the role of solvent molecule in the formation of cross-links. We are also concerned with the correlation between the competitive processes of crystallization and gelation that occur on cooling polymer solutions. Finally, preliminary results of our recent experiments of small angle neutron scattering (SANS) of SPS/o-dichlorobenzene

gels are presented in relation to the dimension of the cross-linking coagurates.

4-2. Experimental

4-2-1. Samples

The SPS samples used were supplied from Idemitsu Petrochemical Co. Ltd. The weight averaged molecular weights were measured by GPC as $7x10^4$, $15x10^4$ and $113.5x10^4$. The tacticities measured by ^{13}C-NMR were in the order of 96% racemic pentad configuration. The solvents (chloroform, carbon tetrachloride, benzene, o-dichlorobenzene etc.) of the commercial source (spectral pure grade) were used without further purification.

4-2-2. Measurements

DSC measurements were performed using a Seiko Model 20. About 15 mg of an SPS/solvent mixture put in a sealed pan was heated at 180°C for dissolving SPS, and then quenched in iced water and held at 0°C for 30 min. Thereafter, the first heating scan started at various heating rates.

Infrared spectra (with $1cm^{-1}$ resolution) were measured using a JASCO FT-IR 8000 spectrometer equipped with a DTGS detector. Spectra were accumulated 50 times to get the S/N ratio high enough for the data manipulation. A solution optical cell with a lead spacer of 100 μm thickness inserted between two KBr windows was constructed.

On cooling SPS solutions, gelation or precipitation

(crystallization) takes place depending on the solvent used. For example, o-dichlorobenzene solution forms gel (or microgel) at any polymer concentration, while decalin solution yields crystalline precipitates. The rates of isothermal gelation or crystallization at various temperatures were measured by the following way. An SPS/solvent mixture sealed in a glass tube was heated first to a certain temperature high enough to be kept as solution. Thereafter, the test tube was transferred in a thermostat held at a selected temperature, and the duration was measured until the gelation (by checking the fluidity of the solution on tilting the test tube) or the precipitation (by visible check of turbidity) started to occur.

SANS measurements were performed using the SANS diffractometer installed in the reactor (JRR-3M) of Tokai Research Establishment, Japan Atomic Energy Research Institute. The cold-neutron beam of 0.6 nm wavelength was used as the radiation source, and the scattered radiation was measured with a two-dimensional detector placed at 4.0 m from the sample. The available Q range was $0.03<Q<0.17 nm^{-1}$. The SPS/deuterated o-dichlorobenzene gel put in a drum-shaped quartz cell with the thickness of 2 or 5 mm (depending on the polymer concentration) were subjected to the SANS measurements.

4-3. Results and Discussion

4-3-1. Molecular conformation formed in SPS gels

For studying the conformation of the SPS molecules formed in solution or gel, FT-IR spectroscopy is very useful because by using

the subtraction technique the interference by the solvent absorptions can be removed and we are able to detect even small spectral changes of polymer molecules. In Figure 4-1, are compared the infrared spectra of SPS in three different states, (1) a chloroform solution (2) an SPS/chloroform gel at room temperature, and (3) a crystalline film of β-SPS.[1] In (1) and (2), the absorption due to chloroform is correctly subtracted, except for the frequency range of 1200-1250 and 650-800 cm^{-1} where the absorption is too strong to be correctly subtracted. It is noted that the gel and the crystalline β-form are very close to each other in the spectral feature, i.e., all the absorption bands characteristic of the TTGG conformation (marked with arrows) appear in both cases. On the contrary, these bands disappear or are substantially weakened in the solution. The main spectral feature of SPS gel are scarcely dependent on the solvent used as shown in Figure 4-2, although small difference are observed in the relative intensity of the bands.

It is generally believed that in physical gels of crystalline polymers, the cross-links are formed by crystallite-like coaguration of polymers.[2] As far as molecular conformation concerns, it is evident that regular sequences of TTGG conformation are formed in gel. It is even surprising that all the conformation-sensitive infrared bands, including even the 935 cm^{-1} band characteristic of long TTGG sequences, appear in gel with the intensities as strong as, or even stronger than, the case of crystalline β phase. For example, the intensities of the 779 and 769 cm^{-1} (TTGG) bands reduced to that of the internal standard band at 750 cm^{-1} (a

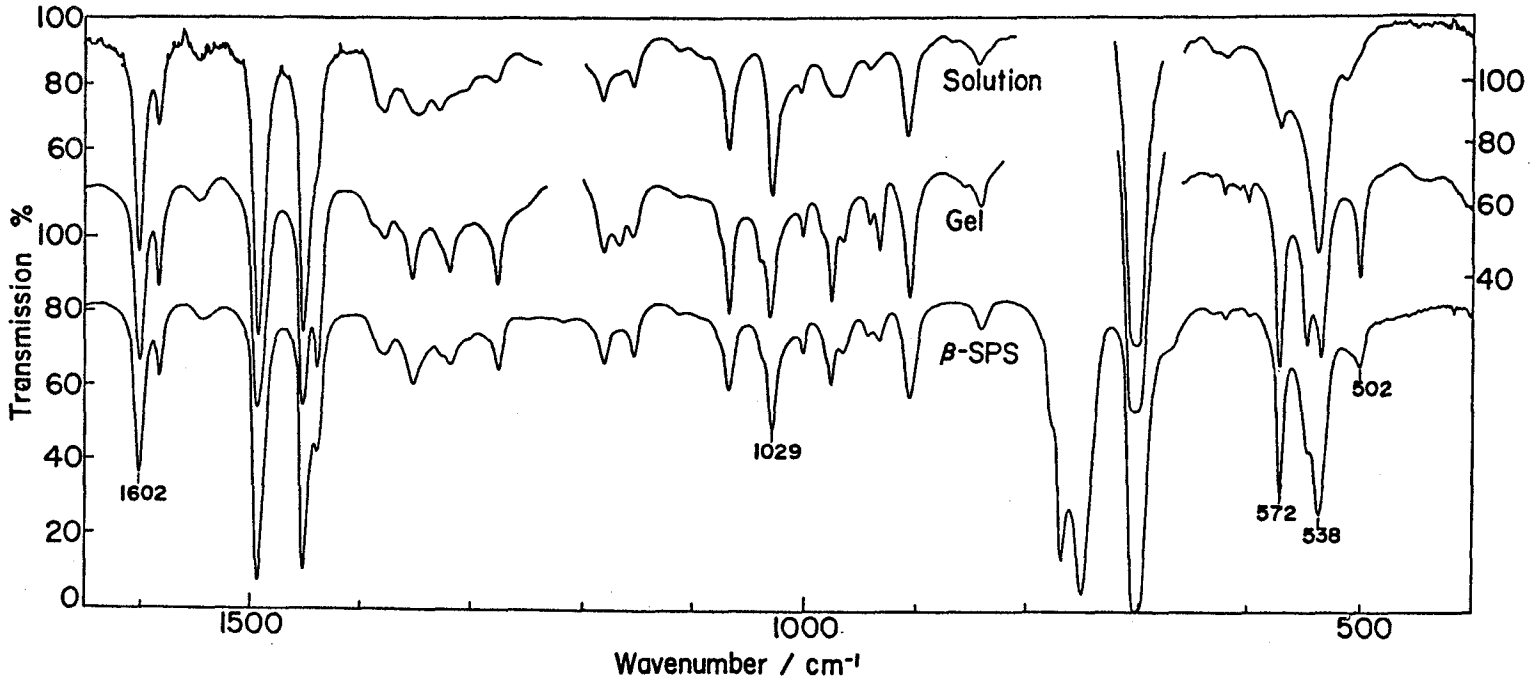

Figure 4-1. Infrared spectra of a chloroform solution (upper), a clear gel (middle), and crystalline β form (bottom) of SPS, measured at a room temperature.

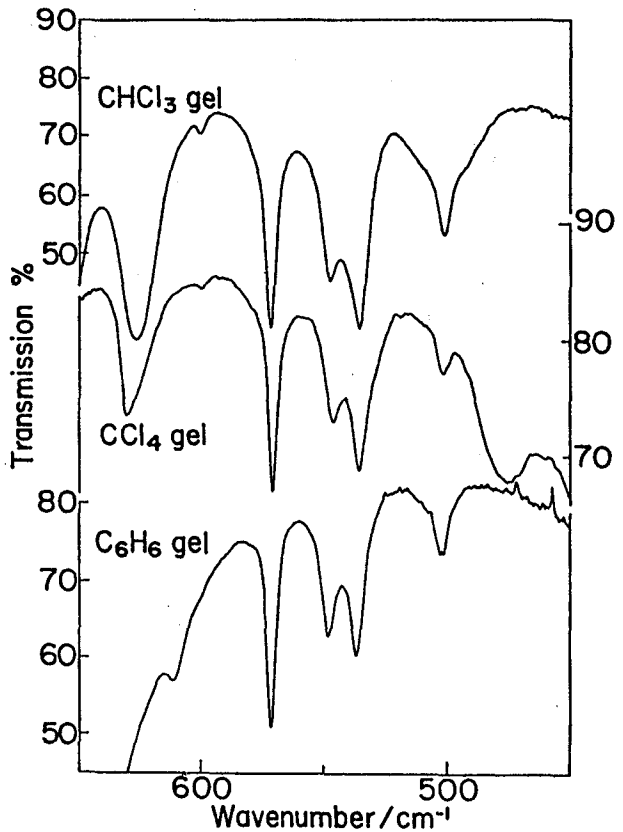

Figure 4-2. Infrared spectra of SPS gels formed from various solvents.

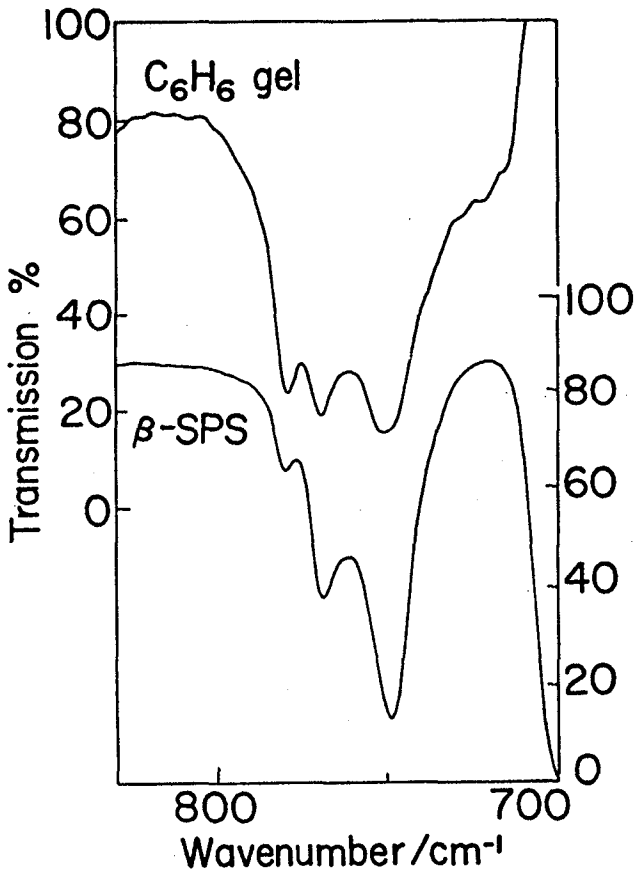

Figure 4-3. Infrared spectra of a clear gel formed from benzene solution (after subtraction of the solvent absorption) and crystalline β form of SPS.

localized C-H out-of-plane deformation of the phenyl ring) are much stronger in SPS/benzene gel than in β-SPS (Figure 4-3). From the observed spectral pattern consisting of the strong TTGG bands superimposed by a very weak background due to disordered conformations, we speculate a picture of SPS gels; i.e., most of the chain segments are accommodated in conformationally ordered parts which are joined each other by rather short disordered segments. Some parts of the ordered conformation might aggregate laterally through intermolecular cohesive forces, forming cross-links. The stability of such a specific regular conformation is considered to be attributed to strong polymer-solvent interactions as discussed below.

4-3-2. Phase diagram of SPS/o-dichlorobenzene

The SPS/o-dichlorobenzene system was chosen for the investigation of the phase diagram of SPS gels, because this system forms a stable gel and the boiling point of the solvent is high enough for measuring the process of sol-gel phase transition.

Figure 4-4 shows the typical DSC thermogram of the SPS/o-dichlorobenzene system (20 w/v%) measured at the heating and cooling rates of 20°C/min. There appears an endothermic peak around 120°C on heating and at 21°C on cooling. Thus, the hysteresis of the sol-gel transition is very large. The gel melting temperature is essentially independent of the molecular weight of SPS as shown in Figure 4-5. The gel melting process was followed by infrared spectroscopy as reproduced in Figure 4-6.

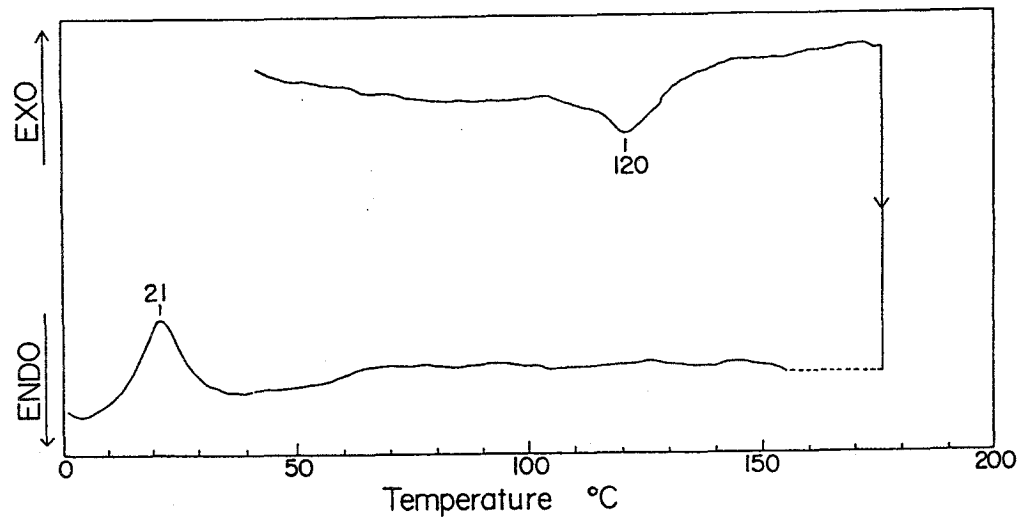

Figure 4-4. Thermogram of SPS/o-dichlorobenzene gel (20 w/v%) quenched at 0°C for 30 min.

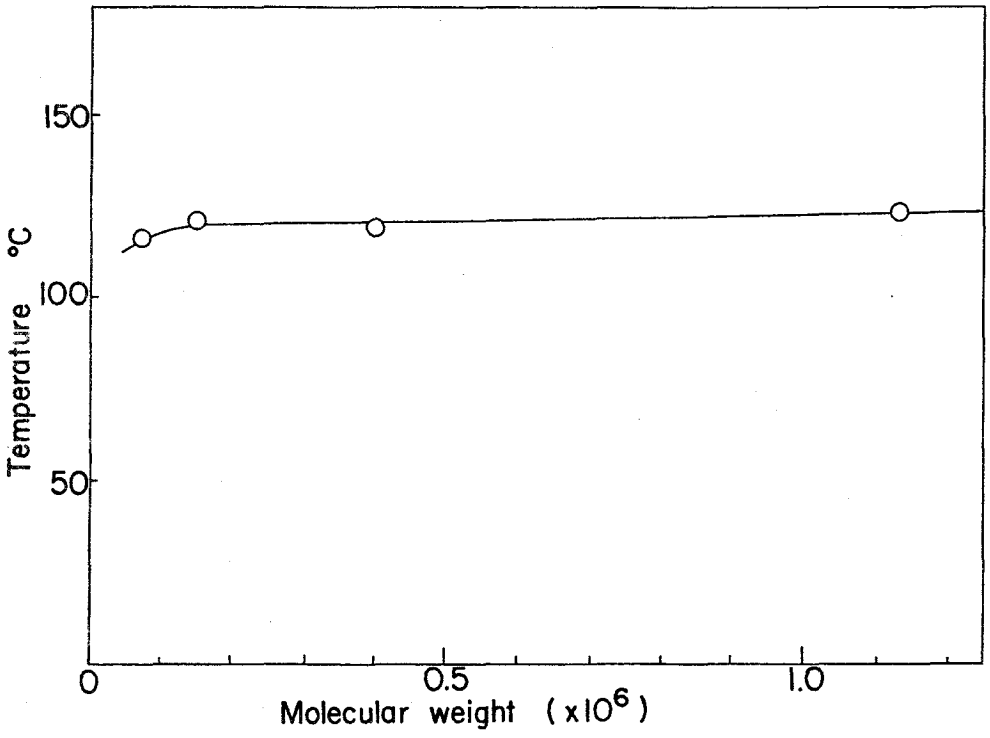

Figure 4-5. Gel melting temperature depending on molecular weight.

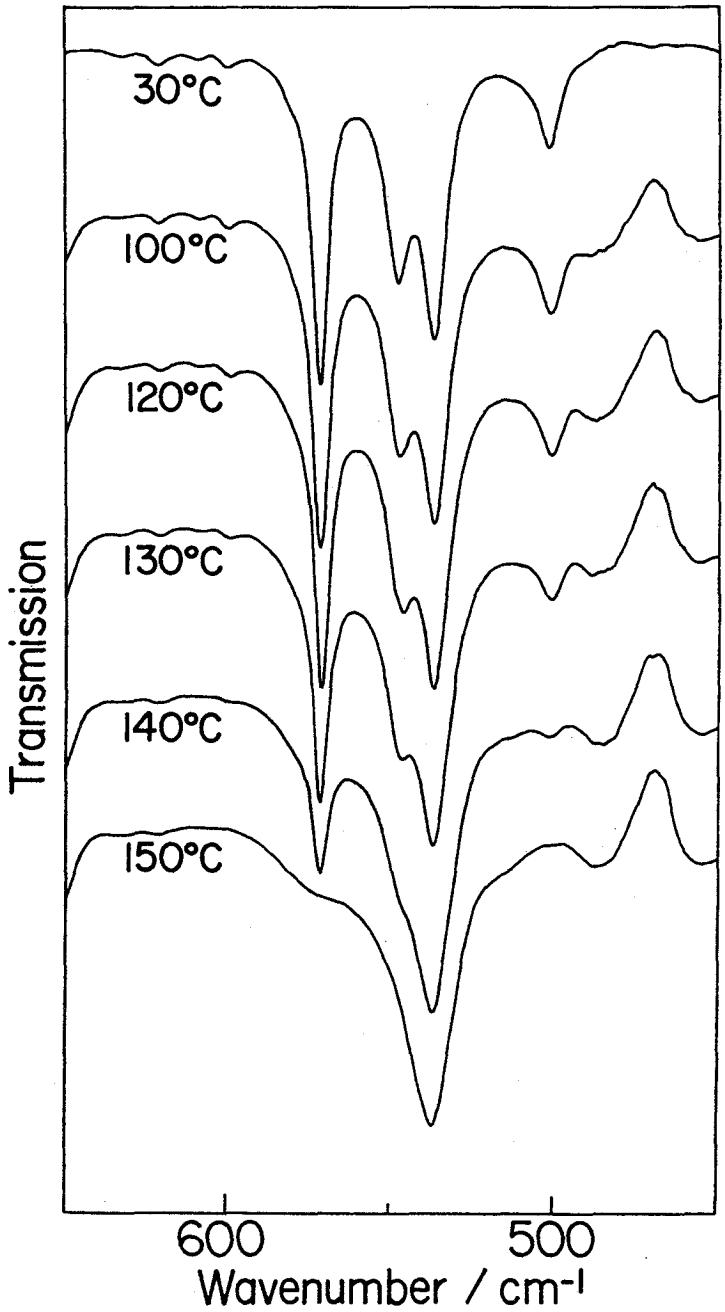

Figure 4-6. Infrared spectral change of SPS/o-dichlorobenzene on heating process.

The spectrum at room temperature is characterized by the appearance of the 572, 547 and 502 cm^{-1} bands due to the TTGG sequences. A sharp depression in intensity of these bands begins to occur at 120°C, corresponding to the melting of gel networks.

Figure 4-7 shows the gel-melting and the gel-forming temperatures of the SPS/o-dichlorobenzene system at various polymer concentrations measured by DSC as a function of the heating or cooling rate. In all cases the melting or forming temperatures vary linearly with the heating or cooling rate. The values extrapolated to zero rate were adopted to depict the temperature-concentration phase diagram as shown in Figure 4-8. The melting and forming temperatures increase monotonically with an increase in polymer concentration (Cp in g/g). The enthalpies of gel-formation ($\Delta H=H_{gel}-H_{sol.}$) measured for various polymer concentrations are plotted against the cooling rate in Figure 4-9. From the ΔH values extrapolated to zero cooling rate, the temperature-enthalpy relationship was obtained as shown in Figure 4-10. With increasing Cp, ΔH increases linearly upto the maximum at Cp=0.45, and then linearly decreases. The ΔH vs. Cp plots of the similar shape have been obtained for the IPS/CS_2[3] and APS/CS_2[4] systems as discussed in the following two chapters. This characteristic ΔH vs Cp relationship indicates that polymer molecules which contribute to gel construct a stoichiometric complex with solvent molecules. In the range Cp<0.45 all the polymer molecules contribute to the complex formation, but there are free solvent molecules. At Cp=0.45 both polymer and solvent molecules present contribute to the complex formation. In the range of Cp>0.45, all the solvent molecules are caught in the

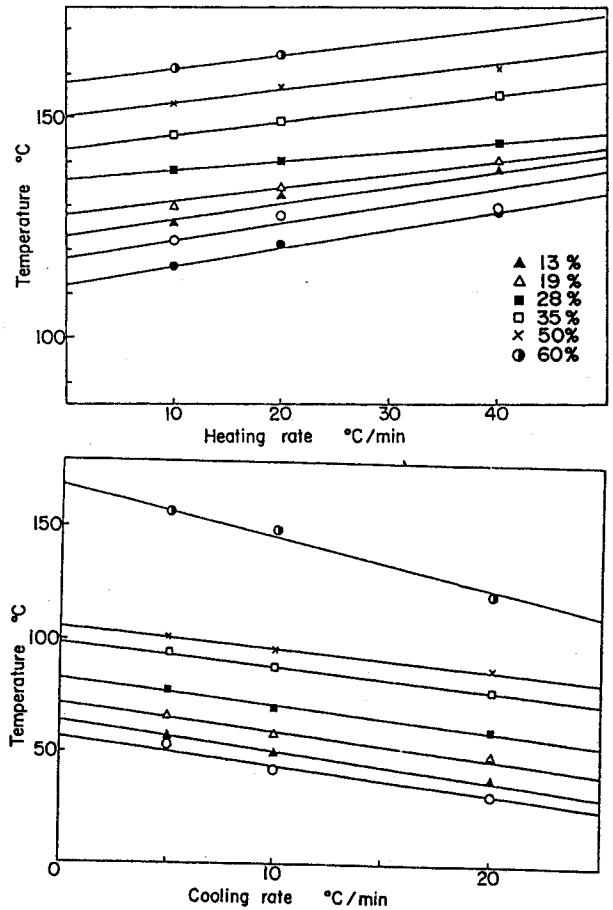

Figure 4-7. Gel melting and forming temperature as a function of the heating and cooling rate, respectively.

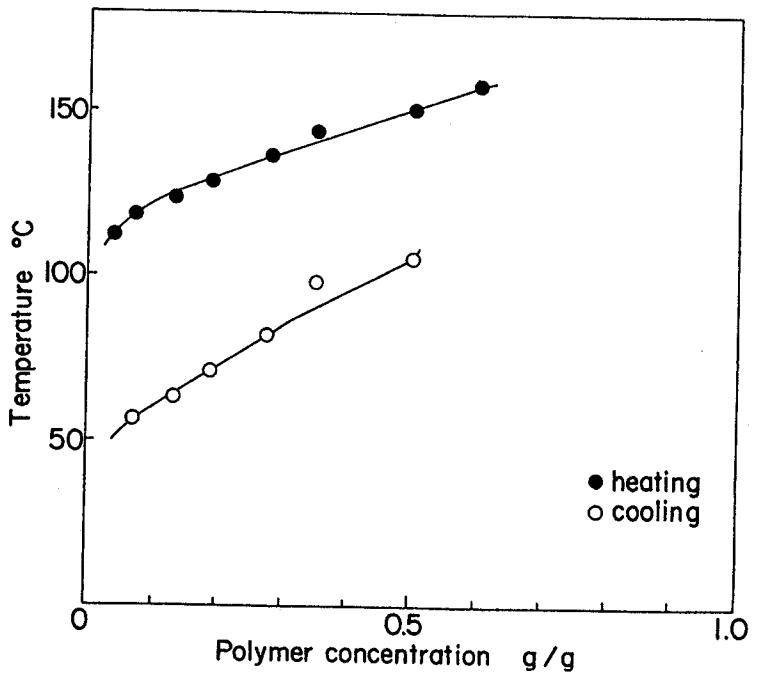

Figure 4-8. The plot of gel melting and forming temperature against concentration.

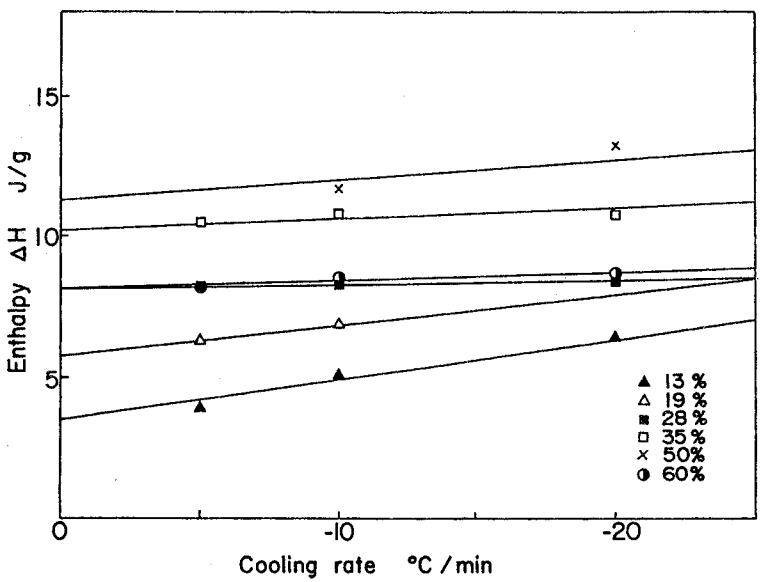

Figure 4-9. Gel forming enthalpies as a function of cooling rate.

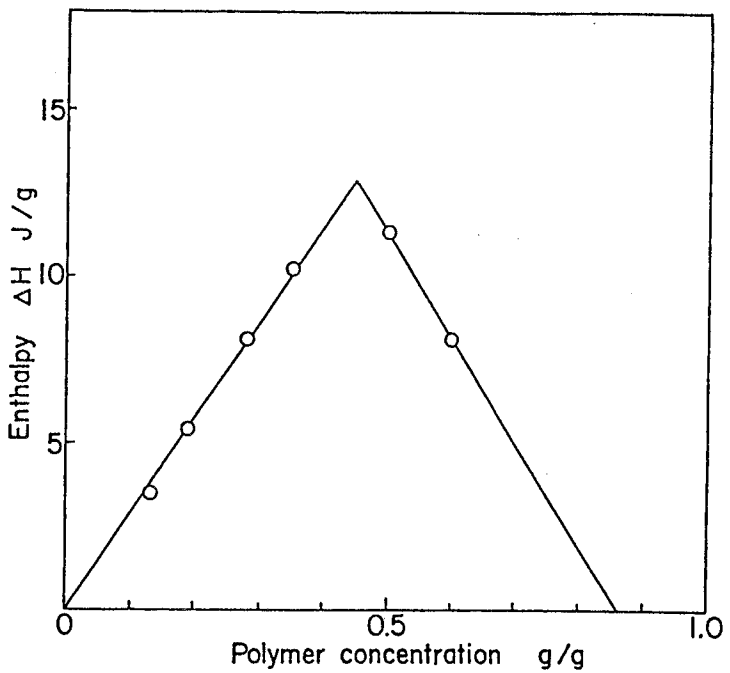

Figure 4-10. The plot of melting enthalpies against concentration.

gel-forming complexes. The average number of adsorbed solvent molecules per monomer unit (R) can be deduced from the following equation

$$R = \frac{1-Cp^*}{Cp^*} \frac{Msol}{Mp} \qquad (4-1)$$

where Cp^* denotes the polymer concentration at the maximum ΔH, and Msol and Mp are the molecular weights of the solvent and the monomeric unit, respectively. For the present case giving $Cp^*=0.45$, the R value was estimated as 0.87, suggesting the formation of about 1:1 polymer-solvent complex in SPS/o-dichlorobenzene gel. Due to the bulkiness of the phenyl group, the size of cavities is large enough for solvent molecules to allow to enter the gel-forming coagurates. It is concluded that the polymer-solvent interactions play important roles to the gelation of polystyrenes. For the case of SPS, the interaction seems strong compared with IPS and APS, as has been discussed in chapter 3. This is the origin of the distinguishable character of SPS of forming very stable gels with various solvents even at room temperature.

4-3-3. Gelation rate of SPS/o-dichlorobenzene gel

The rate of gelation or crystallization depends on the temperature and used solvents. The gel-forming times (t_{gel}) measured by the tilting method are plotted against temperature in Figure 4-11. Around the room temperature, the gelation rate is very rapid and becomes slower with increasing

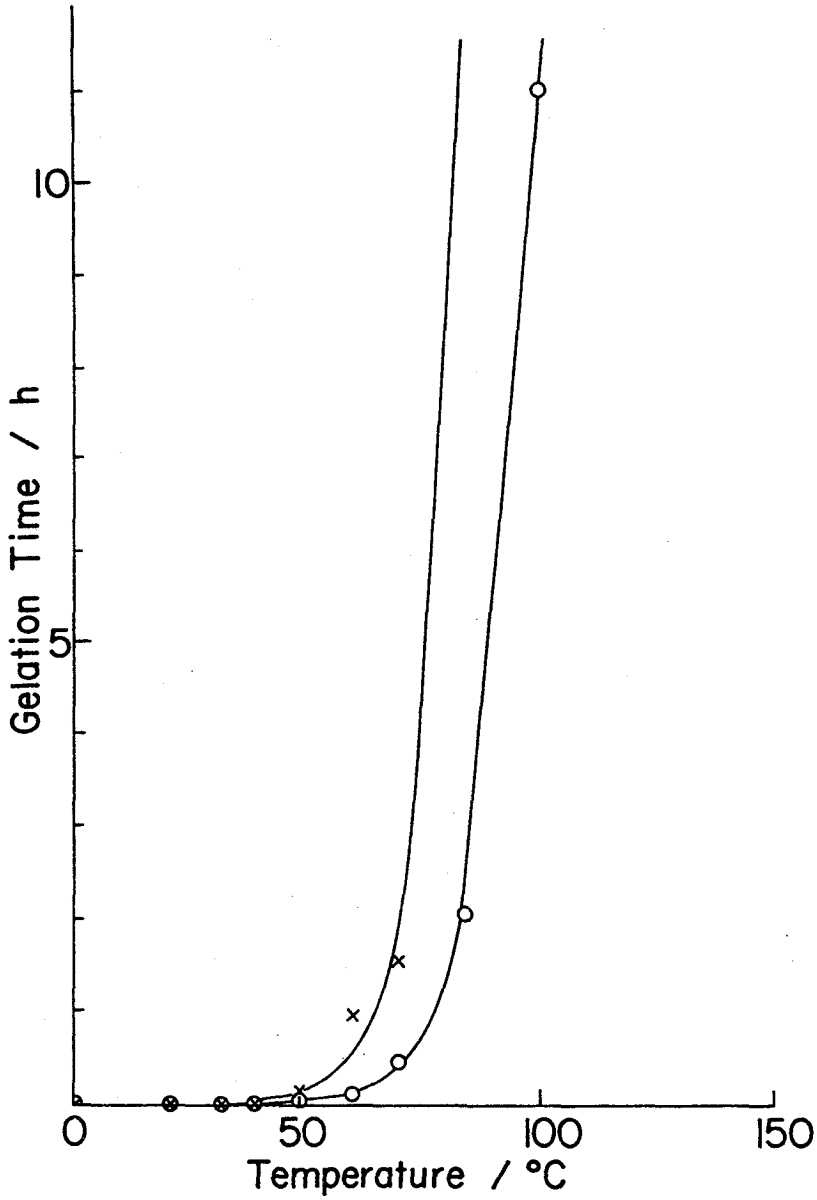

Figure 4-11. Gelation time at definite temperature of SPS/ o-dichlorobenzene system (determined by tilting method); ○: 10 w/v%, x: 5 w/v%.

temperature. Even at a temperature as high as 110°C, gelation proceeds in a 10 w/v% solution.

The gelation rate can be defined as the reciprocal gelation time. The activation energy for the gelation process ($E^{\ddagger}$) is expressed by the following Arrhenius-type equation.

$$1/t_{gel} \propto \exp(-E^{\ddagger}/RT) \qquad (4\text{-}2)$$

where R and T denote the gas constant and the gelation temperature, respectively. Figure 4-12 shows the plots of $\ln(1/t_{gel})$ vs. 1/T. The slope at a given temperature corresponds to the activation energy which varies with T. $E^{\ddagger}$ is expressed as $E^{\ddagger}=(Tm-T)^{\alpha}$, where Tm is a melting temperature and α is the exponent denoting the type of crystallization. Figure 4-13 shows the plots of $\ln E^{\ddagger}$ vs. $\ln(Tm-T)$. The exponent α is determined to be -2 from the slope of the straight part of the resultant curve, indicating the three dimensional growth. In gelation of polyvinyl alcohol and APS, the indices are equal to -2 and -2.8, respectively.[5] In the case of polyethylene single crystals grown from a xylene solution, the corresponding index is equal to -1.[6] This indicates that the crystallization of polyethylene proceeds via a two-dimensional nuclear growth, resulting the lamellar shaped single crystals.

4-3-4. Small angle neutron scattering of SPS/ o-dichlorobenzene

In this section, we show only the preliminary SANS data. Figure 4-14 shows the plot of scattering intensity I(Q) as a

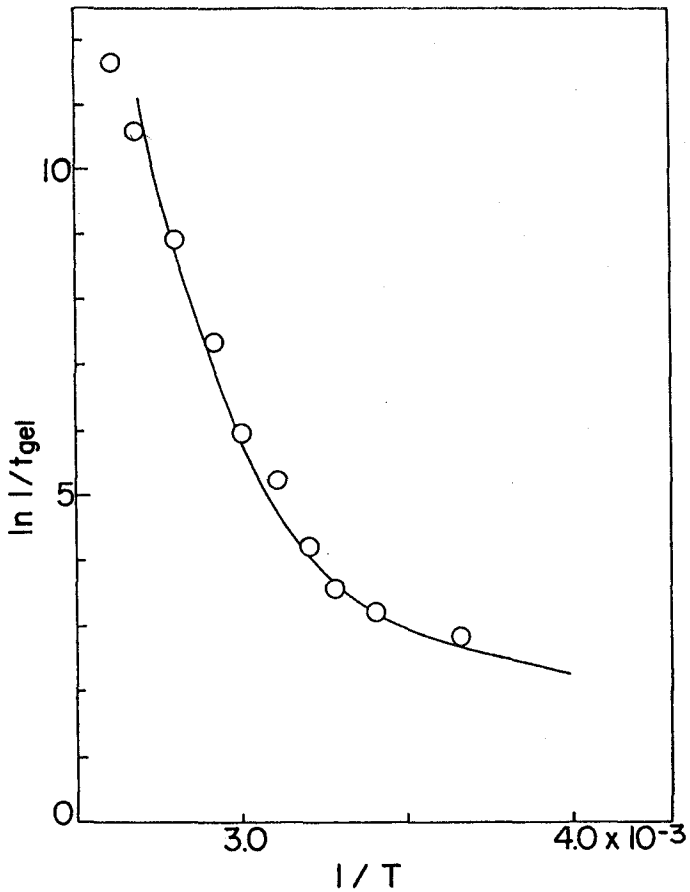

Figure 4-12. Plot of logarithm of the gelation time against reciprocal gelation temperature (10w/v%).

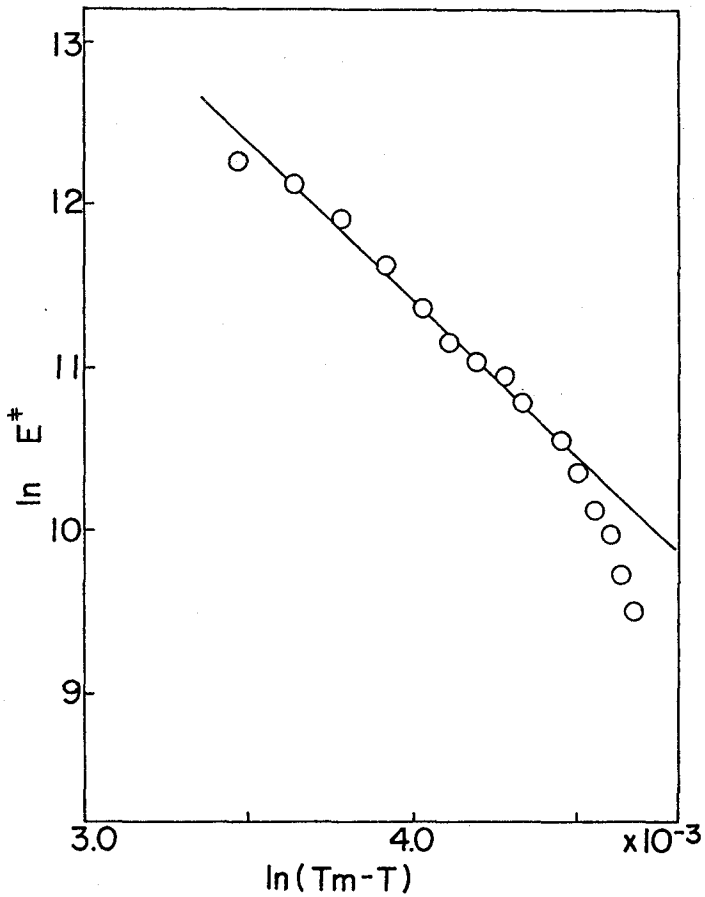

Figure 4-13. Plot of ln E^* vs. ln (Tm-T).

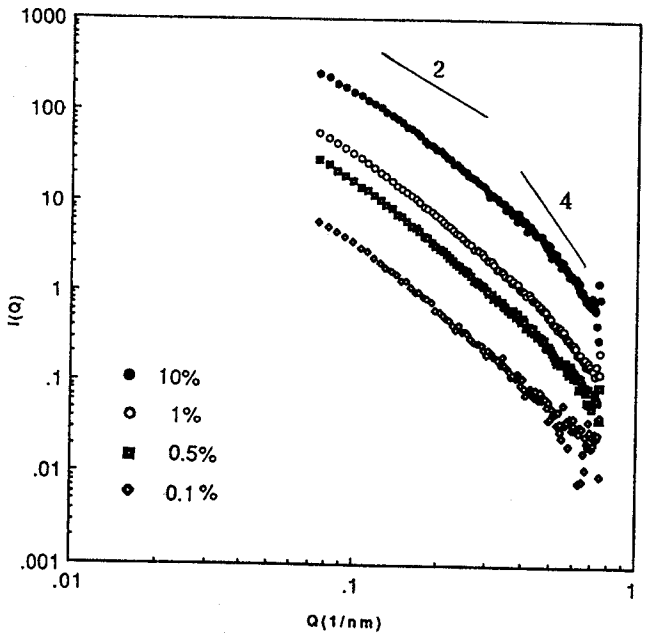

Figure 4-14. Concentration dependence of the SANS scattering intensity in SPS(Mw=15x10^4)/deuterated o-dichlorobenzene gel.

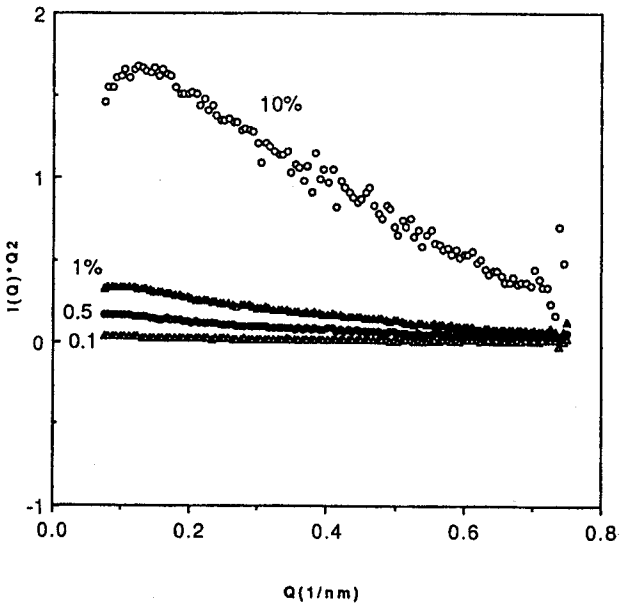

Figure 4-15. Kratky plot in various polymer concentration of SPS(Mw=15x10^4)/deuterated o-dichlorobenzene gel.

function of the scattering vector Q for various polymer concentration. It is well-known that I(Q) is proportional to Q^{-D}, where D is the fractal dimension of gel.[7] As shown in Table 4-1, the D values approach from 2 to 4 with increasing concentration. For 10 w/v% sample, I(Q) obeys so-called Porod's law (D=4).[8] The values of exponent indicate that the gel structure of SPS is different depending on polymer concentration. In Figure 4-15, the Kratky plots at four different concentrations are shown. The experimental data for 0.1% show the shape like a Kratky plateau. On the contrary, an intense maximum is observed for the 10% sample. This feature corresponds to the clustering of chain and the interpretation by the branched polymer model has been attempted.[9-12] The detail analysis is now in progress.

4-3-5. Crystallization from SPS/decalin solution

The SPS/decalin solution is transferred to a turbid suspension on cooling through the precipitation of fine crystallites. The crystallization time as a function of temperature is depicted in Figure 4-16. Evidently, there are two crystallization regimes below and above 70°C. This visual observations are supplemented by DSC and infrared measurements. Typical DSC curve of a sample quenched at 0°C shows the appearance of two endothermic peaks and one exothermic peak around 130°C (Figure 4-17). During this heating process, the infrared spectrum changes as shown in Figure 4-18. The spectrum at room temperature is identical with that of typical TTGG form which is characterized by 572, 548, 502 cm^{-1} bands. With increasing temperature, the intensities

Table 4-1. Fractal dimensions of SPS/ deuterated o-dichlorobenzene gel estimated from SANS measurements.

Mw	Polymer concentration (w/v%)			
	0.1	0.5	1.0	10.0
150000	2.6	2.9	3.6	4.1
400000	2.4	2.8	3.1	4.2
1135000	2.4	2.9	3.2	3.9

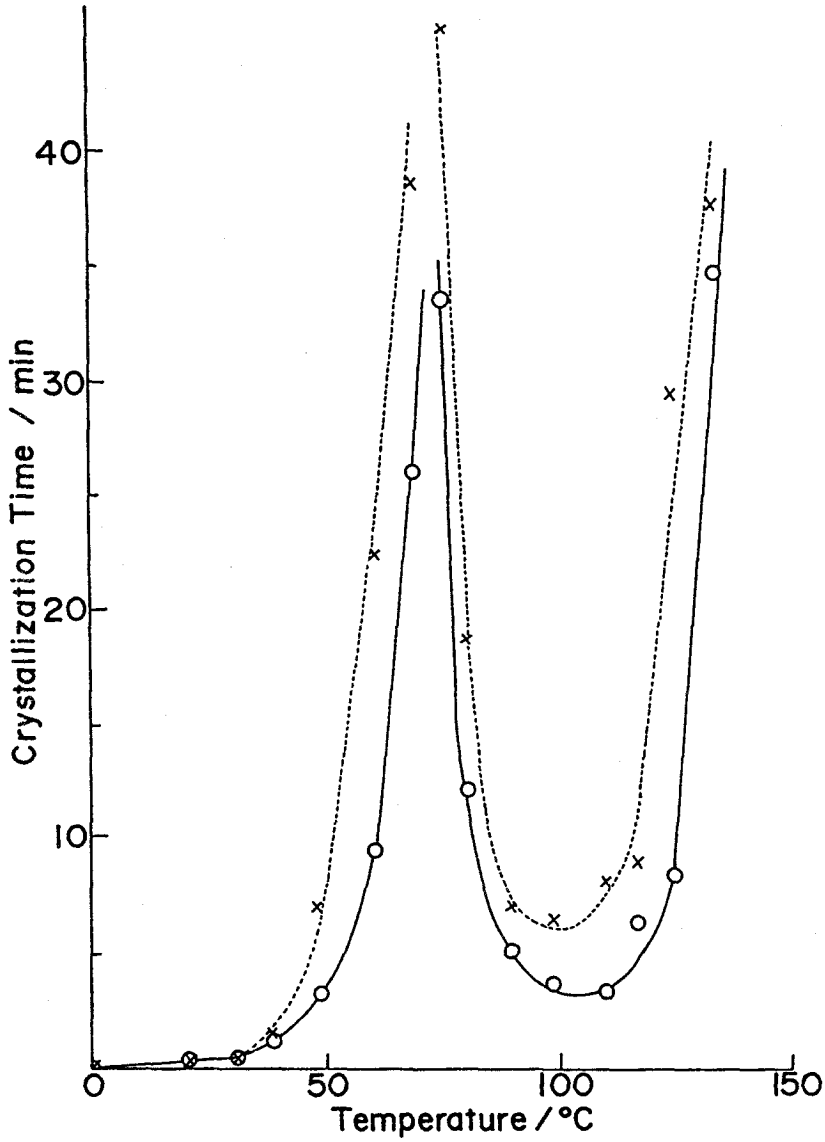

Figure 4-16. Crystallization time at definite temperatures of SPS/decalin system (determined by visual turbidity); ○: 5 w/v%, x: 3 w/v%.

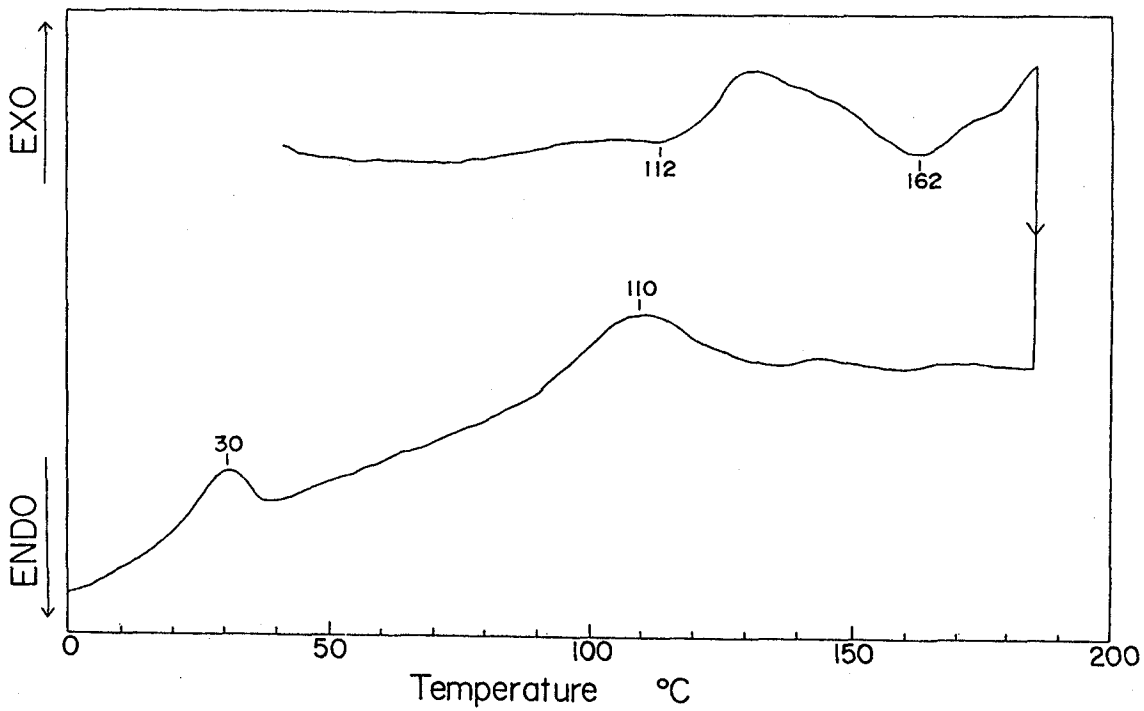

Figure 4-17. Thermogram of SPS/decalin system quenched at 0°C for 30 min.

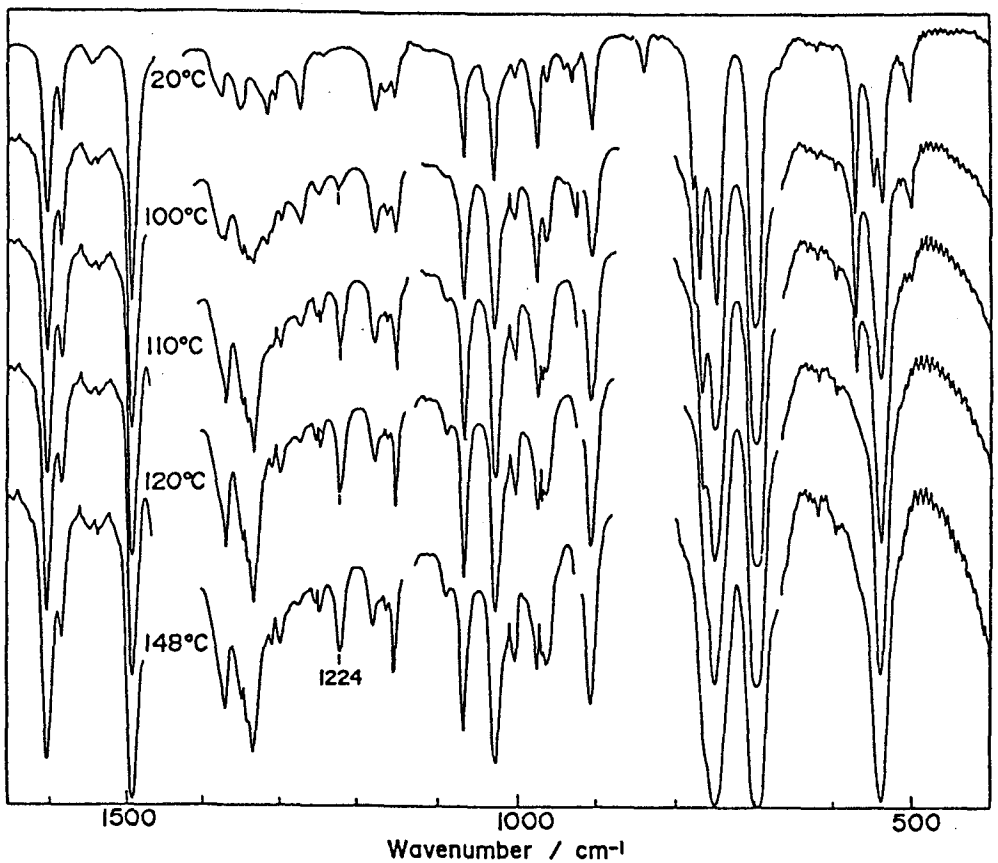

Figure 4-18. Infrared spectral change of SPS/decalin on heating process.

of these bands decreases, and alternatively the 1224 cm^{-1} band which reflects long trans sequences appeared. Therefore, the low and high endothermic peaks in DSC measurement correspond to the melting of TTGG and TT structures, respectively. The intermediate exothermic peak corresponds to the transition from the TTGG to TT form.

As the heating process is complicated because of phase transition, the phase diagrams are determined by cooling process via the similar manner to the case of SPS/o-dichlorobenzene. Figures 4-19 and 4-20 show the cooling rate dependence of the crystal-yielding temperature and the resultant temperature-concentration phase diagram, respectively. Figures 4-21 and 4-22 correspond to the cooling rate dependence of the crystallization enthalpy, and the resultant ΔH vs. Cp relationship, respectively. There is no correlation between ΔH and Cp. Contrary to the case of SPS/o-dichlorobenzene, decalin molecules are not caught in the crystallites.

It is concluded that on cooling SPS solution, gelation or crystallization takes place depending on whether polymer-solvent complexes are formed or not.

References

1) M. Kobayashi, T. Nakaoki, N. Ishihara, Macromolecules, 22, 4377 (1989).
2) P.-G. de Gennes, "Scaling Concepts in Polymer Physics"; Cornell University Press : Ithaca, NY and London, 1979.

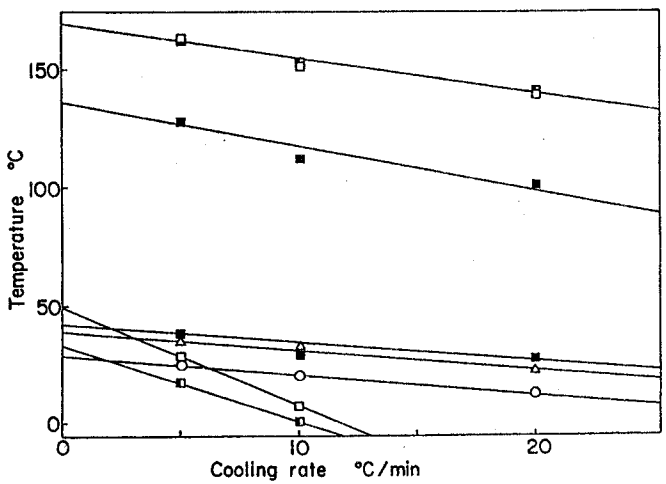

Figure 4-19. Crystal yielding temperature as a function of the cooling rate.

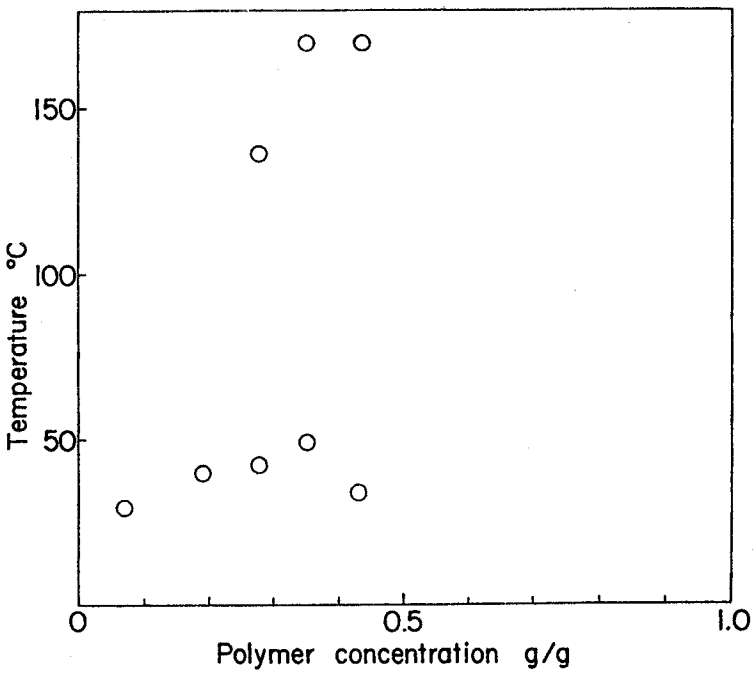

Figure 4-20. The plot of crystal yielding temperature against concentration.

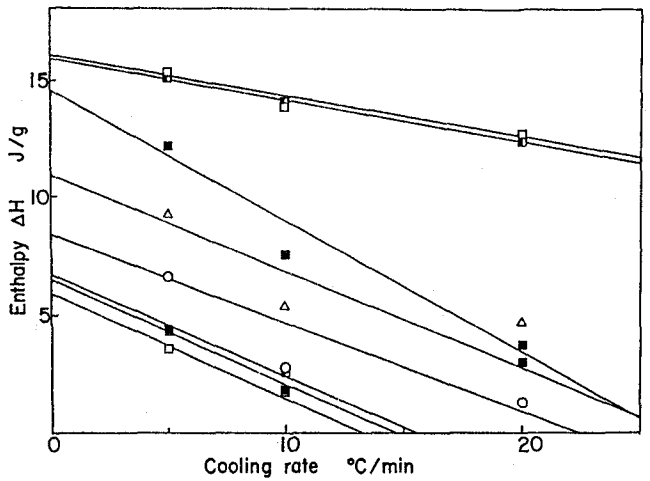

Figure 4-21. Crystal yielding enthalpies as a function of the cooling rate.

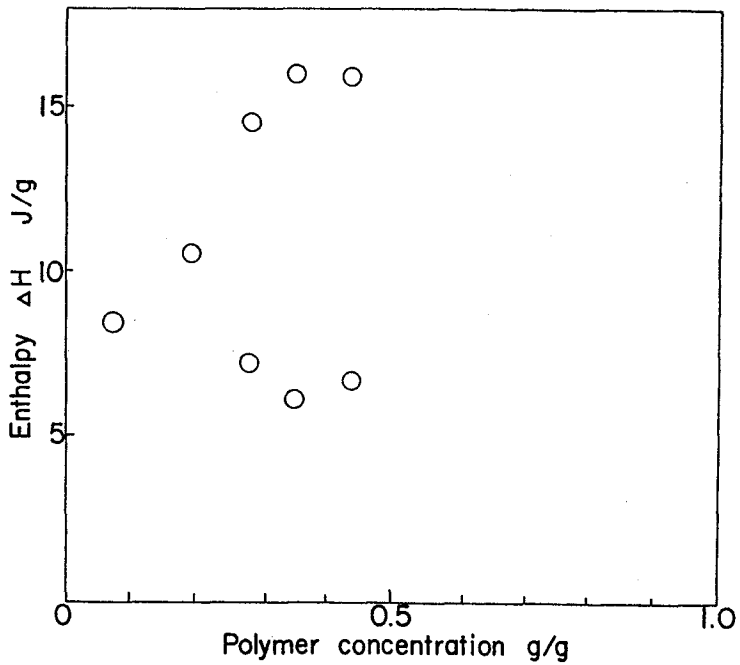

Figure 4-22. The plot of crystal yielding enthalpies against concentration.

3) J.-M. Guenet, Macromolecules, 19, 1961 (1986).

4) J.-M. Guenet, G. B. McKenna, Macromolecules, 21, 1752 (1988).

5) X. -M. Xie, A. Tanioka, K. Miyasaka, Polymer, 31, 281 (1990).

6) M. Cooper, J. Manley, Macromolecules, 8, 219 (1975).

7) F. Family, D. P. Landau, Kinetics of Aggregation and Gelation, 1984, North Holland.

8) G. Porod, Kolloid-Z., 124, 83 (1951).

9) W. Burchard, Macromolecules, 10, 919 (1977).

10) K. Kajiwara, C. A. M. Ribeiro, Macromolecules 7, 121 (1974).

11) K. Kajiwara, W. Burchard, Polymer, 22, 1621 (1981).

12) W. Burchard, K. Kajiwara, D. Nerger, J. Polym. Sci., Polym. Phys. Ed. 10, 157 (1982).

CHAPTER 5

Gelation Mechanism and Structure in Gels of Isotactic Polystyrene

5-1. Introduction

Isotactic polystyrene (IPS) is a representative of synthetic stereoregular polymers and many studies have been done on its molecular structure (the configuration and the conformation as well as their sequential distribution along the molecule) in crystals, glasses, solutions and gels, since it was prepared first by Natta et al. in 1955.[1] It is well established that IPS molecules in crystalline samples assume a (3/1) helical structure consisting of a regular repetition of the trans (T) and gauche (G) conformations of the skeletal C-C bonds.[2,3] During the recent decade, gelation of IPS has been focused to a great deal of attention as a suitable system for studying the molecular mechanism of the formation of physical gel. Keller et al. found that X-ray diffraction taken on partially dried and stretched IPS/decalin gels was different from that of the well-known crystalline phase.[4-8] The appearance of a meridian reflection of the spacing of 0.51 nm suggested the presence of skeletal conformation having a nearly extended form [(12/1) helix]. Thereafter, Sundararajan et al. suggested that the (12/1) helical molecules might be solvated.[9-11] Recently, a series of neutron diffraction experiments of nascent IPS/decalin gels were carried out by Guenet et al. for various combinations of deuterated (D) and hydrogenous (H) species of the polymer and the solvent.[12-16] They found that the 0.51 nm reflection appeared

in H-IPS/D-decalin, D-IPS/D-decalin and also in pure D-decalin, but disappeared in D-IPS/H-decalin. Therefore, they concluded that the 0.51 nm^{-1} reflection should not be ascribed to the (12/1) helicies of IPS, but to the solvent molecules. As a possible structure of IPS/decalin gel, they proposed a ladder like model consisting of (3/1) type helices that form a nematic liquid-crystal mediated by solvent molecules between polymer chains.

In this chapter, the molecular structure formed in IPS gels is considered on the basis of the results obtained by vibrational spectroscopic study, in relation to the molecular mechanism of gel formation.

5-2. Experimental

5-2-1. Samples

Polymerization of IPS was carried out with a $TiCl_3$-$Al(C_2H_5)_3$ Ziegler-Natta catalyst in n-heptane at 70°C. The polymers obtained were washed with methanol and then heated in boiling water. The atactic component was extracted with boiling methyl ethyl ketone (MEK). The IPS samples obtained were dissolved in hot toluene and the solutions, after cooling, were separated from gelatinous precipitates by centrifugation. The polymers were reprecipitated with methanol, collected and dried. The diad isotacticity of the IPS samples were evaluated as over 96% by ^{13}C-NMR. Samples of isotactic poly 2-monodeuterostyrene $\{CH_2\text{-}CD\cdot C_6H_5\}_n$ (IPS-2-d_1), isotactic poly 1,1-dideuterostyrene $\{CD_2\text{-}CH\cdot C_6H_5\}_n$ (IPS-1,1-d_2) and isotactic poly ring-pentadeuterostyrene $\{CH_2\text{-}CH\cdot C_6D_5\}_n$ (IPS-r-d_5) were prepared in a previous work done by Kobayashi et al.[17]

Gels of IPS/decalin and IPS/carbon disulfide (CS_2) systems were investigated. The IPS/decalin dried gels were prepared by quenching (at $0^{\circ}C$) a hot decalin solution (kept at $150^{\circ}C$) followed by standing in vacuo. The IPS/CS_2 gels were prepared by cooling the solutions below $-50^{\circ}C$ (the gelation temperature depends on polymer concentration).

5-2-2. Measurements

Infrared spectra (with 1 cm^{-1} resolution) were measured by using a JASCO FT-IR 8000 spectrometer equipped with a DTGS detector. Spectra were accumulated 50 times. A home-made solution cell with a lead spacer of 100 μm thickness inserted between two KBr windows was used. For measurements at low temperatures, an Oxford flow-type cryostat was used. ^{13}C-NMR spectrum was measured with a JEOL GSX-400 spectrometer, operating at 100.40MHz.

5-3. Results and Discussion

5-3-1. Molecular structure of IPS formed in gel

To elucidate the skeletal conformation of IPS molecules in gel, the spectral features of the conformation-sensitive infrared bands associated with the TG skeletal conformation were compared between highly crystalline solid and CS_2 gel.

It has been established that the infrared spectrum of IPS/CS_2 solutions exhibits a dramatic thermoreversible change on cooling.[18] The conformation-sensitive bands due to the regular TG sequence increase continuously as the temperature is lowered, as shown in

Figure 5-1. On this cooling process, physical gelation takes place below -40°C as is detected by a steep change in the half-width of the ^{13}C-NMR signals (Figure 5-2).

The infrared spectral change on cooling indicates that gelation is accompanied with the ordering in molecular conformation. The bands which become prominent on gelation are very close to those of crystalline IPS in frequency, relative intensity, as well as in shape. This indicates that TG-type regular sequences are formed during gelation and the total amount and the average sequential length of the ordered part increase as the temperature is lowered (Detail analysis will be made in the following section). The small difference in frequency for the 923 (918) and 899 (896) cm^{-1} bands (the frequency in the gel are given in parentheses) between the crystalline and gel phases, and the appearance of additional bands at 1070 and 1062 cm^{-1} in the gel, are ascribed to strong polymer-solvent interactions that cause small conformational changes. These considerations are also confirmed by CP/MAS ^{13}C-NMR spectrum measured on a IPS/decalin dried gel. The infrared spectra of IPS/decalin dried gel measured by Painter et al.[19] was regarded as the same as that of IPS/CS_2 gel. In Figure 5-3, the CP/MAS spectrum of IPS/decalin dried gel is compared with the normal ^{13}C-NMR spectrum of decalin. As will be described in Chapter 7, CP/MAS spectrum reflects sensitively the conformation of the skeletal chain. If the near-trans conformation proposed by Keller et al. existed, the methylene signal should appear at 48 ppm (see Chapter 7). There is no peak around this region, indicating that nearly all trans structure

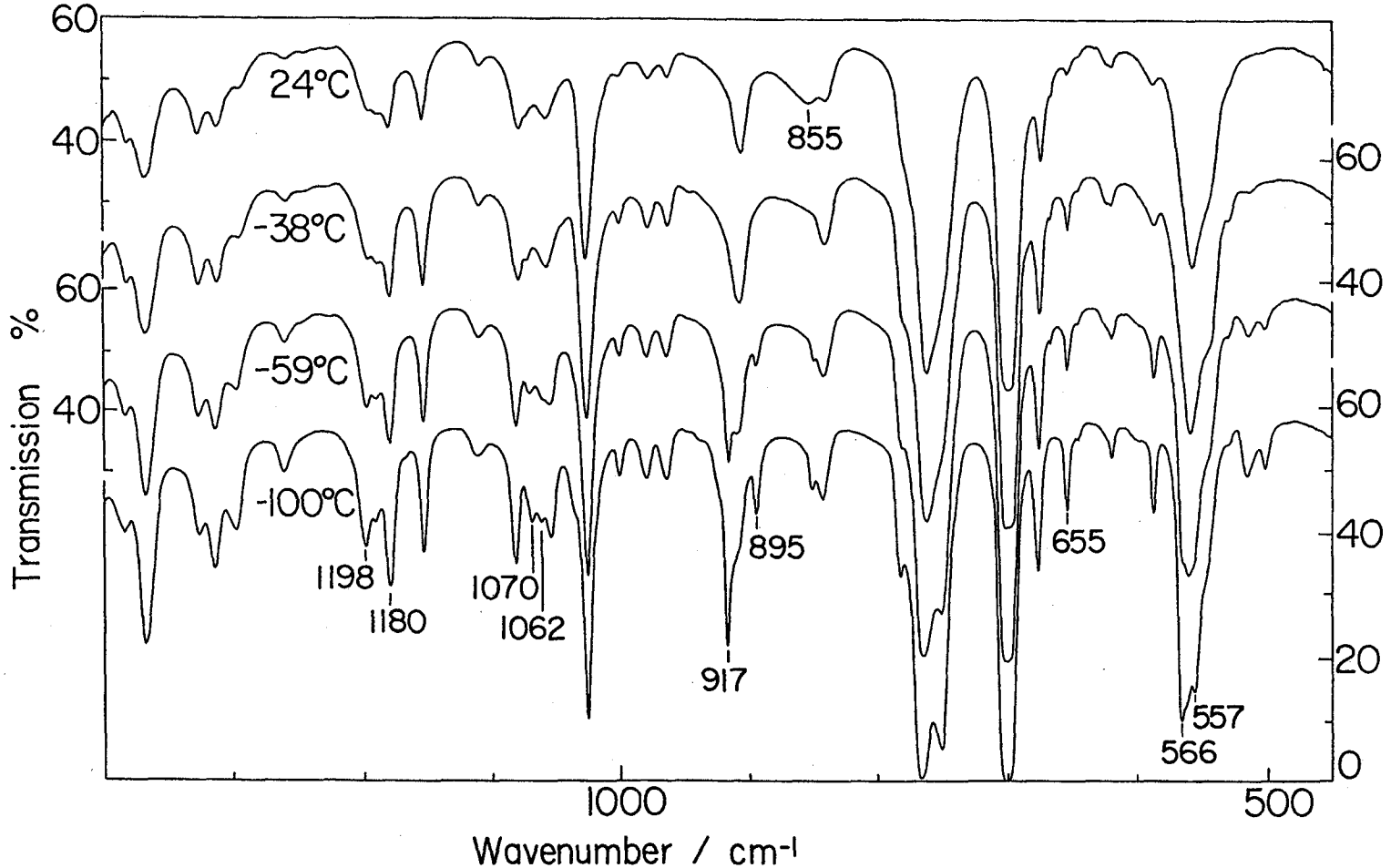

Figure 5-1. Temperature dependence of the infrared spectra of a IPS/CS_2 solution.

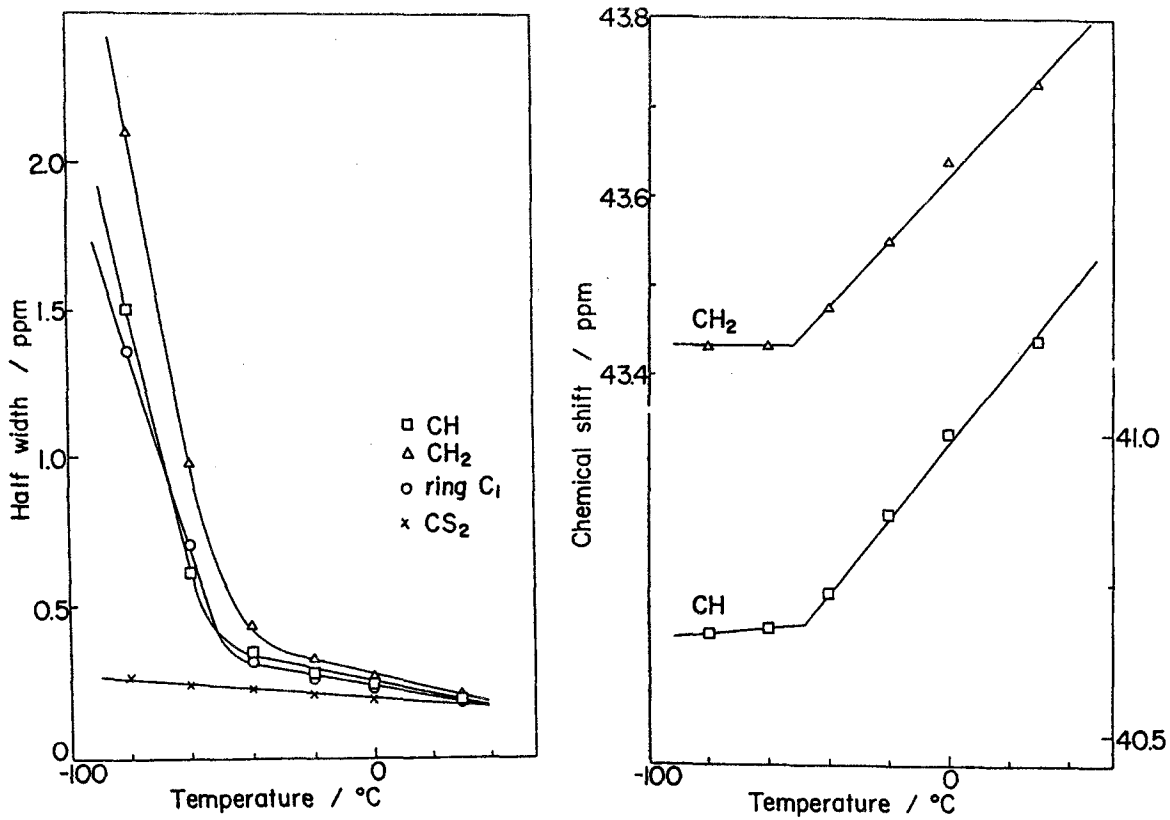

Figure 5-2. Temperature dependence of the half-width and chemical shift of the ^{13}C-NMR signals of a IPS/CS_2 system.

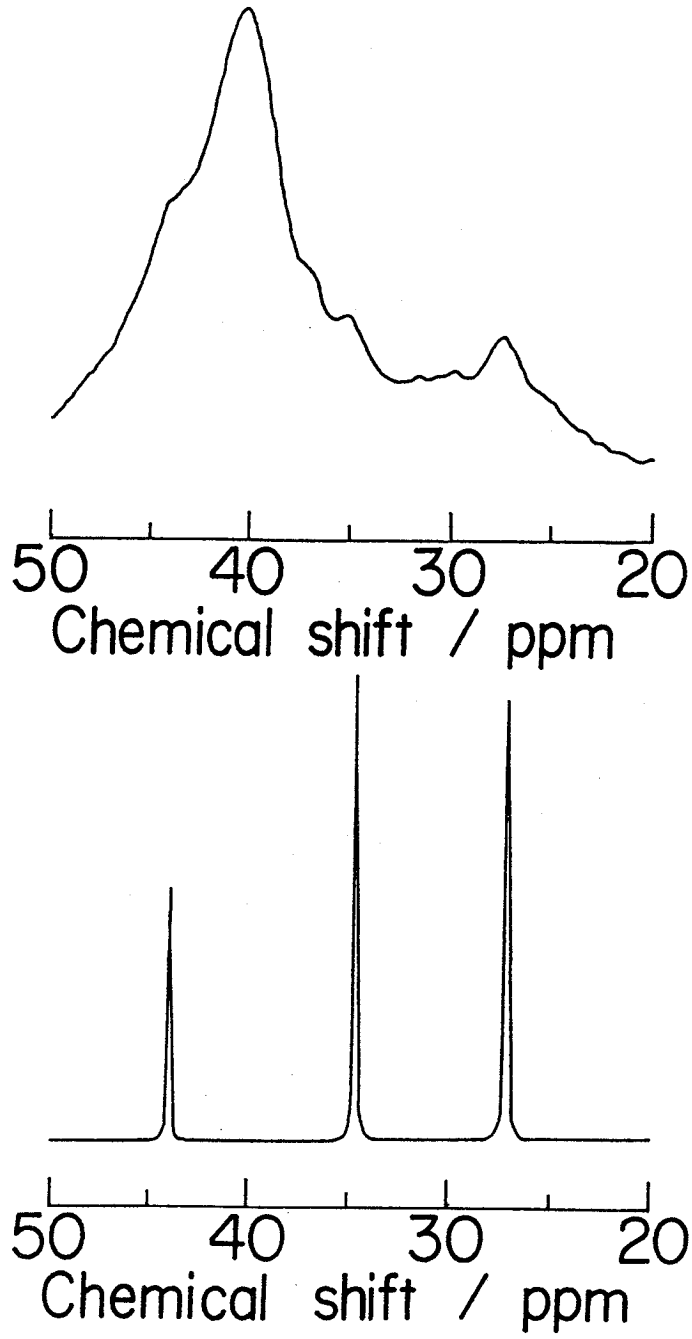

Figure 5-3. CP/MAS ^{13}C-NMR spectrum of IPS/decalin dried gel (upper), and ^{13}C-NMR spectrum of decalin (bottom).

does not exist in gel. (The three peaks at 44.0, 34.6 and 27.1 ppm originate from decalin because their chemical shift corresponds to that of liquid decalin) The solvent molecules are caught in gel with less mobility judging from the fact there are no sharp peaks due to the solvent molecules.

Thus, we conclude that the ordered conformation formed in IPS gel should be of the TG type, rather than the near-TT [(12/1) helix] type proposed previously for the IPS/decalin gel. The type of ordered conformation constructed in the gel seems hardly influenced by the solvent used. In fact, the infrared spectrum of an IPS/decalin gel (at room temperature), after subtracting the absorption of the solvent and the background due to the disordered part of the polymers by computer manipulation, resembles that of our IPS/CS_2 gel at -100°C. Bearing the significant spectral difference between the α and β phases of SPS in mind, it is naturally considered that the spectral feature of the near-TT (12/1) conformation should be very different from that of the (3/1) helix.

Comparing the infrared spectra of crystalline IPS and IPS/CS_2 gel measured at low temperature, there are some marked differences (Figure 5-4). Base on the spectral features, the bands appearing in gel are classified in the following three types. (1) Gel specific bands which disappear in crystalline IPS (1070, 1062, 854, 517 and 503 cm^{-1}) (2) Bands providing intensities different from crystalline IPS (1198, 1188, 983 cm^{-1}) (3) Bands whose wavenumbers are shifted from those of the 3/1 helix (917, 892 cm^{-1}). All these bands are associated with the vibrations of the phenyl group. The origin of these differences will be discussed in what follows.

1. The behavior of 983 cm^{-1} band : This band was assigned to

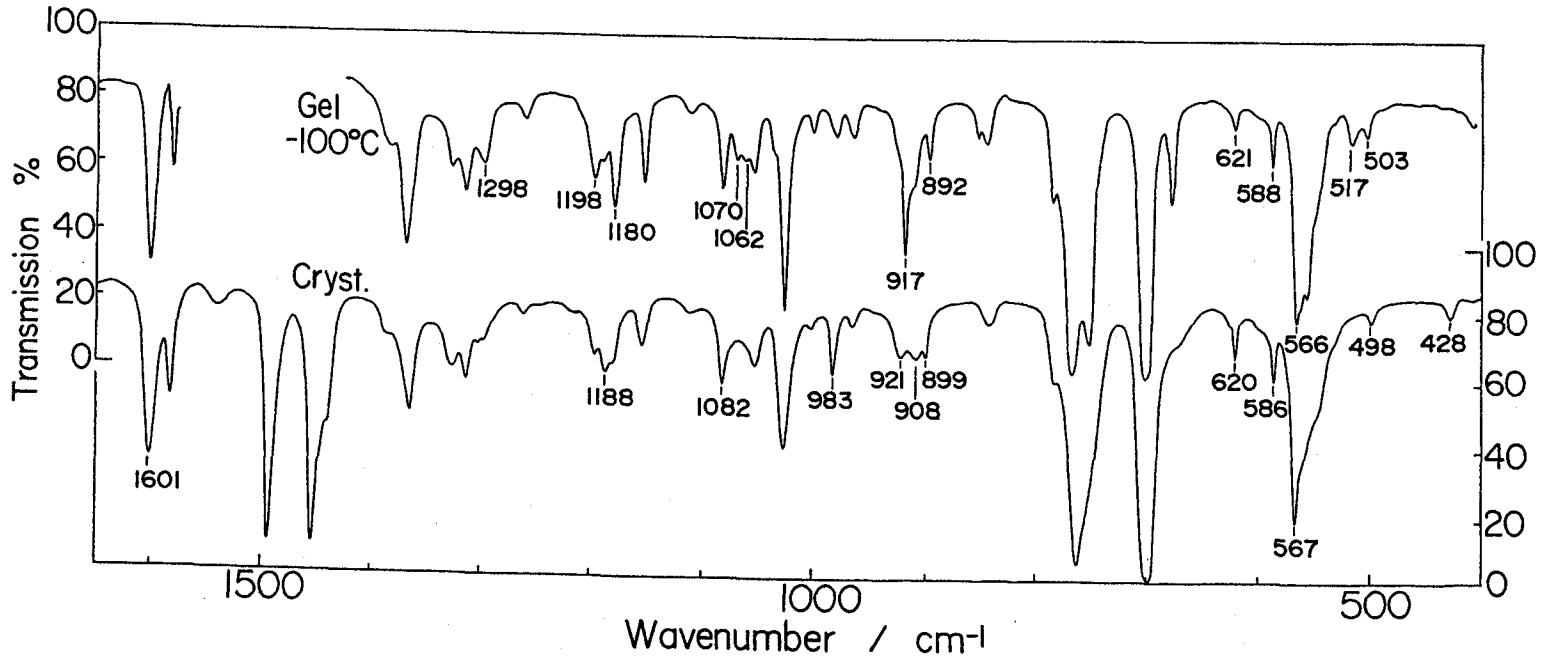

Figure 5-4. Infrared spectra of crystalline and gel at -100°C.

a pure C-H out-of-plane ring mode.[20,21] In the crystalline phase, the 983 cm^{-1} band behaves as a typical crystallization-sensitive band with intensity proportional to the degree of crystallinity of the sample. In gel, on the contrary, the intensity does not increase with decreasing temperature and remains at a level as low as in the glassy state, even at $-100^{o}C$. As to the origin of the crystallization-sensitive character, two different sources, intermolecular and intramolecular, are possible. The former originates from a specific spatial arrangement of the molecules in the crystal lattice. In this case, the arrangement of the phenyl ring plays an important role, since the band is assigned to a C-H out-of-plane ring mode. The latter is concerned with concerns a specific conformation of the phenyl ring with respect to the skeletal chain.

In order to identify the correct source of the crystallization-sensitive character of the 983 cm^{-1} band, the author investigated the intensity of the band for isotactic copolymers of styrene and ring deuterated styrene and also for blends of IPS and IPS-r-d_5, in both highly crystalline and glassy states. In Figure 5-5, the spectra of a copolymer (with 52.1 mol% styrene monomer) and a blend (with 51.2 mol% IPS) are reproduced. If the sensitivity originates from the intermolecular interaction, the band intensity should decrease remarkably with an increase in the degree of isotope dilution for both the blend and the copolymer. On the other hand, if the sensitivity is caused by a particular conformation of the phenyl ring, the band intensity should remain unaltered with variation in the isotope composition, since the degree of

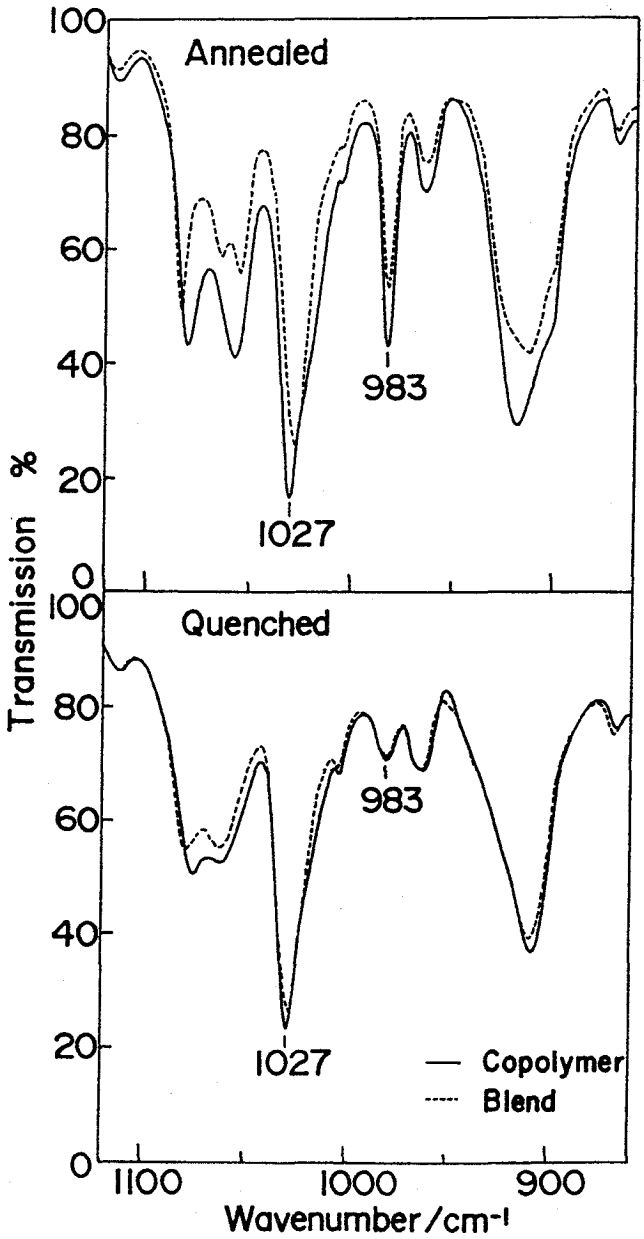

Figure 5-5. Infrared spectra of an isotactic styrene-styrene-r-d_5 copolymer (styrene, 52.1 mol %)(——) and an IPS-IPS-r-d_5 blend (styrene, 51.2 mol %)(---) in highly crystalline (upper) and glassy (lower) states. On crystallization, the 983 cm^{-1} band gains intensity in both the copolymers and the blend, as in IPS homopolymer.

crystallinity is high over the whole composition range.

The peak intensity of the 983 cm^{-1} band (reduced to that of the 1027 cm^{-1} band used as the internal standard, because this band is proportional to the fraction of hydrated polystyrene as shown in Figure 5-6) of the copolymers and the blends is plotted against the molar concentration of undeuterated styrene units in Figure 5-7. Since there are no absorptions around 983 cm^{-1} and 1027 cm^{-1} in IPS-r-d_5 homopolymer (Figure 5-8), only the undeuterated phenyl rings are responsible for the peak intensity. In both the copolymers and blends, the peak intensity remains nearly constant over the whole concentration range. The slight reduction with increasing dilution may be due to an experimental artifact in drawing the baseline. This means that the crystallization-sensitive character of the 983 cm^{-1} band originates from a specific conformation of the phenyl groups which remain undisturbed in the highly crystalline copolymers and blends, as in IPS homopolymer. Therefore, the intensity depressions in the cooled gel comes from the disordered orientation of the phenyl rings.

2. Origin of the gel specific bands : The origin of the gel specific bands is investigated by using partially deuterated samples. Figure 5-9 shows the temperature dependence of infrared spectra of IPS-2-d_1. The intensity of 983 cm^{-1} band and the appearance of gel specific bands of 854, 517 and 503 cm^{-1} are common behaviors with IPS gel. Figure 5-10 shows infrared spectral change of IPS-1,1-d_2 on cooling. Also in this case, gel characteristic bands are common with IPS gel. Therefore, the vibrations of methine and methylene are hardly influenced by the formation of gel. On the contrary, as shown in Figure 5-11,

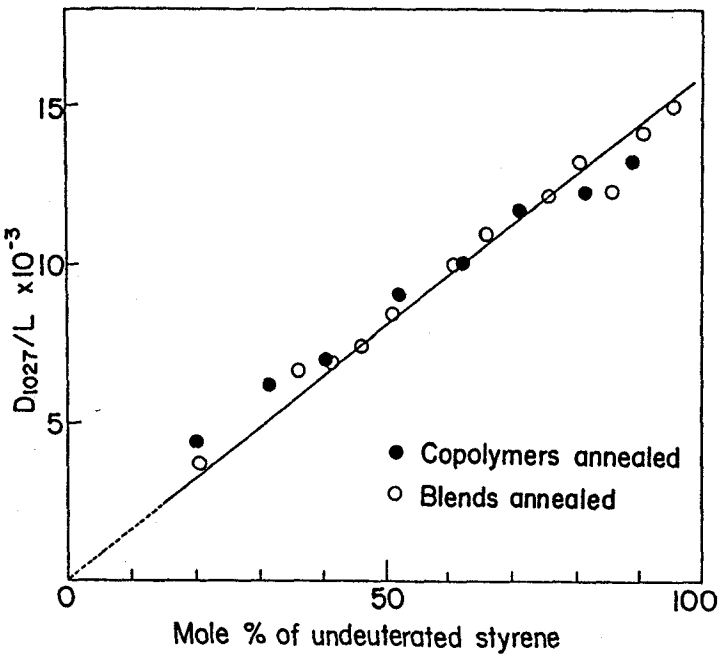

Figure 5-6. The plot of the intensities at 1027 cm^{-1} band against mole fraction.

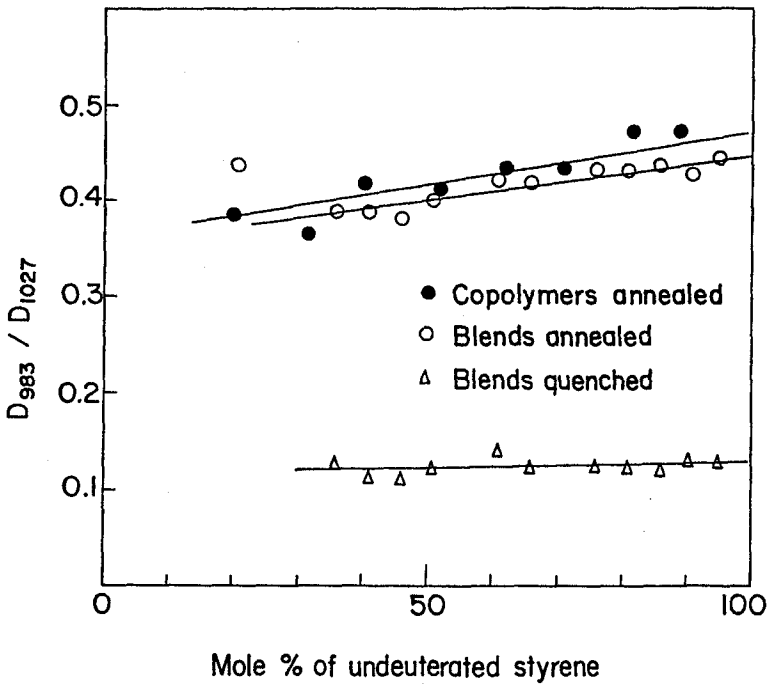

Figure 5-7. Dependence of the peak intensity of the 983 cm^{-1} band in isotactic S-S-r-d_5 copolymer and IPS-IPS-r-d_5 blend on isotope composition.

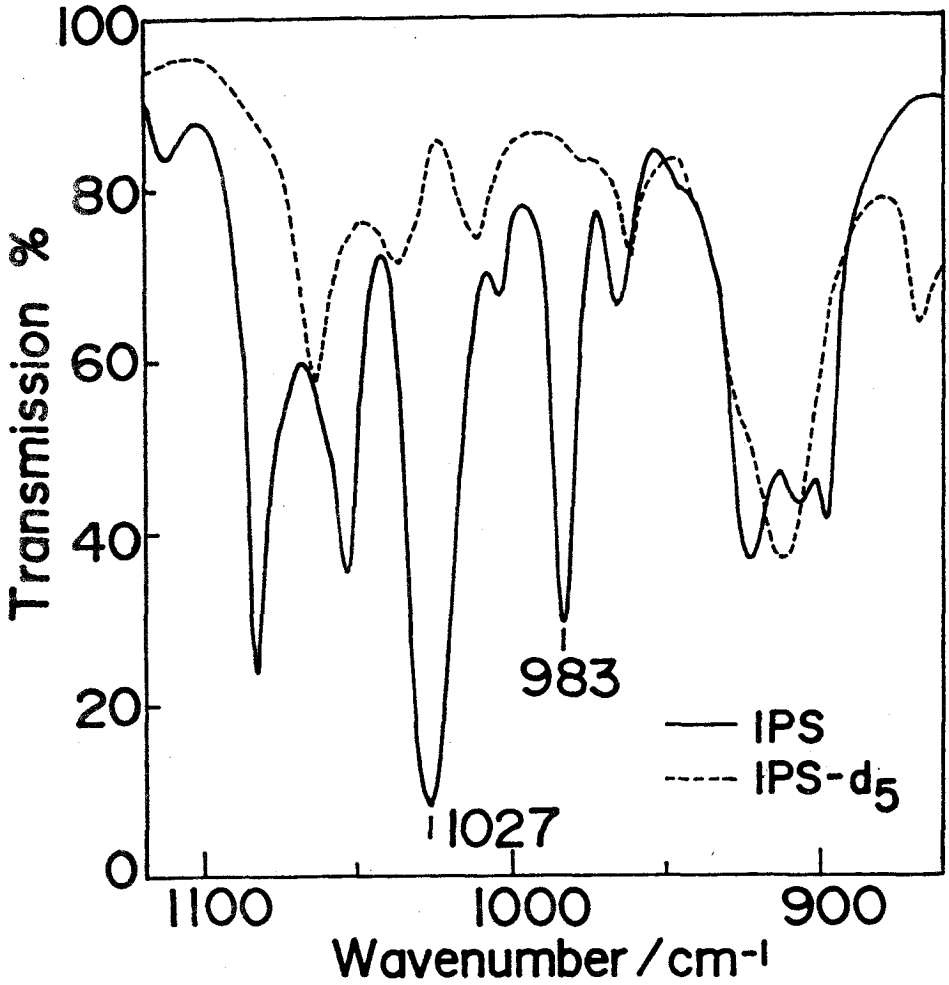

Figure 5-8. Infrared spectra of IPS (——) and IPS-r-d_5 (---) homopolymers in the highly-crystalline state.

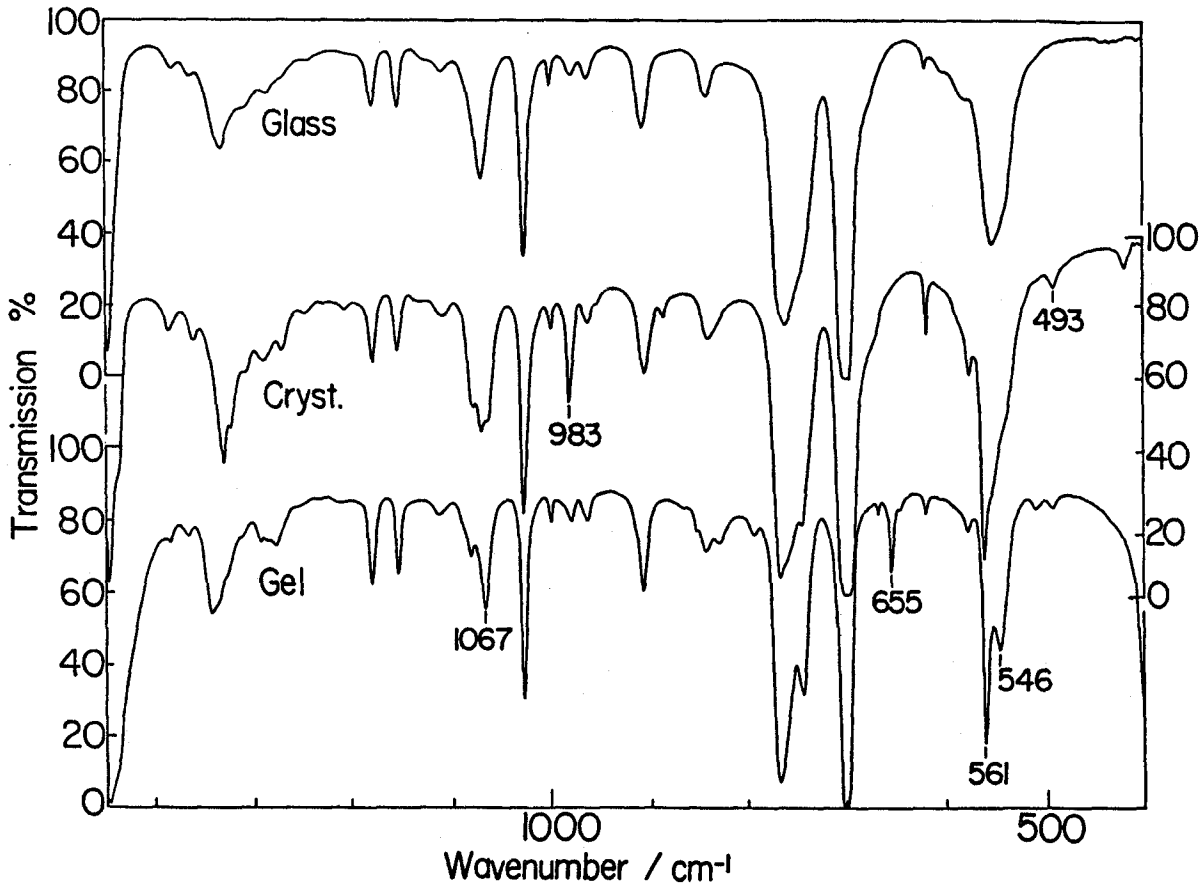

Figure 5-9. Temperature dependence of the infrared spectra of IPS-d_1 glass, crystal and /CS_2 gel (20 w/v%, -100°C).

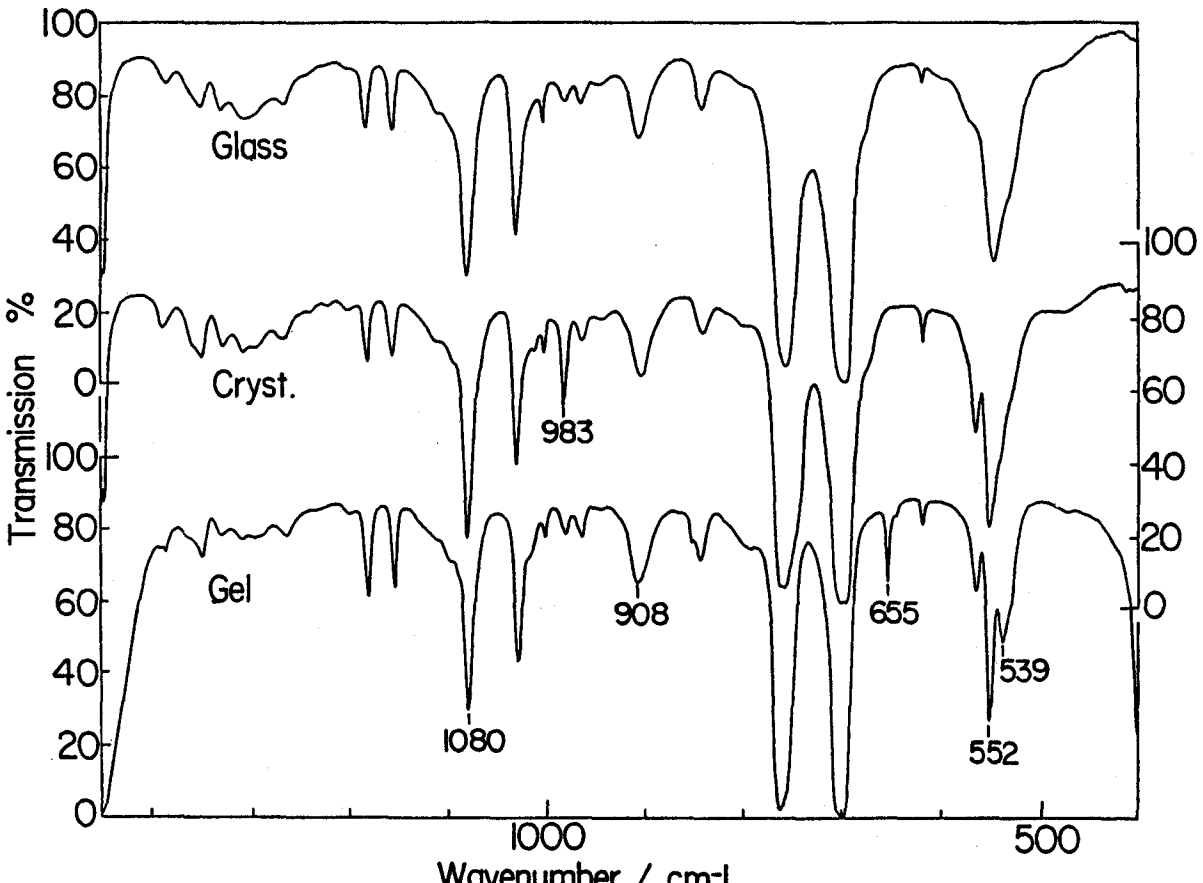

Figure 5-10. Temperature dependence of the infrared spectra of IPS-d_2 glass, crystal and /CS_2 gel (20 w/v%, -100°C).

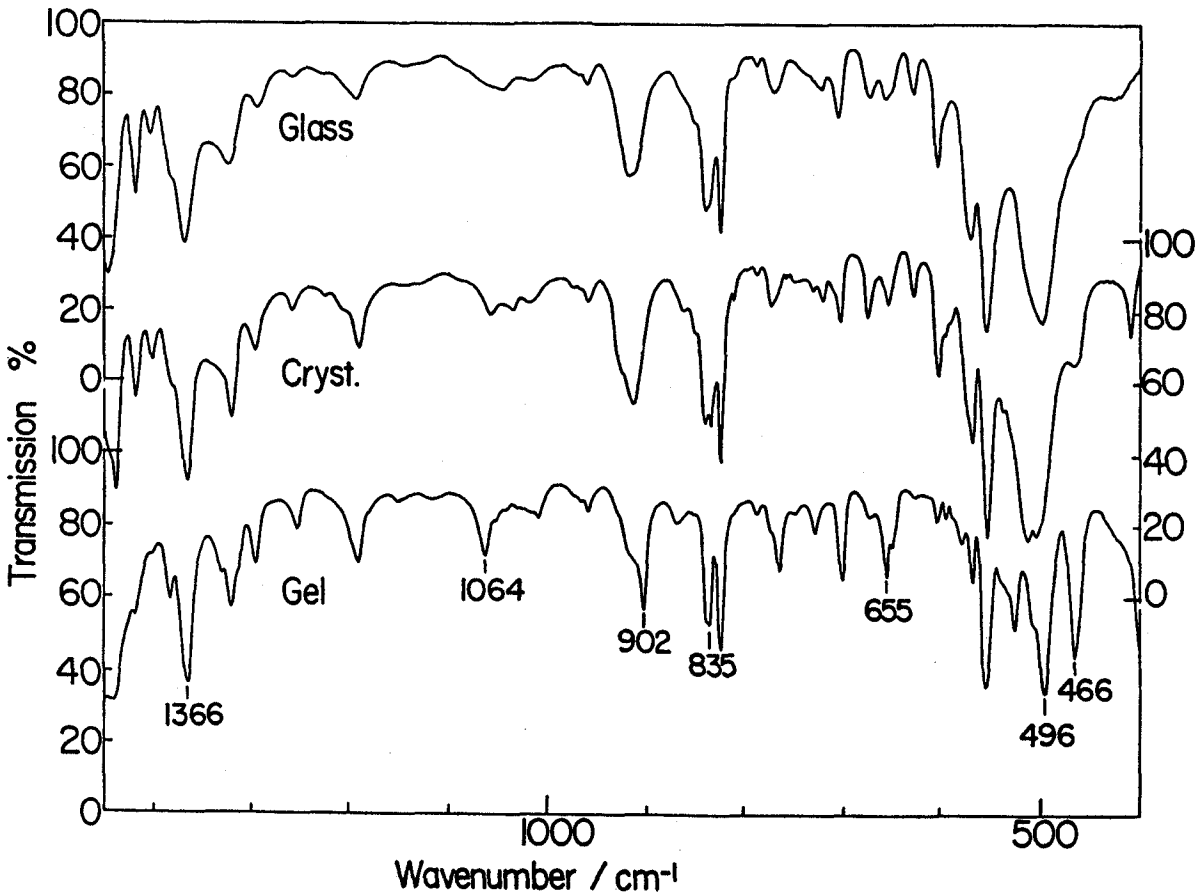

Figure 5-11. Temperature dependence of the infrared spectra of IPS-r-d_5 glass, crystal and /CS_2 gel (20 w/v%, -100°C).

the infrared spectrum of IPS-r-d_5 gel is remarkably different from that of crystalline IPS.

Judging from the behavior of these gelation bands of three partially deuterated samples, only the ring modes are especially influenced on gelation.

Consequently, it is concluded that the infrared spectral features characteristic of IPS gels comes from the disordered conformation around the C(skeletal)-C(ring) bond. Such a disorder may be induced by the insertion of solvent molecules in the intermolecular space, while the skeletal chain takes a partially-ordered TG conformation.

5-3-2. Critical sequence length of conformation-sensitive bands

The conformational sensitive character of the infrared bands originates from the intramolecular vibrational coupling among the monomeric units regularly arranged along the polymer chain. It should be emphasized that the sensitivity of the band intensity to the conformational order differs from band to band. As a figure of the sensitivity, a concept of the critical sequence length has been introduced.[17] It is defined as the shortest length of the sequence of a particular conformation, ex. TG or TTGG, (represented by the number of the structural units m) necessary for the appearance of the sensitive band. For IPS, the values of m were derived from the relationship between the band intensity and the mole fraction of styrene/2-deuterated styrene copolymers. On the basis of this method, the temperature dependence of band

intensity in polymer solution was interpreted by following procedure.[18]

The total fraction F(m) of the regular sequence containing m monomer units can be represented by the equation

$$F(m)=p^{m-1}[m-(m-1)p] \qquad (5-1)$$

$$\sigma=(1-p)/p \qquad (5-2)$$

where p is the mole fraction of regular part, and σ means the ratio of irregular to regular parts. Therefore, σ can be represented by free energy difference per mole of monomeric units ($\Delta G=G_{irregular}-G_{regular}$) between the irregular and the regular helical state.

$$\sigma=\exp(-\Delta G/RT) \qquad (5-3)$$

$$\Delta G=\Delta H-T\Delta S \qquad (5-4)$$

where ΔH and ΔS are the corresponding enthalpy and entropy differences, respectively. F(m) is estimated as the ratio of observed intensity of a given band to that for the perfect crystalline ; $F(m)=R/R_0$. The value of m for 917 cm^{-1} band of IPS has been estimated as to be 10 (determined from isotope dilution[17]). From the experimental values of F(10) vs. T for this band, values of $\sigma(T)$ at T were calculated by equation 5-1. Figure 5-12 shows a plot of log σ vs. 1/T, which according to equation 5-4 gives ΔH and ΔS as shown in the Figure. With these values, the theoretical curves are derived for various values of m (solid lines in Figure 5-13). Thus, with the measured intensities of

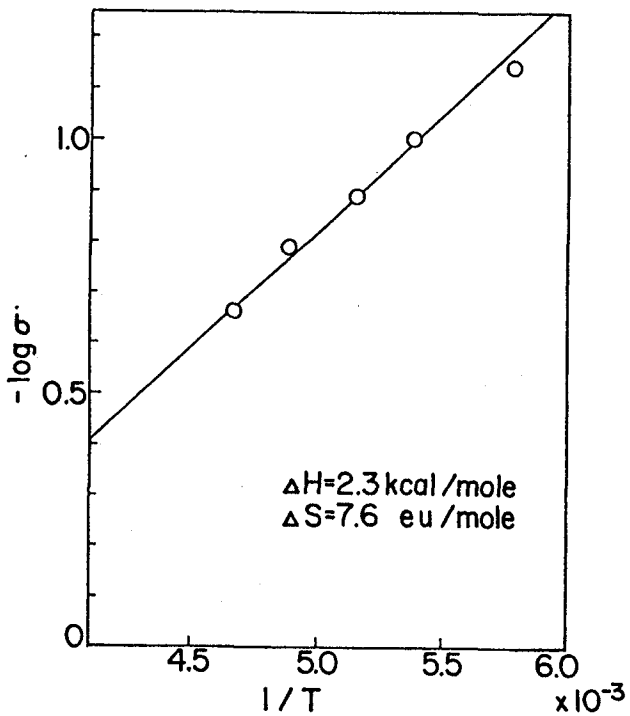

Figure 5-12. The -log σ vs. 1/T plot (m=10) for the 917 cm^{-1} band of IPS.

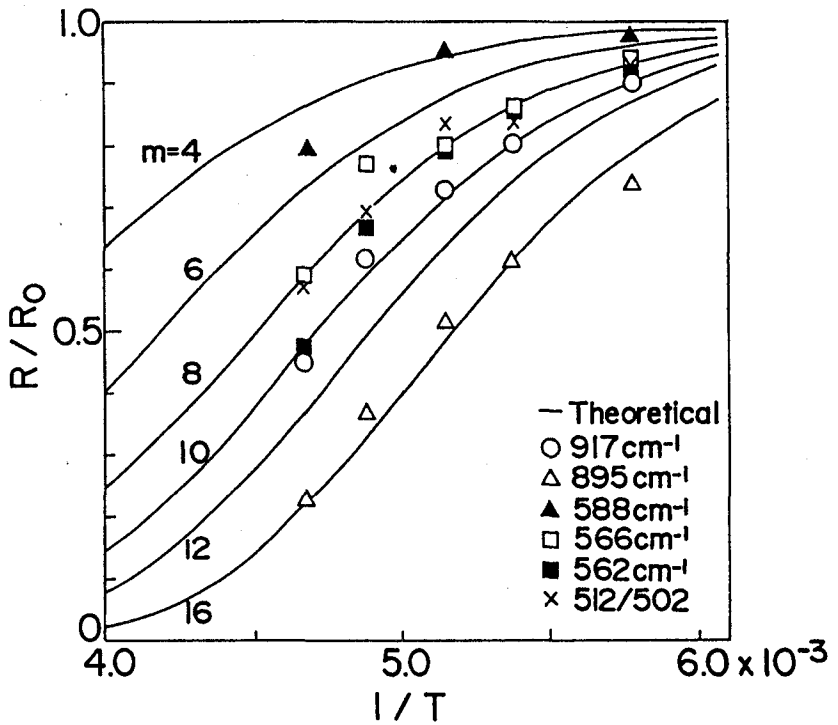

Figure 5-13. Temperature dependence of infrared intensities of the helix bands of IPS.

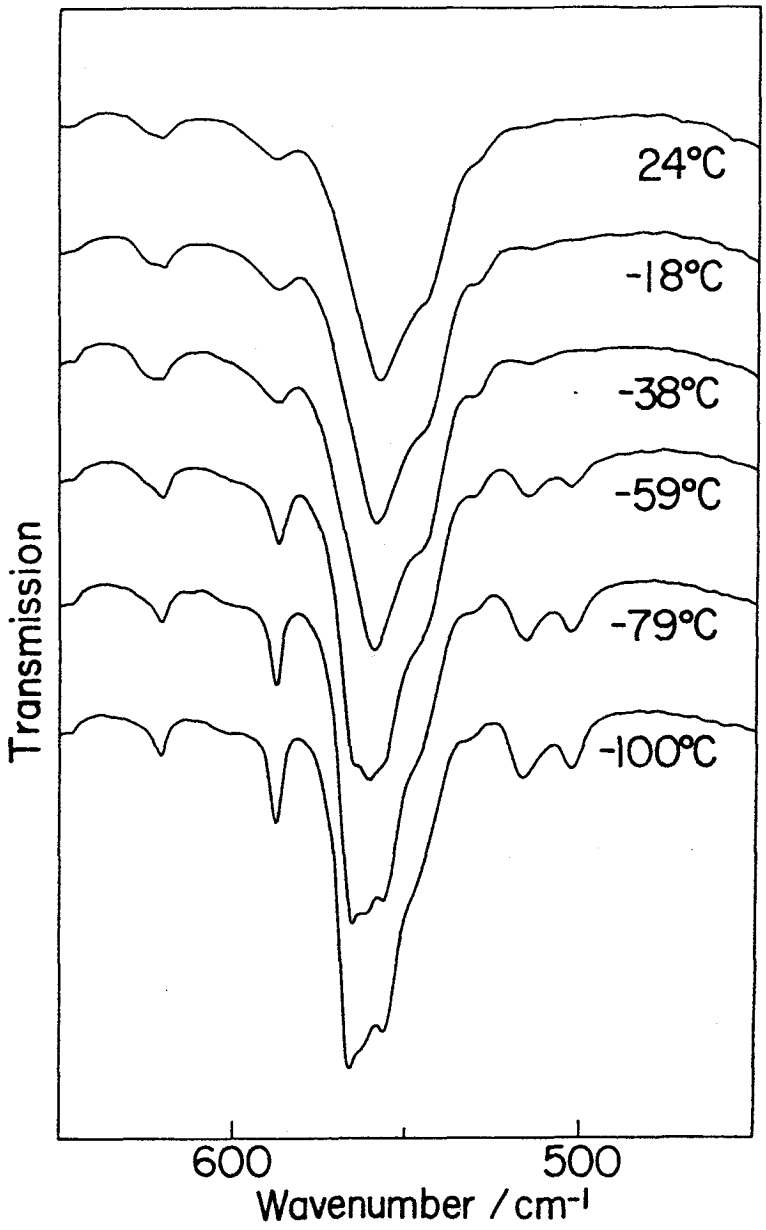

Figure 5-14. Temperature dependence of the infrared spectrum in the 500-600 cm^{-1} range of an IPS/CS_2 gel (20 w/v%).

these conformational sensitive bands of IPS, along with the m values, we are able to evaluate the orderliness of the TG conformation.

The ordering process of the skeletal conformation during the gelation of an IPS/CS_2 (20w/v%) system was followed by monitoring the intensity changes of the bands in the range of 500-600 cm^{-1} (Figure 5-14). The absorption profile was divided into seven Lorentzian components by band separation method, and the integrated intensity of each component was plotted against temperature (Figure 5-15). On cooling, the intensities of the 566, 562 and 517 cm^{-1} bands due to the TG form begin to increase steeply at the gelation point (~-50°C), while those of the 546 and 566 cm^{-1} bands due to the TT form start to decrease at the same temperature. The m values of these bands were determined from the temperature dependence of their absorbances. For a particular band, the absorbance was measured at a temperature T. The R_0 value is obtained from the absorbance of the highly crystalline sample, where it becomes independent of temperature. Thus, one can estimate the m value for each helix band by comparing the $R(T)/R_0$ vs. $1/T$ plot with the calculated curves of F(m) (Figure 5-13). The results are listed in Table 5-1. The 500-600 cm^{-1} region is comparatively sensitive to the short conformational ordering, corresponding to m=6-8. The appearance of the 894 cm^{-1} band having m=16 indicates that regular sequences longer than 5 turns of the (3/1) helix are formed in gel.

It has been confirmed that the intensity of infrared spectra is closely related to the conformational stability of the polymer molecules, and gives the important information for local ordering

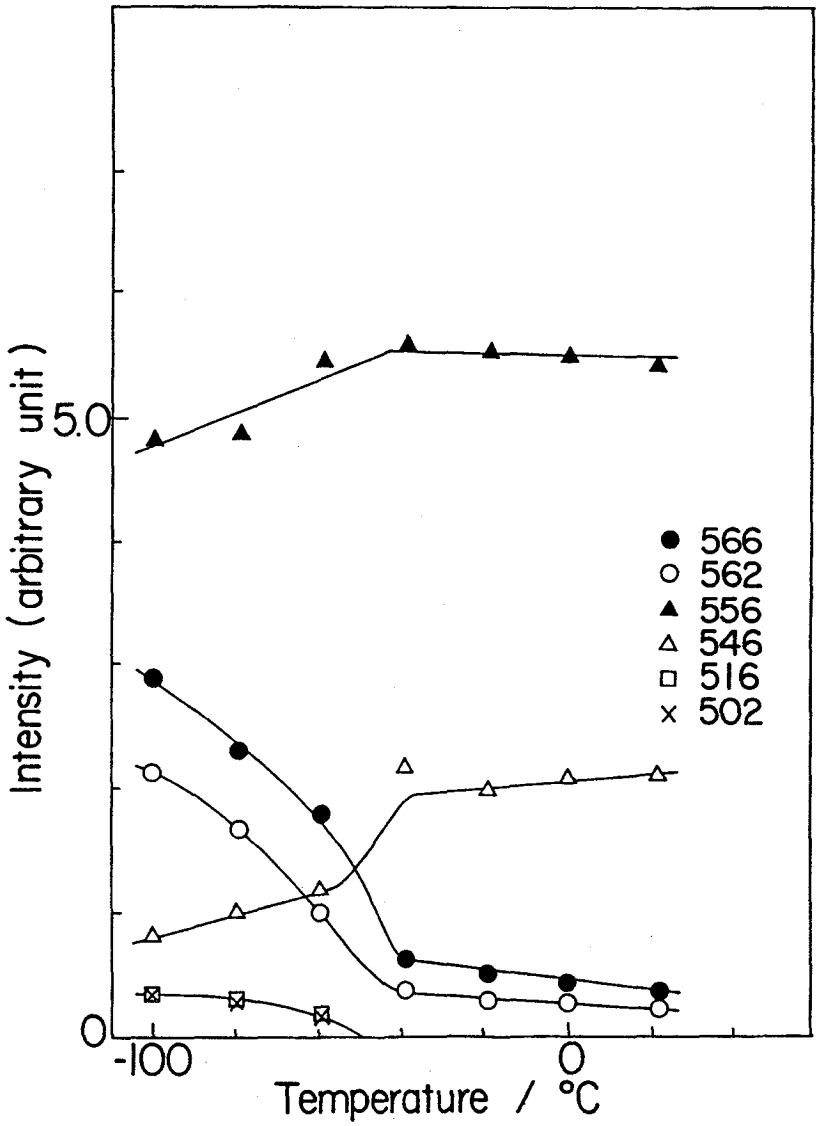

Figure 5-15. Temperature dependence of the integrated intensities of the bands characteristic of the local conformation in IPS/CS_2 gel (20 w/v%).

Table 5-1. Critical sequence length (m) of each regularity-sensitive band.

band/cm^{-1}	m/monomer unit
917	10
894	16
588	4-6
566	8
562	8
512	6-8
502	6-8

of a polymer chain in gel. It is worthy to note that the bands in 500-600 cm^{-1} corresponds to short conformational order ($m \sim 6$-8). This result will be applied to the following chapter.

References

1) G. Natta, P. Pino, P. Corradini, F. Danusso, E. Mantica, J. Am. Chem. Soc., 77, 1700 (1955).

2) G. Natta, F. Danusso, G. Moraglio, G. Natta, Makromol. Chem., 28, 166 (1958).

3) G. Natta, P. Corradini, I. W. Bassi, Nuovo Cimento, Suppl., 15, 68 (1960).

4) M. Girolamo, A. Keller, K. Miyasaka, N. Overbergh, J. Polym. Sci., Polym. Phys. Ed., 14, 39 (1976).

5) E. D. T. Atkins, D. H. Isaac, A. Keller, K. Miyasaka, J. Polym. Sci., Polym. Phys. Ed., 15, 211 (1977).

6) E. D. T. Atkins, D. H. Isaac, A. Keller, J. Polym. Sci., Polym. Phys. Ed., 18, 71 (1980).

7) E. D. T. Atkins, A. Keller, J. S. Shapiro, P. J. Lemstra, Polymer, 22, 1161 (1981).

8) E. D. T. Atkins, M. J. Hill, D. A. Jarvis, A. Keller, E. Sarhene, J. S. Shapiro, Colloid & Polymer Sci., 232, 22 (1984).

9) P. R. Sundararajan, Macromolecules, 12, 575 (1979).

10) P. R. Sundararajan, N. J. Tyrer, Macromolecules, 15, 1004 (1982).

11) N. J. Tyrer, T. L. Bluhm, P. R. Sundararajan, Macromolecules, 17, 2296 (1984).

12) J. -M. Guenet, Macromolecules, 19, 1961 (1986).

13) J. -M. Guenet, G. B. McKenna, Macromolecules, 21, 1752 (1988).

14) M. Klein, J. -M. Guenet, Macromolecules, 22, 3716 (1989).

15) M. Klein, A. Brulet, J. -M. Guenet, Macromolecules, 23, 540 (1990).

16) M. Klein, A. Mathis, A. Menelle, J. -M. Guenet, Macromolecules, 23, 4591 (1990).

17) M. Kobayashi, K. Akita, H. Tadokoro, Die Makromol. Chem., 118, 324 (1968).

18) M. Kobayashi, K. Tsumura, H. Tadokoro, J. Polym. Sci., A-2, 6, 1493 (1968).

19) P. C. Painter, R. E. Kessler, R. W. Snyder, J. Polym. Sci., Polym. Phys. Ed., 18, 723 (1980).

20) P. C. Painter, J. L. Koenig, J. Polym. Sci., Polym. Phys. Ed., 15, 1885 (1977).

21) R. W. Snyder, P. C. Painter, Polymer, 22, 1633 (1981).

CHAPTER 6

Gelation Mechanism and Structure in Gels of Atactic Polystyrene

6-1. Introduction

The thermoreversible gelation of crystallizable polymers can be ascribed to the formation of microcrystallites. In the case of syndiotactic (SPS) and isotactic (IPS) polystyrenes, we revealed that gelation was accompanied with the formation of crystallite-like coagurates consisting of polymer-solvent. However, gels formed from non-crystallizable polymers contain more complex problem. Wellinghoff et al. reported that non-crystalline atactic polystyrene (APS) also forms thermoreversible gel.[1] Tan et al. carried out systematic thermal analyses, and presented the temperature-concentration phase diagram.[2] Later, Guenet et al. demonstrated that gel melting enthalpy took a critical point at a particular concentration like the cases of SPS and IPS, indicating that the cross-links consisted of a stoichiometric complex between polymer and solvent molecules.[4] Recently neutron scattering method has been developed to analyze the gel structure, because the use of deuterated polymer gives the large difference in diffraction power from that of solvent. Small angle neutron scattering (SANS) measurements on the sol-gel transition of APS/CS_2 system have been carried out by Izumi et al.[6-11] They showed that the scattering exponents along the gelation curve cross over from -2 to -4. Guenet et al. carried out a wide angle neutron diffraction experiment, and elucidated the formation of

a local ordered structure.[12,13] This structure was confirmed from the increase in intensity at 1.095 nm on gelation of APS/CS_2 solution. Although they considered the peak associated with the distance between first neighboring stems, the distance observed is a little large in comparison with the lattice constants of IPS and SPS crystallines. So they considered that the lattice spread by the formation of a polymer-solvent complex derived from thermodynamic studies.[4]

Nowadays, we are able to prepare polystyrene samples with various tacticities covering the whole range from highly isotactic to highly syndiotactic. Therefore, the polystyrene-solvent system is the most suitable one to study the role of the stereoregularity in the molecular level mechanism of the gelation process.

6-2. Experimental

6-2-1. Samples

The APS sample prepared by radical polymerization was supplied from Sekisui Chemical Co. Ltd. (Styron 666-7). The diad syndiotacticity was evaluated as 65% by ^{1}H-NMR. In order to investigate the relationship between the stereoregularity and gelation mechanism, we carried out epimerization reaction by using IPS sample as a starting material. Epimerization was conducted by heating at 100^{o}C IPS dissolved in hexamethyl phosphoramide containing potassium t-butoxide.[14,15] The tacticity of the resultant polymer was adjusted by the reaction time. The epimerized samples are referred as EPSn, n being the reaction

time in hour. Gels of these samples were prepared by dissolving in carbon disulfide (CS_2)(20 w/v%), and then cooling below -50°C.

6-2-2. Measurements

Infrared spectra (with 1 cm^{-1} resolution) were measured by using a JASCO FT-IR 8000 spectrometer equipped with a DTGS detector. Spectra were accumulated 50 times. A home-made solution cell with a lead spacer of 100 μm thickness inserted between KBr windows was used. For measurements at low temperatures, an Oxford flow-type cryostat was used. ^{1}H-NMR spectrum was recorded at 400 MHz using a JEOL GSX 400 spectrometer, on a 1,1,2,2-tetrachloroethane-d_2 solution (5 w/v%) at 120°C. Figure 6-1 shows the ^{1}H-NMR spectra of APS and EPS. The peaks at 2.2 and 1.9 ppm arise from the methine protons. The 2.2 ppm signal is assigned to the meso-meso (mm) triads and that at 1.9 ppm to the superposition of the racemo-racemo (rr) and meso-racemo (mr).[14,15] The tacticities are evaluated as listed in Table 6-1. Figure 6-2 shows the fraction of rr+(rm+mr) triads as a function of reaction time. Our results are a little smaller than calculation.[14] The longer the reaction time, the smaller the value of isotacticity. These values were converted to diad tacticity by assuming Bernoullian statistics. The present samples cover the range 0.4-0.87 of the meso diad (Pm).

6-3. Results and Discussion

6-3-1. Gel structure of APS

Radical polymerization of styrene (Styron 666-7) is the

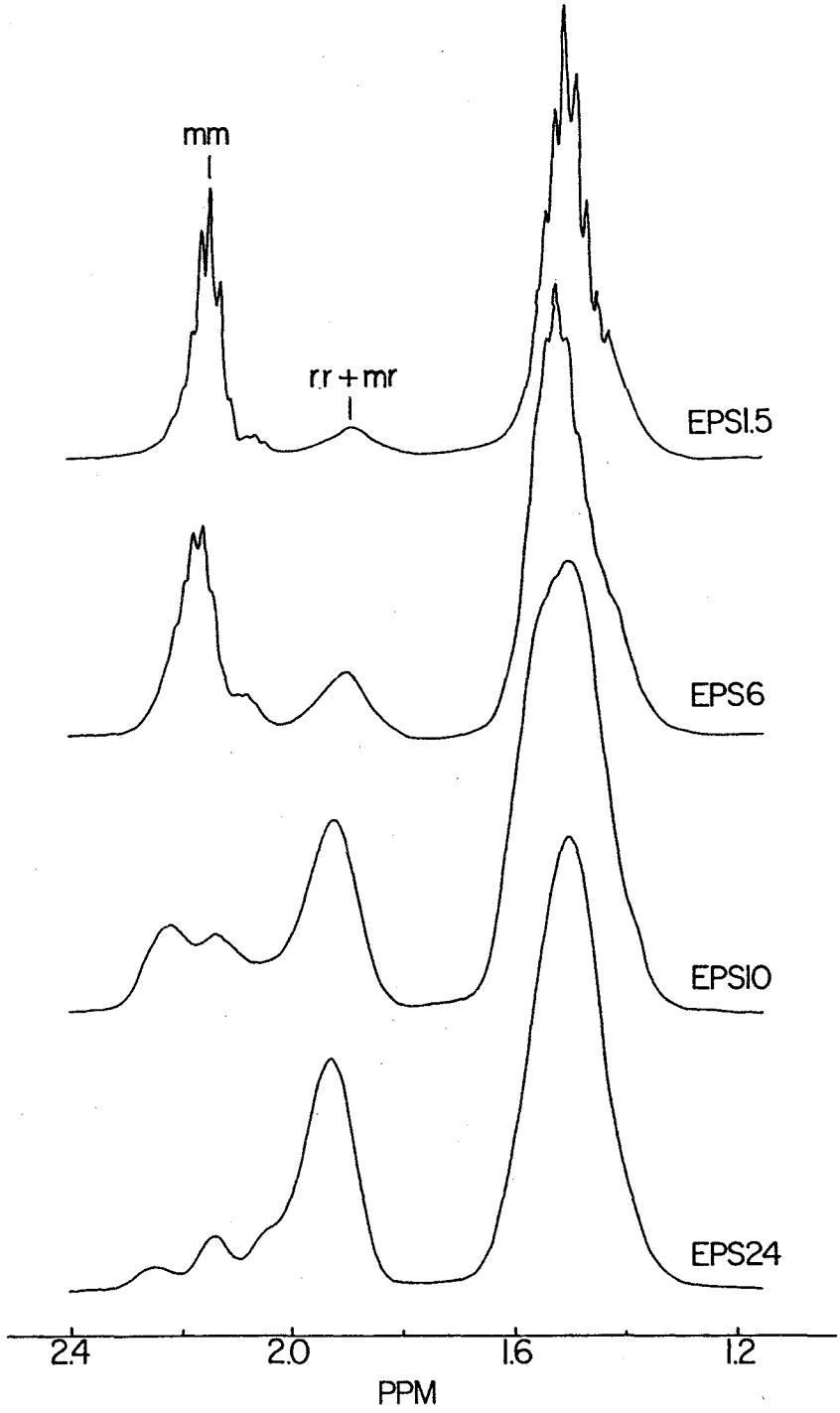

Figure 6-1. ^{1}H-NMR spectra of EPS at 120^{o}C.

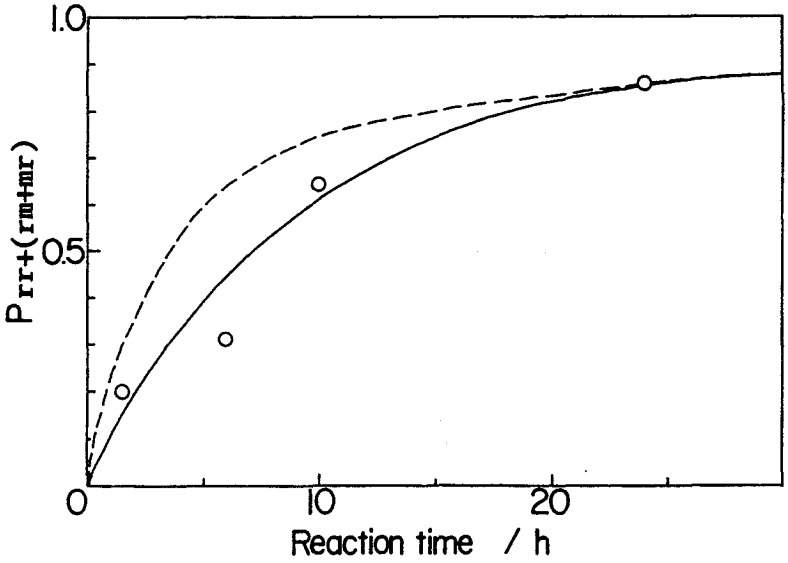

Figure 6-2. Reaction time dependence of triad tacticity.

Table 6-1. Stereoregularity of epimerized and radical-polymerized polystyrenes.

	Pmm	Pm	n_m
EPS1.5	0.80	0.87	11.1
EPS6	0.69	0.80	8.1
EPS10	0.36	0.57	2.9
EPS24	0.14	0.40	1.7
APS-R	0.06	0.35	-

Pmm and Pm: Probability of meso triad and diad, respectively.

n_m: Average length of isotactic sequences.[15]

most typical for preparing APS samples. As shown in Table 6-1, this sample takes predominantly syndiotactic sequences (Pr=0.65). The gelation of APS/CS_2 system was detected by temperature dependence of the half-width of the ^{13}C-NMR signals. This shows that the mobility of polymer chain is restricted by making three dimensional network structures. Infrared spectrum is very sensitive to analyze a short conformational change. In Figure 6-4, the gelation process of an APS/CS_2 system (20w/v%) was followed by infrared spectroscopy. Unlike the IPS/CS_2 system, no remarkable spectral change was observed in mid-infrared region on cooling except for the appearance of the 1280 cm^{-1} band characteristic of the TTGG conformation of the syndiotactic part. This indicates that construction of the long regular sequences of TG (the stable form of the isotactic part) and/or TTGG (the stable form of the syndiotactic part in solvated states) is restricted because of short stereoregular sequence length. In the 500-600 cm^{-1} region, a detectable change in the absorption profile is observed, reflecting the change in the local conformation. The bands in this region are associated with out-of-plane modes of phenyl ring. The frequencies are dependent on the local skeletal conformation. The spectral features of APS gels do not depend on the solvent as shown in Figure 6-5, although relative intensities vary a little with condition of gelation.

This 500-600 cm^{-1} region seems to be very complicated by superposition of several absorption bands, but is able to fit by using band profiles of SPS and IPS as shown in Figure 6-6 [Three peaks for SPS (572, 548 and 540 cm^{-1}) and four peaks for IPS (566,

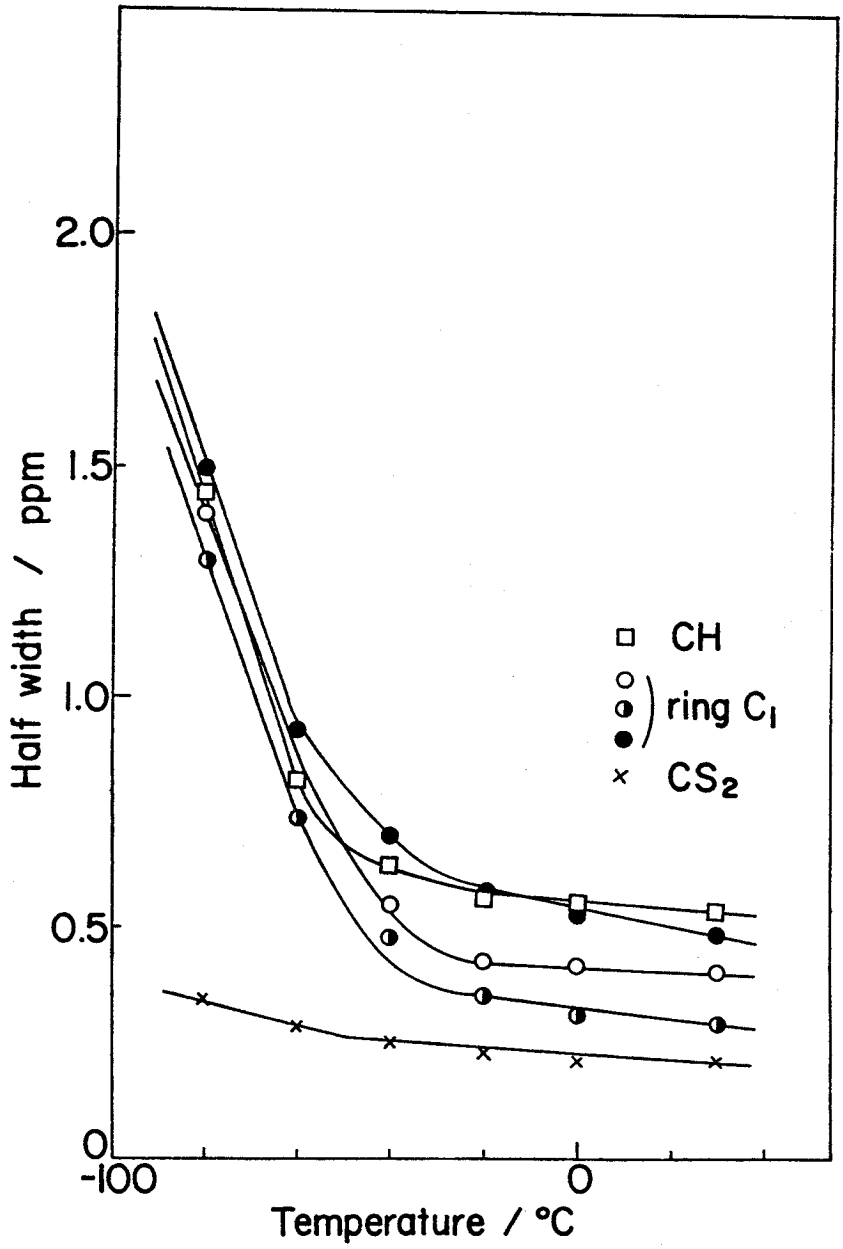

Figure 6-3. Temperature dependence of the half-width of the ^{13}C-NMR signals of a APS/CS_2 solution (20 w/v%).

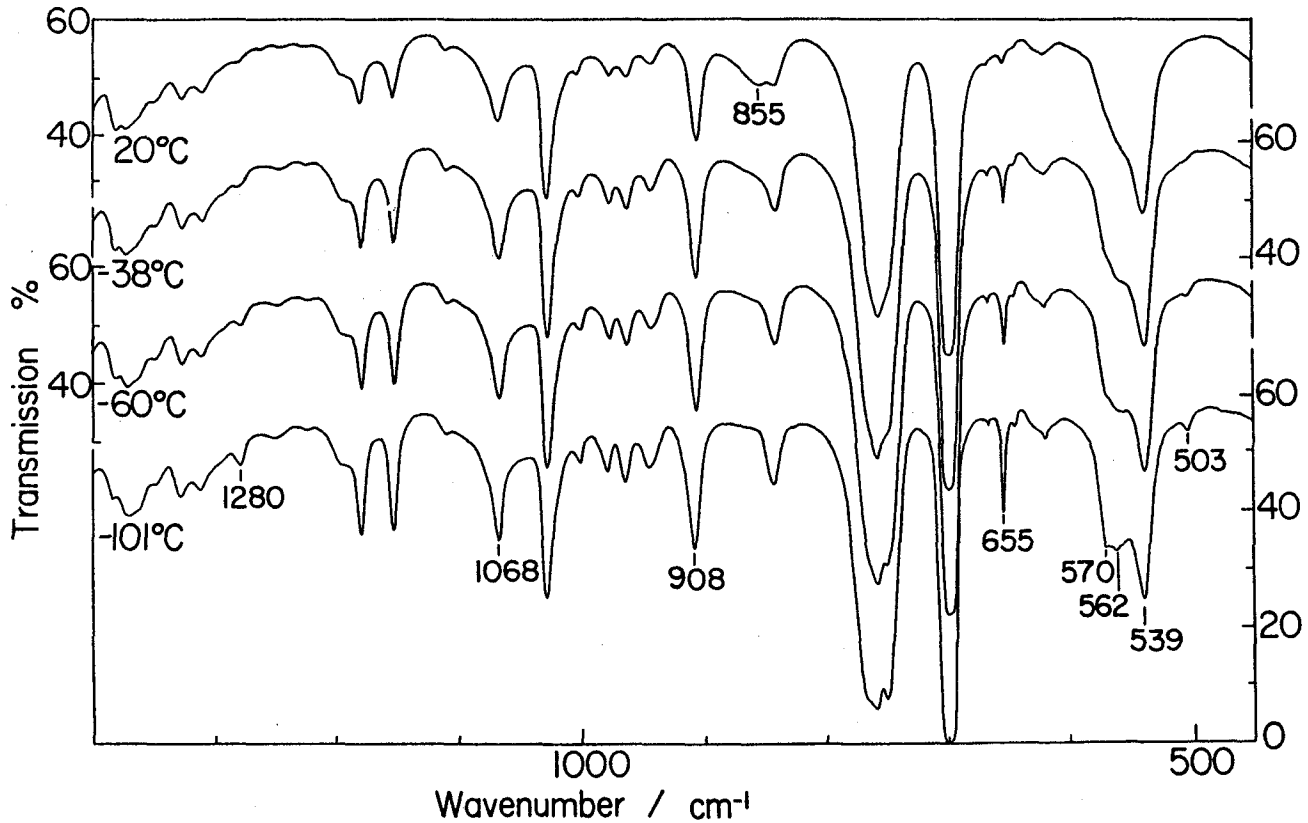

Figure 6-4. The temperature dependence of the infrared spectrum of a APS/CS_2 solution (20 w/v%).

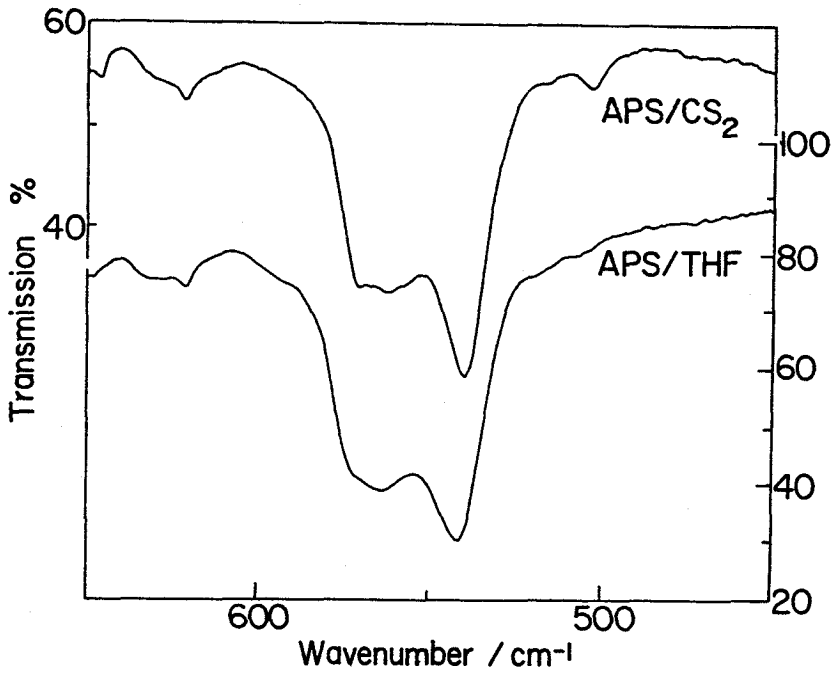

Figure 6-5. Infrared spectra of APS/CS_2 and THF gels at -100°C.

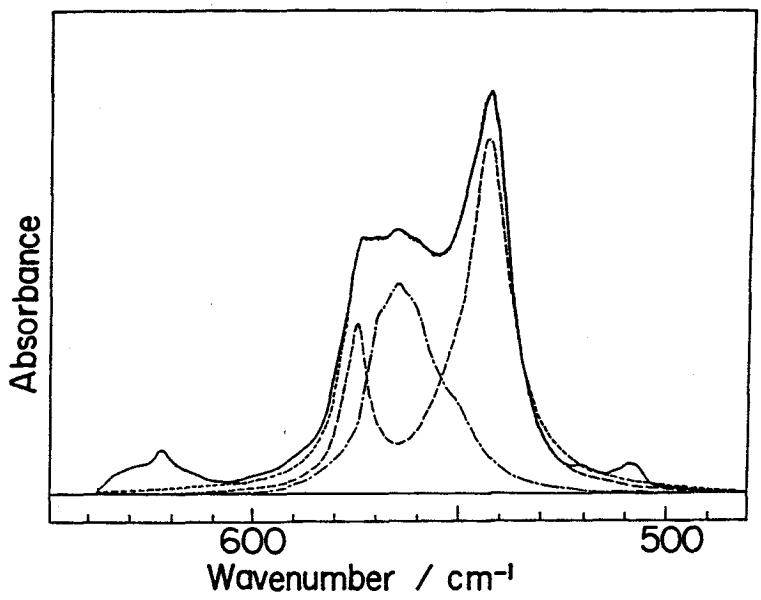

Figure 6-6. Infrared spectrum of APS/CS_2 gel after curve fitting, ——: observed, ---: calculated, — —: syndiotactic component, -·-: isotactic component.

562, 556 and 546 cm^{-1}) were used.]. A good agreement was obtained between observed and calculated curves. The integrated intensities of each bands are plotted against temperature (Figure 6-7). The most conspicuous increase in intensity on gelation is observed for the 572 cm^{-1} band associated with the TTGG form, while the 566 and 562 cm^{-1} bands due to the TG form undergo a slight and continuous increase on cooling. From the analysis of critical sequence length of IPS gel (see Chapter 5), the appearance of bands in 500-600 cm^{-1} corresponds to m=6-8. Therefore, the cross-links consist of ca. 2 turns of TTGG for SPS.

The appearance of 572 cm^{-1} band suggests that the formation of short TTGG sequences promote gelation even in such non-crystallizable polymers. However, compared with SPS gel the intensity of 572 cm^{-1} band is not so strong even at -100°C, suggesting the low density of cross-links. Judging from the fact that no crystallization takes place in a bulk state, it is worth noting that the solvent plays a significant role for stabilizing conformation. Namely, the existence of ordered structure in spite of non-crystallizable in solid state is due to the formation of complex structure with solvent molecules.

6-3-2. The relationship between gel structure and stereoregularity

In order to investigate the gel structure depending on stereoregularity, we measured infrared spectra of EPS/CS_2 gel. As the stereoregular sequences of EPS samples are not so long, the gelation bands are restricted in analogy with the case of

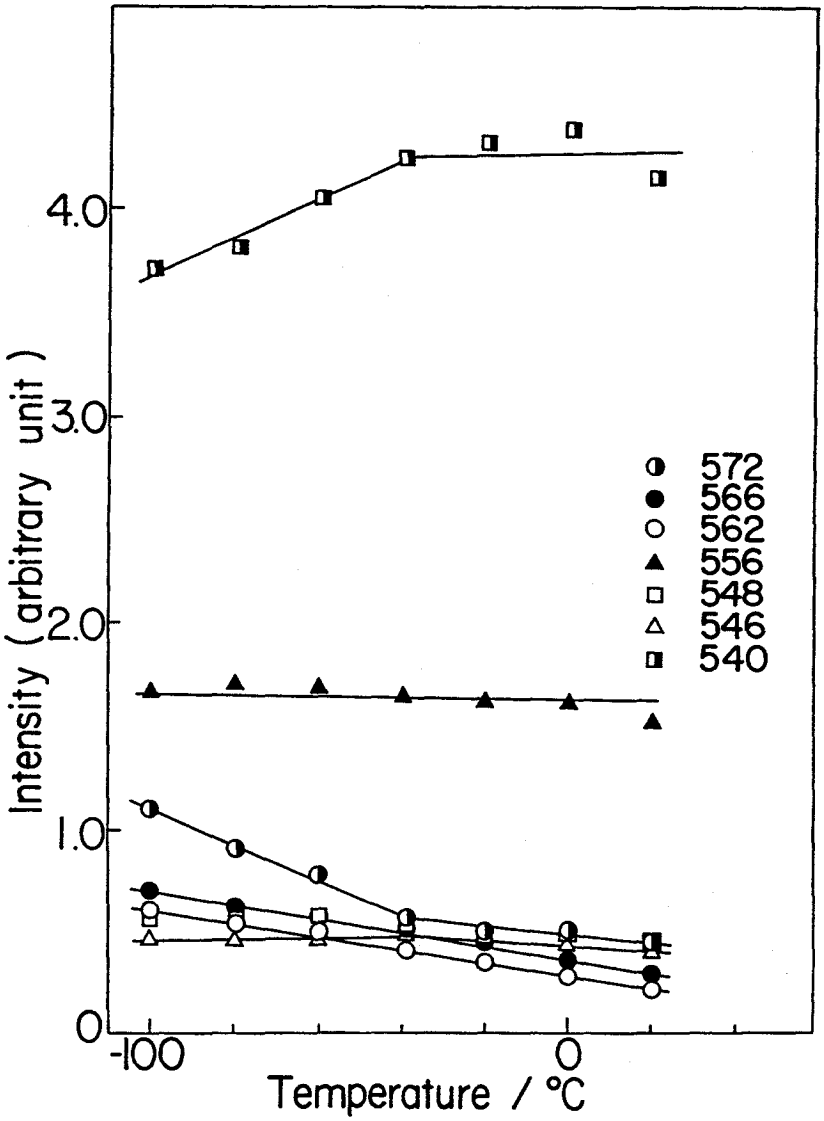

Figure 6-7. Temperature dependence of the integrated intensities of the bands characteristic of the local conformation in APS/CS_2 gel.

radical polymerized APS gel. Figure 6-8 shows infrared spectra of IPS, EPS1.5 and EPS6 gels at about -100°C in 850-960 cm^{-1} region. The intensities of 917 and 894 cm^{-1} bands are very strong in IPS gel compared with that of EPS1.5 and EPS6 gels. As revealed in chapter 5, these bands correspond to the m=10 and m=16, respectively. In the spectrum of EPS1.5 gel, the presence of these bands indicates that the long ordered sequences with m>10 still remain, whereas they do not appear in that of EPS6 gel. This is consistent with the analysis of average length of isotactic sequences (11 for EPS1.5 and 8 for EPS6) shown in Table 6-1.

Figure 6-9 shows the infrared spectral change on gelation of four different stereoregular polystyrenes in 500-600 cm^{-1} region. In isotactic-rich samples like EPS1.5, the 566 and 562 cm^{-1} bands due to the TG sequences of IPS increase in intensity with decreasing temperature. Contrary to the bands around 900 cm^{-1}, the intensities of these bands are kept to some magnification even for the samples of very low isotacticity, because both bands are related to short conformational arrangements. With increasing syndiotacticity, the 572 cm^{-1} band characteristic of TTGG sequences of SPS appear. The type of the ordered molecular conformation that contributes to the gelation crosses over the TG sequences of the isotactic parts to the TTGG sequences of the syndiotactic parts at the critical value $Pm \sim 0.7$ of the meso diad tacticity. As the TTGG structures of SPS is more stable than that of IPS, the critical tacticity for gelation is closer to one taking complete isotactic sequences.

These results demonstrate that the physical gelation of non-crystalline polymer is accompanied by the formation of locally

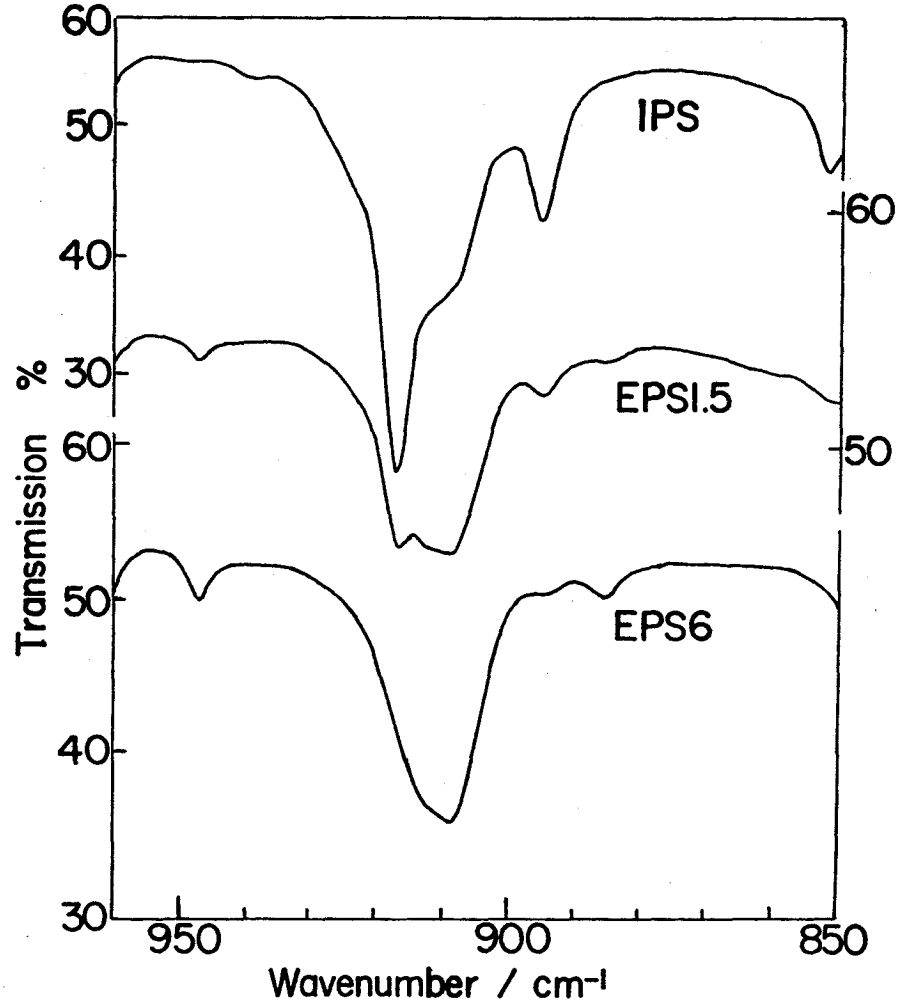

Figure 6-8. Infrared spectra of IPS and EPS gels at -100°C. The 917 and 894 cm^{-1} bands correspond to m=10 and m=16, respectively.

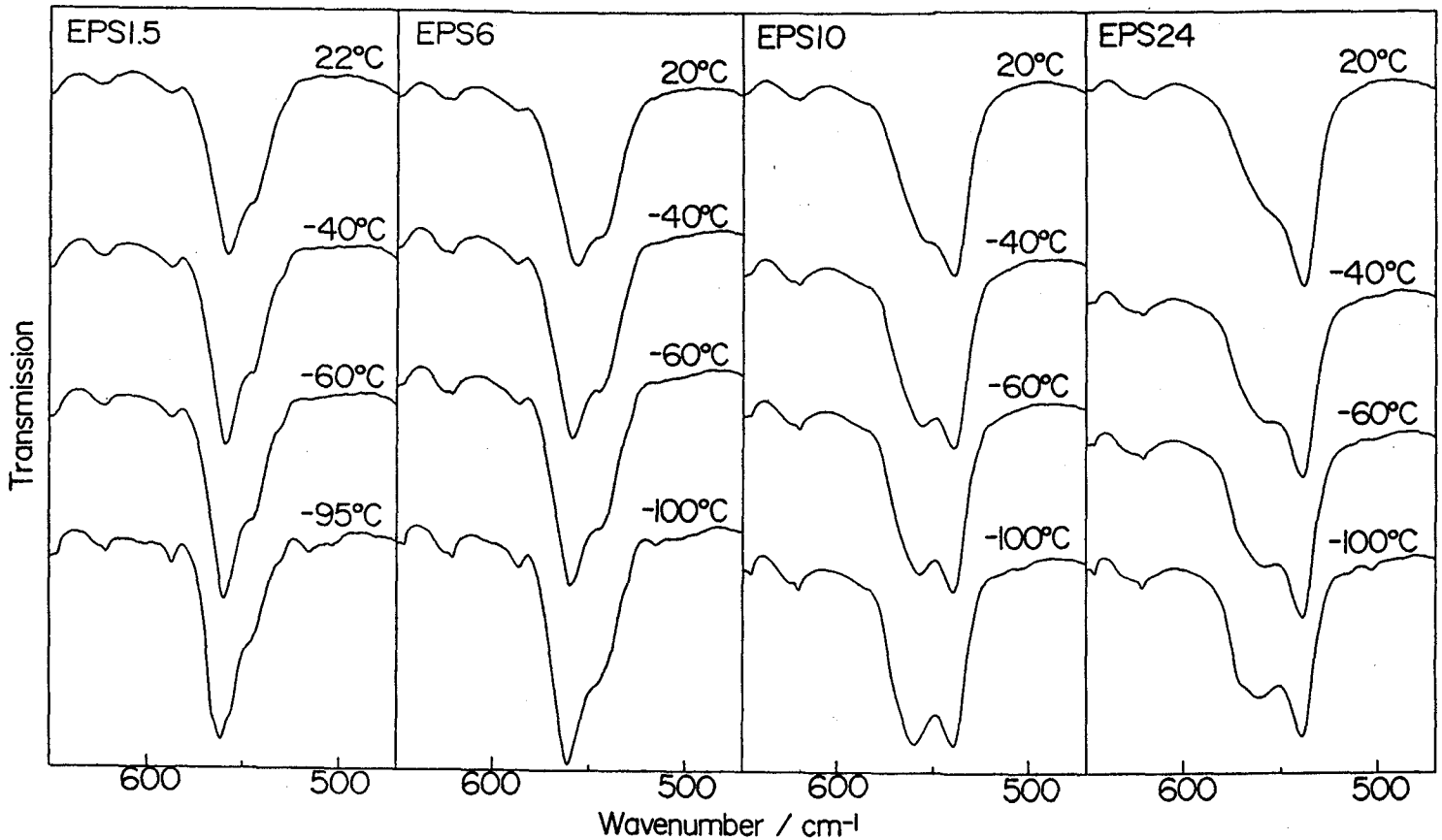

Figure 6-9. Infrared spectral change on a cooling process of various EPS/CS_2 gels (20 w/v%).

ordered conformation formed in the respective stereoregular sequences.

In conclusion for various stereoregular polystyrenes from highly syndiotactic to isotactic samples, the gelation mechanism is interpreted as the same whatever the polymer is crystallizable or non-crystallizable. Namely, gelation requires conformational arrangement of polymer molecules to which solvation presumably plays important roles.

References

1) S. J. Wellinghoff, J. Shaw, E. Baer, Macromolecules, **12**, 932 (1979).
2) H. Tan, A. Hiltner, E. Moet, E. Baer, Macromolecules, **16**, 28 (1983).
3) R. M. Hikmet, S. Callister, A. Keller, Polymer, **29**, 1378 (1988).
4) J. Francois, J. Y. S. Gan, J. M. Guenet, Macromolecules, **19**, 2755 (1986).
5) X.-M. Xie, A. Tanioka, K. Miyasaka, Polymer, **31**, 281 (1990).
6) Y. Izumi, Y. Miyake, M. Iizumi, N. Minakawa, S. Katano, Rep. Prog. Polym. Phys. Jpn., **29**, 5 (1986).
7) Y. Izumi, Y. Miyake, S. Katano, N. Minakawa, M. Iizumi, Rep. Prog. Polym. Phys. Jpn., **29**, 7 (1986).
8) Y. Izumi, Y. Miyake, M. Furusaka, H. Kumano, K. Kurita, KENS Report VI, IV, 151 (1985/1986).
9) Y. Izumi, Y. Miyake, K. Inoue, Rep. Prog. Polym. Phys. Jpn., **30**, 3 (1987).

10) Y. Izumi, T. Matsuo, Y. Miyake, M. Arai, M. Furusaka, S. Hirota, K. Kurata, KENS Report, VII, 103 (1987/1988).

11) Y. Izumi, T. Matsuo, Y. Miyake, S. Katano, N. Minakawa, M. Iizumi, S. Furuhashi, M. Arai, M. Furusaka, S. Hirota, K. Kurita, Rep. Prog. Polym. Phys. Jpn., **31**, 5 (1988).

12) J. -M. Guenet, M. Klein, A. Menelle, Macromolecules, **22**, 493 (1989).

13) J. -M. Guenet, M. Klein, Makromol. Chem. Macromol. Symp., **39**, 85 (1990).

14) L. Shepherd, T. K. Chen, H. J. Harwood, Polym. Bull., **1**, 445 (1979).

15) J. Francois, J. Gan, D. Sarazin, J. M. Guenet, Polymer, **29**, 898 (1988).

CHAPTER 7

Glassy state of various stereoregular polystyrenes

7-1. Introduction

Elucidation of molecular level structure of polymer glasses and melts has been one of the main subjects of polymer science. Both syndiotactic (SPS) and isotactic polystyrene (IPS) samples form a glassy state when they are rapidly quenched from the melt in iced water. Atactic polystyrene (APS) is in a glassy state below the glass transition temperature Tg=82^{o}C. Although molecular structure in IPS and APS glasses has been studied by infrared and Raman spectroscopy,[1-3] there still remain uncertainties. Therefore, investigation of SPS glass in comparison with IPS and APS glasses seems of importance for understanding the role of stereochemical configuration in the molecular conformation and physical properties of polystyrene glasses.[1-3]

The purpose in this chapter is to clarify the tacticity dependence of local chain conformation and spatial dimension of molecular chain.

7-2. Experimental

7-2-1. Samples

Descriptions of the SPS, IPS, APS and epimerized polystyrene (EPS) samples used are in the previous chapters.

The glassy films are prepared from heating the polymer films a little above the melting point, and then quenching in iced water.

7-2-2. Measurements

Infrared spectra (with 1 cm^{-1} resolution) were taken by using JASCO FT-IR 8000 spectrometer equipped with a DTGS detector. Raman spectra were taken with a JASCO R-500 double monochromator with the 514.5-nm excitation light from an Ar^{+} laser.

The densities of glassy film were measured by the flotation method. The flotation medium used was water-glycerin mixing in which the samples were neither dissolved nor swollen. The densities were determined at 25°C by using a Lipkin-type pyknometer.

7-3. Results and Discussion

7-3-1. Preferred conformation in the Glassy State

Infrared and Raman spectra are sensitive to the local conformation of polymer molecules. Figures 7-1 and 7-2 show infrared and Raman spectra of SPS, APS and IPS, respectively. In infrared spectra, differences among three samples are found in the regions around 1200, 1070, 750 and 550 cm^{-1}. In Raman spectra, the bands around 1200 and 750 cm^{-1} depend on stereoregularity.

The bands in the region of 650-450 cm^{-1} are due to the phenyl ring modes. They reflect the local conformation rather than its sequential array. The infrared spectra in this region of SPS, IPS and APS in various states are compared in Figure 7-3. In crystalline α-SPS, there is only one sharp band at 537 cm^{-1}. In glassy SPS, there appear broad peaks at the both side of the 537 cm^{-1} band. They correspond to the bands at 572 and 502 cm^{-1}

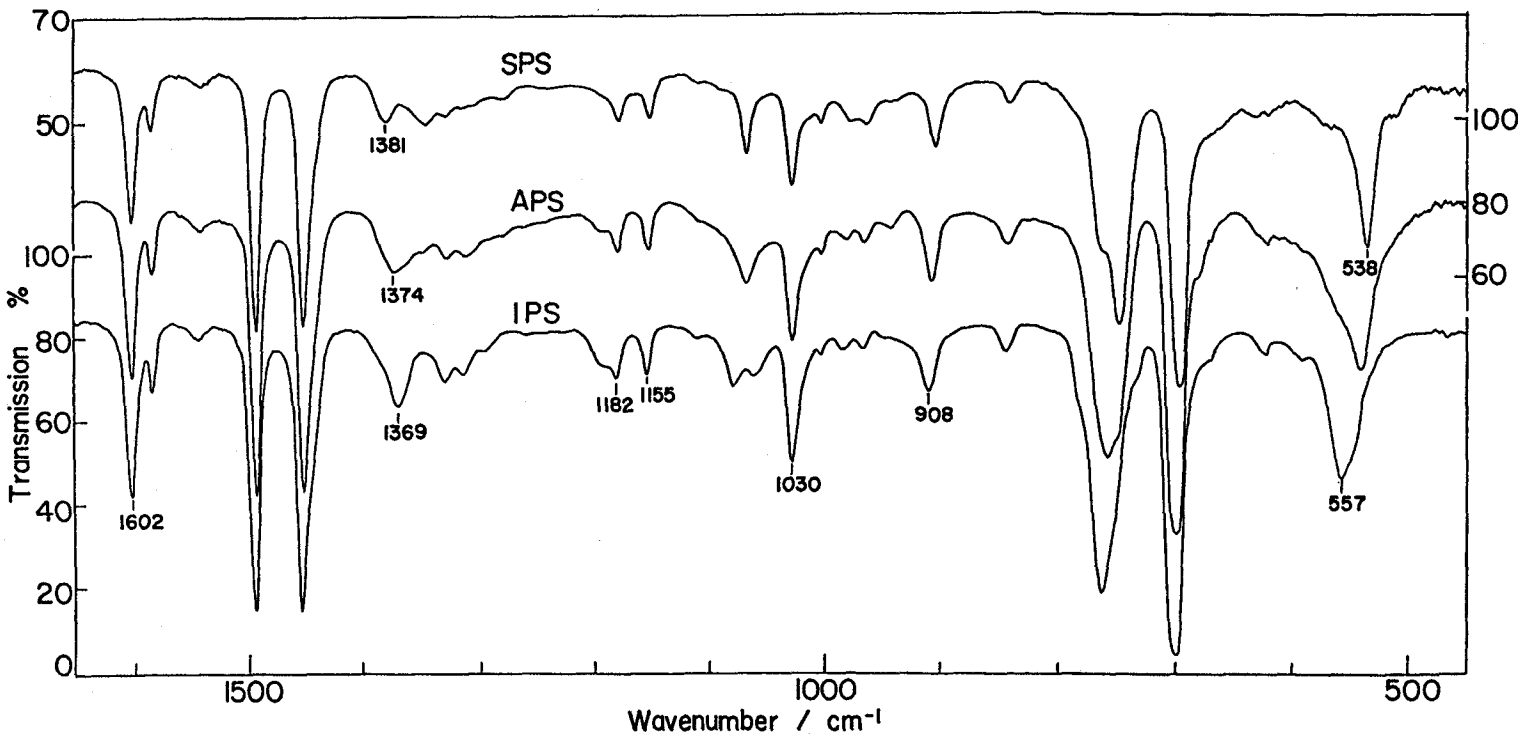

Figure 7-1. Infrared spectra of glassy films of SPS, APS and IPS.

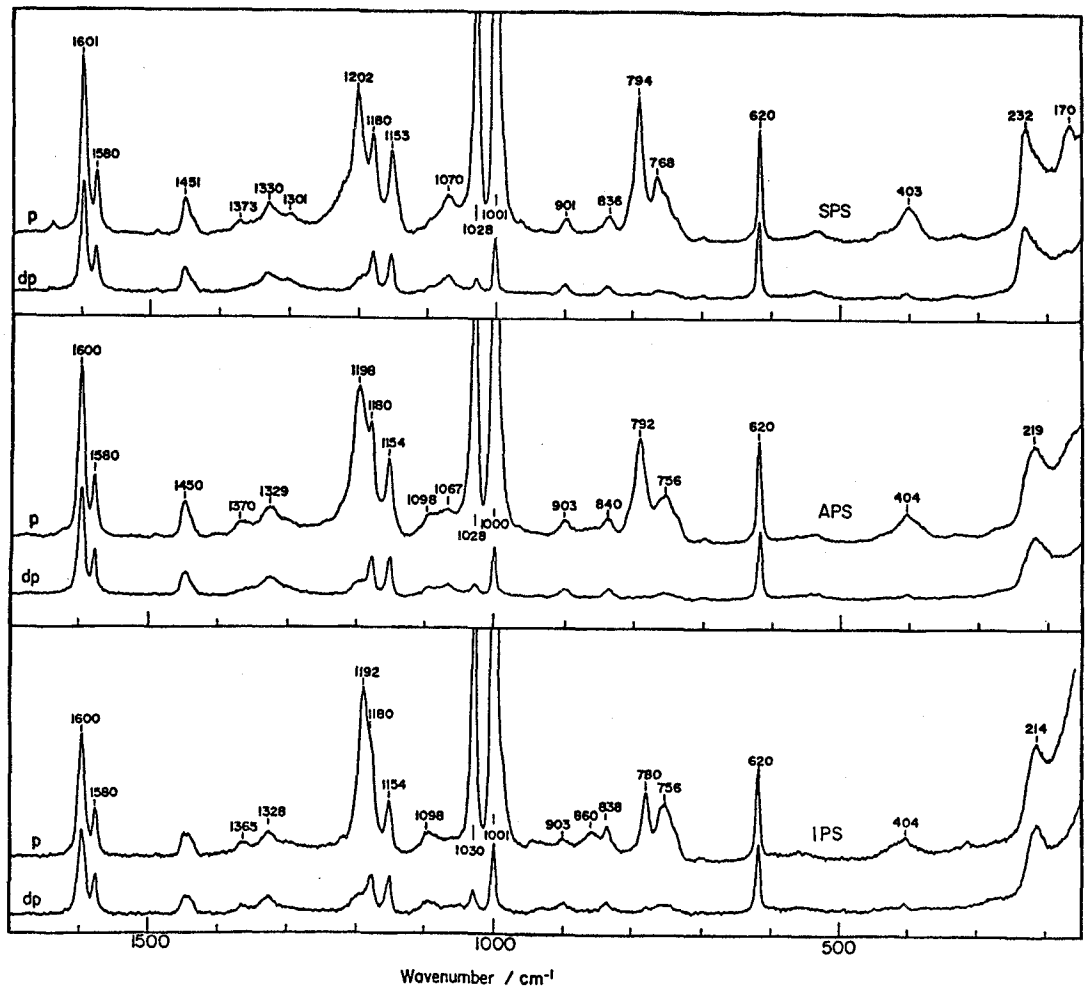

Figure 7-2. Polarized Raman spectra of glassy SPS, APS and IPS.

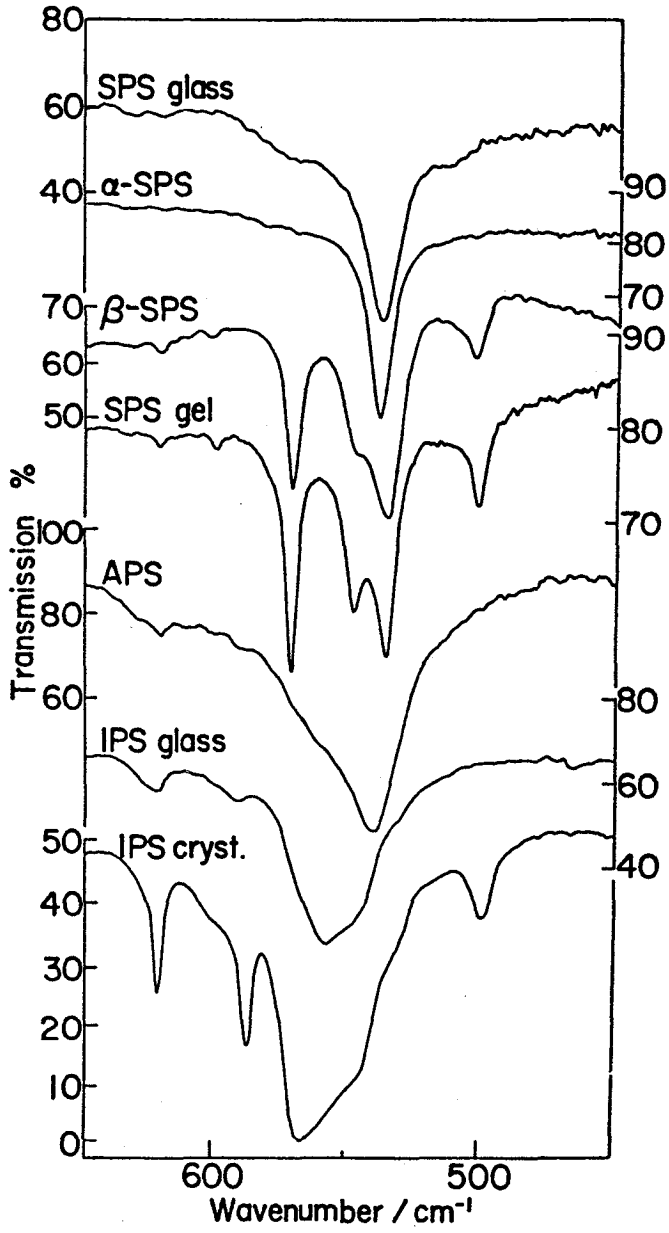

Figure 7-3. Infrared spectra in the 650-450 cm^{-1} region of SPS, APS and IPS in various states.

of crystalline β-SPS. At the same time, the 537 cm^{-1} band becomes a little broder, suggesting a superposition of the absorptions corresponding to the 548 and 536 cm^{-1} of β-SPS. In glassy IPS, all the bands, except for that at 500 cm^{-1}, characteristic of the TG conformation appear, though some of them are weakened and broadened. From these experimental facts, we conclude that there exist some fraction of gauche C-C bonds in glassy SPS. Judging from the relative intensities of the gauche bands, the trans content may be greater in glassy SPS than in glassy IPS. However, from the disappearance of the 1224 cm^{-1} band, there must be no detectable amount of long TT sequences in glassy SPS.

7-3-2. CP/MAS ^{13}C-NMR spectra

Solid-state CP/MAS ^{13}C-NMR spectrum is very sensitive to conformational change. First we attempt the assignment of signals by using that of crystalline states. In Figure 7-4 are shown the ^{13}C-NMR spectra in the region of the aliphatic carbon atoms measured on three different crystalline samples of SPS (upper three) compared with that of IPS (bottom). The SPS spectra are, from the top, that of the α_1, α_2 and β phases. The band profile of each sample was divided into several Lorentzian components by the curve-fitting computer manipulation. In this process, we took the ^{13}C spectra of the glassy samples of SPS, IPS and APS (Figure 7-5) into account for separating the signals due to the amorphous region (the chain lines) from those of the crystalline region (the broken lines). The isotactic ^{13}C chemical shifts of the components thus obtained, along

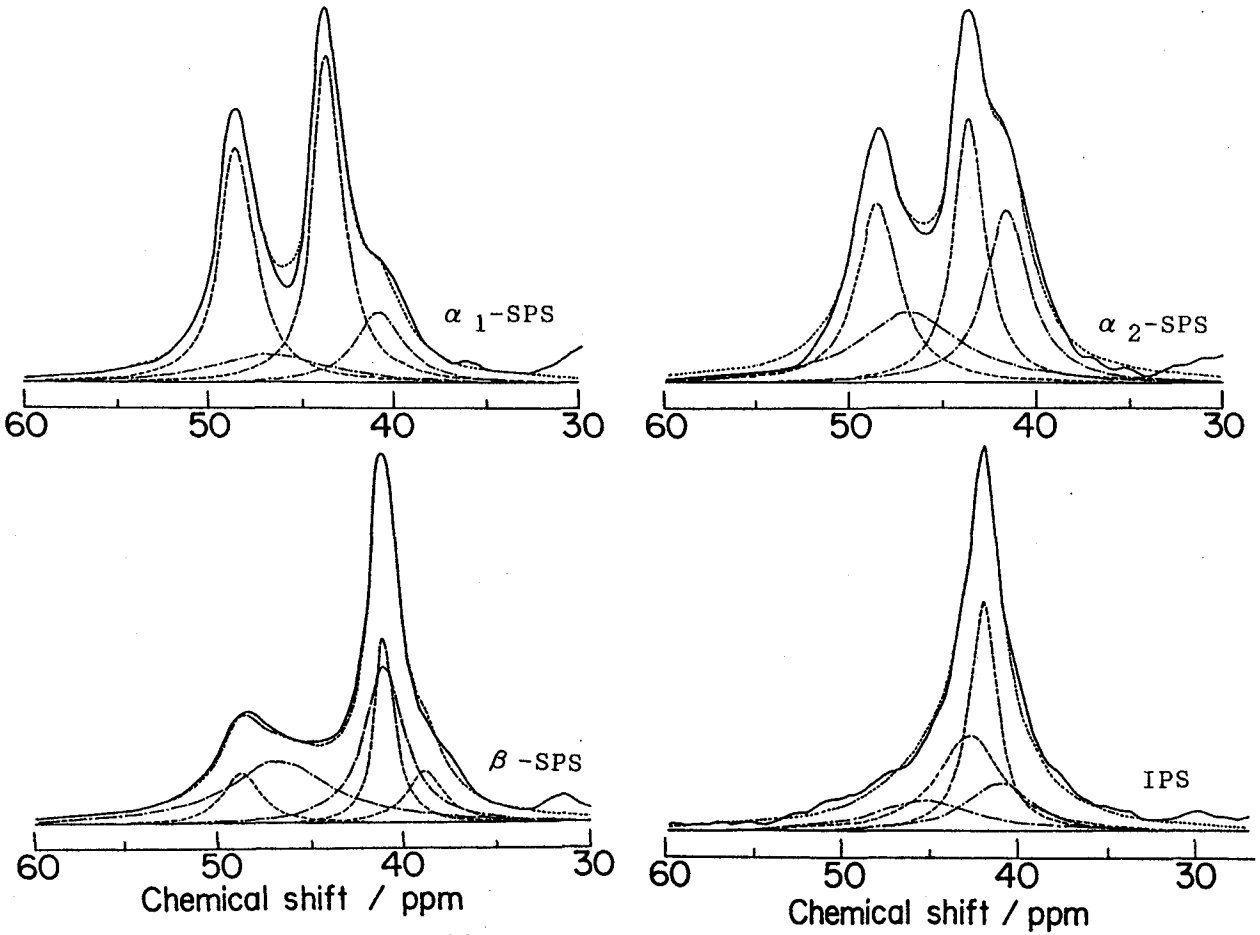

Figure 7-4. CP/MAS ^{13}C-NMR spectra of α_1-SPS, α_2-SPS, β-SPS and IPS. ——: obs., ····· : calc., ---: crystal component, —·—: amorphous component.

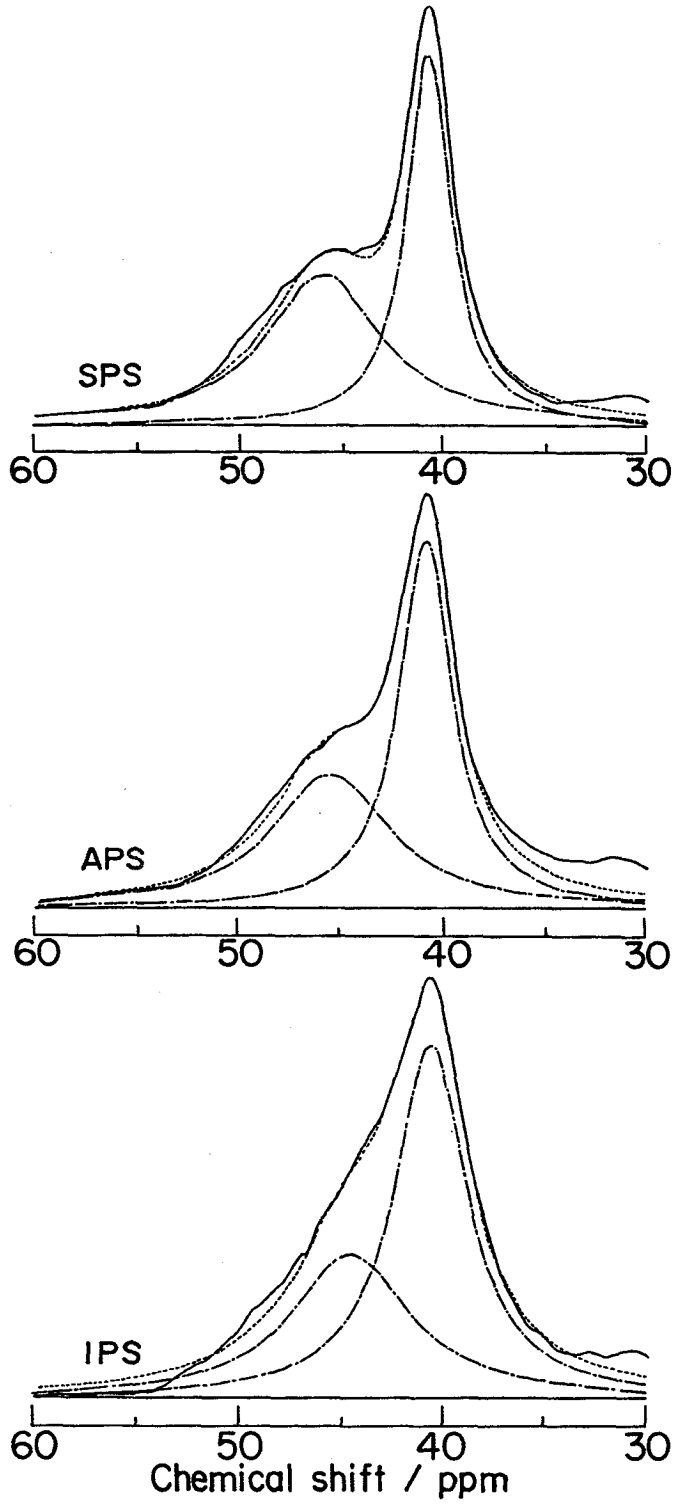

Figure 7-5. CP/MAS ^{13}C-NMR spectra of glassy SPS, APS and IPS.

with their assignments, are summarized in Table 7-1. The degree of crystallinity evaluated from the integrated intensity ratio of the crystalline and amorphous regions is also given.

In the case of the α_1 and α_2 phases, the CH_2 and CH carbon signals due to the crystalline region appear as a singlet centered at 47.5 and 42.5 ppm, respectively. The singlet pattern originates from the TT conformation where all of the monomeric units are equivalent to each other. In the crystalline region of β phase, the CH_2 signal appears as a doublet centered at 48.5 and 38.3 ppm having the same intensity, while the CH signal appears as a singlet at 40.5 ppm. The characteristic spectral pattern can be interpreted by the TTGG conformation. The CH_2 occupies two distinct sites (the inner and outer sites), whereas the CH occupies one equivalent site.

The dependence of ^{13}C chemical shifts on molecular conformation in the solid state has been interpreted in terms of an empirical rule "3-bond interactions" or "γ-gauche shielding effects". This claims that a carbon is subjected to a strong shielding by the carbon atoms which are separated from it by three bonds and located at the gauche position with respect to it. The inner CH_2 suffers a strong γ-gauche shielding and gives rise to the upfield shift by 10 ppm compared to the outer and inner CH_2 of α-SPS. The CH in the TTGG form also suffers a strong γ-gauche shielding (causing an upfield shift by about 2 ppm) compared to that in the TT or TTGG form. These experimental results are well understood by the aid of Figure 7-6.

In the case of polyethylene, the signal of the amorphous carbon atoms is 2-3 ppm upfield shifted from that of the crystalline

Table 7-1. ^{13}C-NMR Chemical shifts of polystyrenes in solid states (ppm measured from TMS).

Sample	CH_2	CH	Crystallinity
α_1-SPS	47.5	42.8	71-74 %
α_2-SPS	47.5	42.4	50-52 %
β-SPS	48.5 (outer)	40.5	35 %
	38.3 (inner)		
SPS Glass	46.0	40.7	0 %
IPS Cryst.	42.5	41.8	65 %
IPS Glass	45.0	41.0	0 %
APS Glass	45.6	40.8	0 %

Methylene

CH - CH_2 - CH - $\underline{CH_2}$ - CH - CH_2 -CH

G	G	T	T	G	G	TTGG (inner)	38.3 ppm
T	T	G	G	T	T	TTGG (outer)	48.5 ppm
T	T	T	T	T	T	TT	47.5 ppm
T	G	T	G	T	G	TG	42.5 ppm

Methine

CH_2 - CH - CH_2 - $\underline{CH}$ - CH_2 - CH - CH_2

T	G	G	T	T	G	TTGG	40.5 ppm
T	T	T	T	T	T	TT	42.5 ppm
G	T	G	T	G	T	TG	41.8 ppm

Figure 7-6. γ-Gauche shielding in polystyrene of various conformations and ^{13}C chemical shifts.

carbons.[6] The same trend is observed in glassy SPS; the CH_2 and CH signals are upfield shifted by about 2 ppm from those of α-SPS. This is also interpreted by the same effect caused by the CH_2 signal in the glassy state increases in the order of IPS<APS<SPS. This result is attributed to the trans-rich structure in glassy SPS compared to IPS and APS.

7-3-2. Long-range conformational structure and stiffness of polymer molecules in the glassy state

The molecular form as a whole in the glassy state might be influenced by the preferred local conformation as well as the stiffness of the polymer molecule. It is known that such long range conformational order as well as the stiffness of the disordered polymer molecules is reflected in the frequency of a particular low-frequency Raman-active mode, the so-called "disordered longitudinal acoustic mode", abbreviated as D-LAM. The D-LAM band has been identified first in the low-frequency isotropic Raman spectra of a series of liquid n-alkanes[7] and thereafter in those of polyethylene[8] and poly(tetrafluoroethylene).[9] This band was also found in various polymers in the liquid and glassy states.[10] In the present work, we measured the D-LAM bands of SPS, IPS, and APS in the glassy state. Figure 7-7 reproduces the polarized (p) and depolarized (dp) Stokes Raman profiles of the three samples measured on melt-quenched film specimens. As proposed by Snyder et al.,[11] we obtained the isotropic spectrum $I_{iso}(\nu)$ free from the background by subtracting the dp component from the p component. The scattering power $S(\nu)$ was obtained

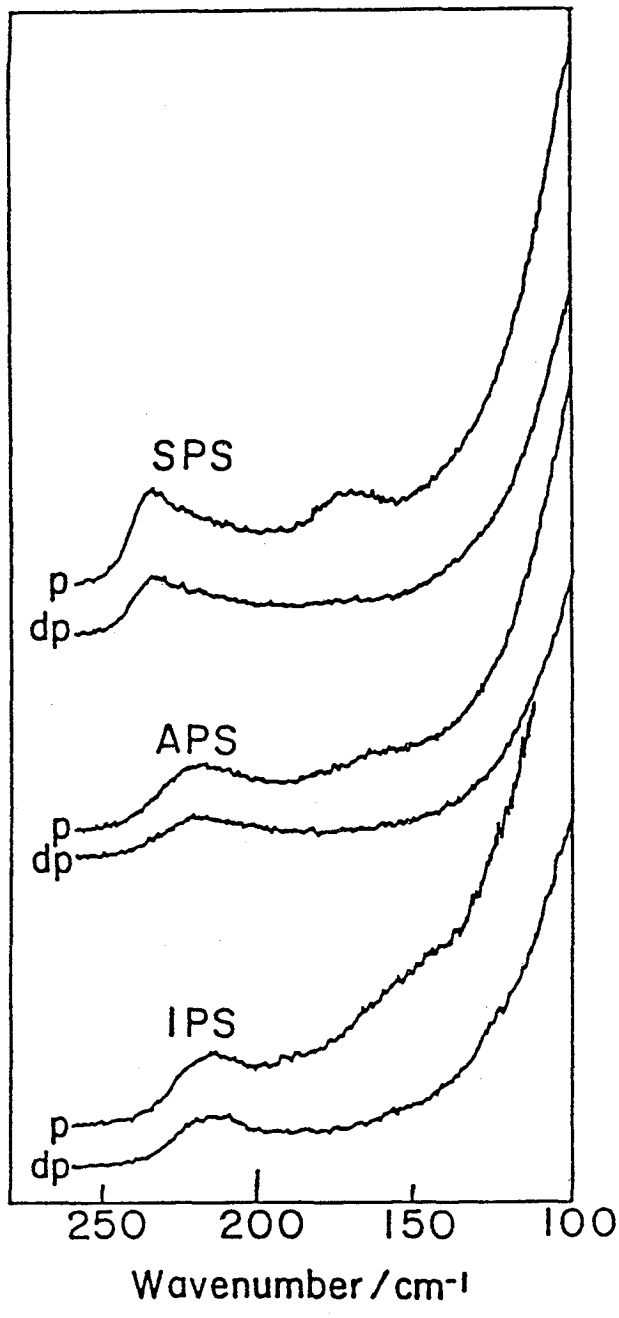

Figure 7-7. Low-frequency Raman spectra of SPS, APS and IPS glasses.

according to the equation

$$S(\nu)=BI_{iso}(\nu) \qquad (7\text{-}1)$$

$$B=1-\exp(-hc\nu/k_BT) \qquad (7\text{-}2)$$

where ν denotes the Stokes Raman shift (in cm^{-1}), T the absolute temperature, c the velocity of light in vacuo, h the Planck constant, and k_B the Boltzmann constant. Figure 7-8 shows $S(\nu)$ thus transferred from Figure 7-7.

The peak frequency of the D-LAM band increases in the order IPS<APS<SPS. The shift of the D-LAM frequency means that either the long-range conformational order decreases or the stiffness increases in this order. The long-range conformational order in three samples should be almost the same, since the presence of long TT (in SPS) or TG (in IPS) sequences was not detected, and they differ from each other in the local conformation caused by different stereochemical configuration, as mentioned in the previous chapter. Therefore, the difference in D-LAM frequency is probably to be ascribed to the difference in stiffness of a chain segment is expected to increase with an increase in the content of the TT conformation.

The difference in the local conformation is reflected also in the density of the glass. The density of SPS, IPS and EPS samples are listed in Table 7-2. Significant differences are found among stereoregular isomers. Figure 7-9 plotted densities depending on the diad tacticity. The straight line was obtained and the observed values decreased with increasing syndiotacticity. As a glassy SPS is regarded to be of a TT rich, its locally rod-

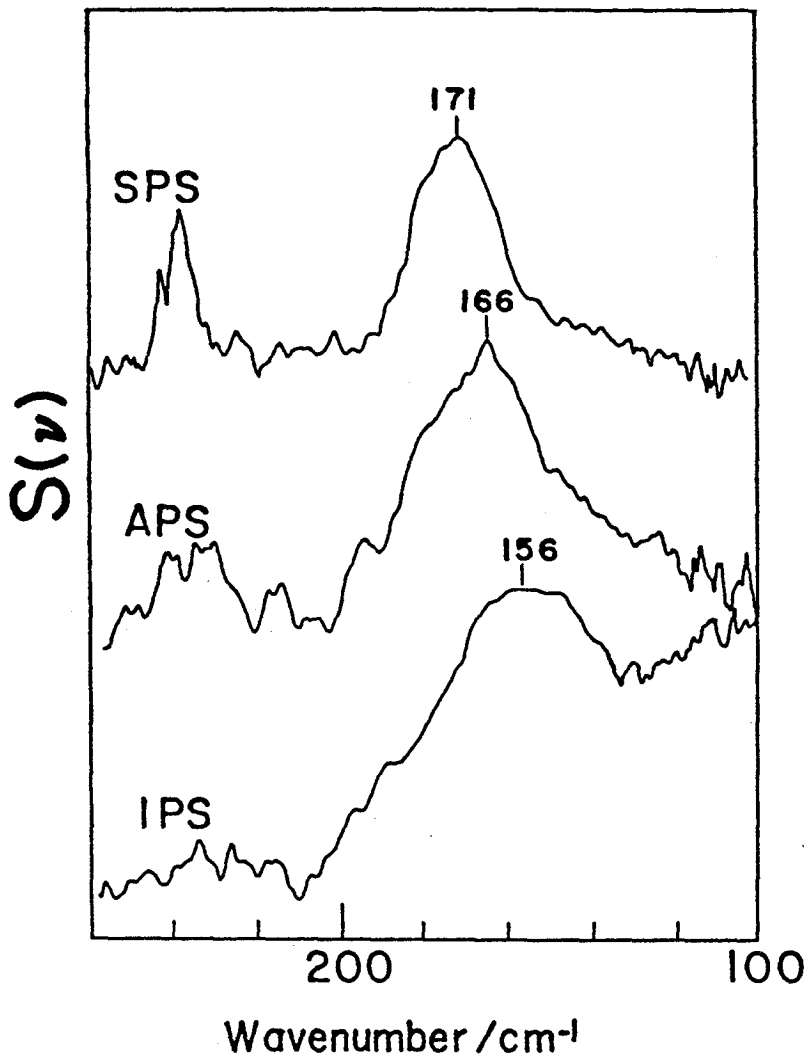

Figure 7-8. Scattering powers of the D-LAM of SPS, APS and IPS glasses.

Table 7-2. Density of glassy state of various stereoregular polystyrenes.

	Density / g/cm^3
IPS	1.0575
EPS6	1.0550
EPS10	1.0527
EPS24	1.0510
APS	1.0477
SPS	1.0448

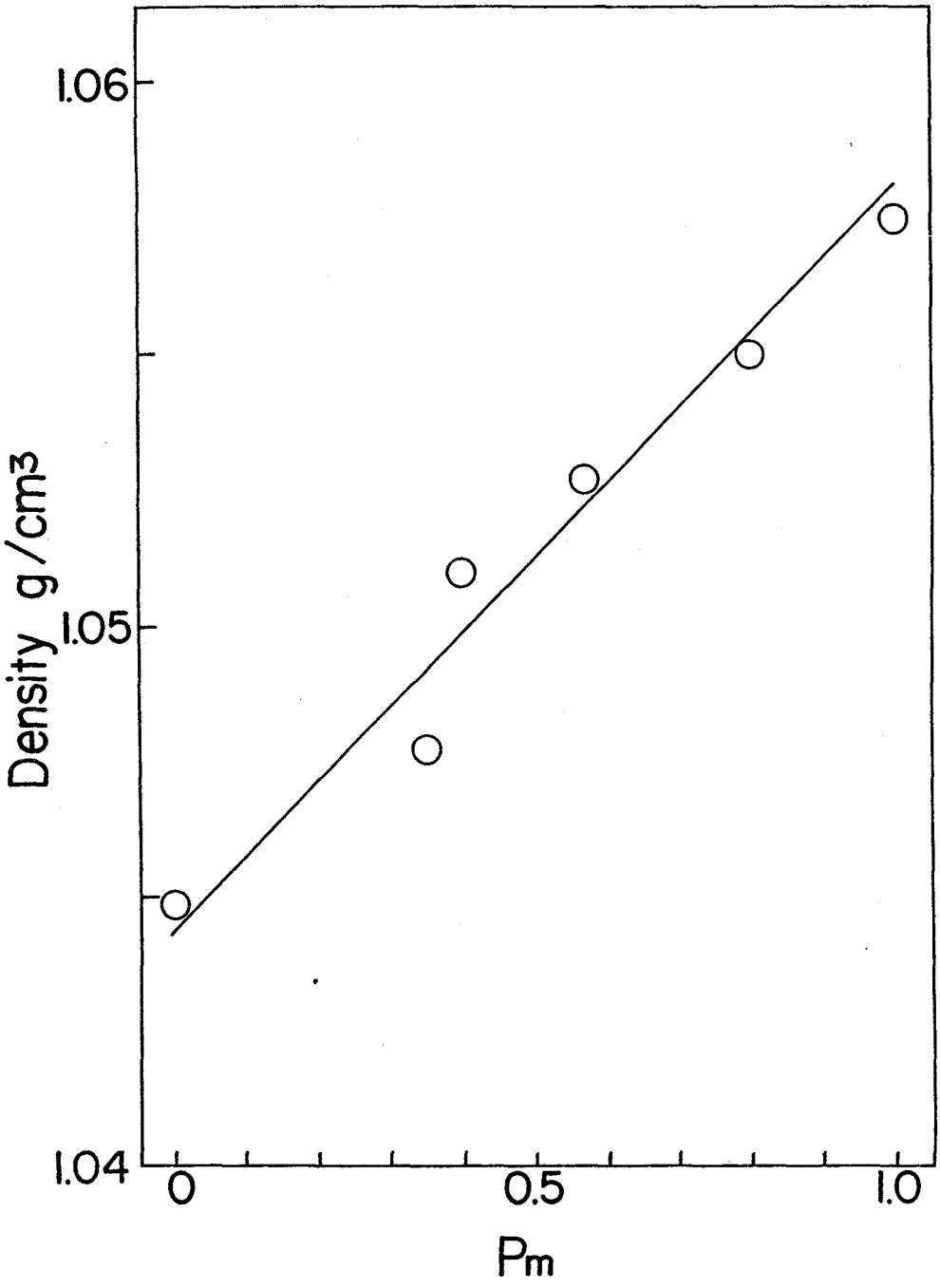

Figure 7-9. Densities of polystyrene glasses.

like structure leads to the smallest value of density among them. This result corresponds to the tacticity dependence of radius gyration $\langle Rg^2 \rangle$; the experimental values of IPS and APS obtained from SANS by Guenet et al. are approximately 150 and 210 A (if $Mw=5x10^5$), respectively.[12,13] This seems quite reasonable because the unperturbed radius of gyration in syndiotactic rich APS sample expands, so that the density decreases as the content of straight (TT) segments increases.

In conclusion, molecular conformation and size of molecular chain in a glassy state are described as a function of the degree of stereoregularity. The preferred molecular conformation is different between SPS and IPS glasses. SPS glass tends to take trans sequences, whereas IPS glass fairly contains gauche conformation. The analysis from molecular order connects with the interpretation of densities and mean square radius of gyration depending on stereoregularity.

References

1) M. Kobayashi, K. Akita, H. Tadokoro, Makromol. Chem., 113, 324 (1968).
2) B. Jasse, J. L. Koenig, J. Polym. Sci., Polym. Phys. Ed., 17, 799 (1979).
3) B. Jasse, R. S. Chao, J. L. Koenig, J. Raman Spectrosc., 8, 244 (1979).
4) J. M. O'Reilly, D. M. Teegarden, G. D. Wignall, Macromolecules, 18, 2747 (1985).

5) D. Y. Yoon, P. J. Flory, Macromolecules **9**, 299 (1976).

6) A. E. Tonelli, F. C. Schilling, Acc. Chem. Res., **14**, 233 (1981).

7) R. F. Schaufelle, J. Chem. Phys., **49**, 4168 (1968).

8) R. G. Snyder, J. Chem. Phyas., **76**, 3921 (1982).

9) R. G. Snyder, N. E. Schlotter, R. Alamo, L. Mandelkern, Macromolecules, **19**, 621 (1986).

10) R. G. Snyder, S. L. Wunder, Macromoleculs, **19**, 496 (1986).

11) R. G. Snyder, S. J. Krause, J. R. Scherer, J. Polym. Sci., Polym. Phys. Ed., **16**, 1593 (1978).

12) J. P. Cotton, D. Decker, H. Benoit, B. Farnoux, J. Higgins, G. Jannink, R. Ober, C. Picot, J. des Cloizeaux, Macromolecules, **7**, 863 (1974).

13) J. -M. Guenet, C. Picot, Macromolecules, **16**, 205 (1983).

CHAPTER 8

Concluding Remarks

This thesis has dealt with the following subjects on various stereoregular polystyrenes.

1) Molecular conformation and crystal polymorphism of newly synthesized syndiotactic polystyrene.

2) The relationship between the gel structure at cross-linking points and stereoregularity.

3) Structure of SPS, IPS and APS in the glassy state.

The summary of each chapter is described in what follows.

CHAPTER 2.

Two stable conformations in crystalline states of SPS were investigated by vibrational spectroscopy and X-ray diffraction. It was revealed that the α phase, obtained by crystallization from the melt or by annealing the cast or melt-quenched film samples, consists of the molecules having the all-trans (TT) skeletal conformation, and the β phase, obtained by crystallization from solutions or by exposing glassy samples in an atmosphere of solvent vapor, consists of the molecules having the TTGG skeletal conformation. The infrared bands characteristic of these specific conformations were observed and compared with those of isotactic polystyrene with TG conformation. The crystallization process from the glassy state and the solid state phase transition from β to α phase were followed by the infrared spectral change and DSC thermogram. The TT form is found to be more stable than the TTGG form under ambient condition.

CHAPTER 3.

Crystal polymorphism of SPS was investigated by means of X-ray diffraction, infrared spectroscopy and electron microscopic measurements. Depending on the crystallization condition, five or more crystal modifications were obtained. There are two crystal forms consisting of the planar zigzag molecules (α_1 and α_2). As for the TTGG conformation, two crystal modifications called β_1 and β_2 were found. The presence of polymer-solvent complexes (γ) was indicated by some experimental evidences. Infrared and X-ray measurements revealed that the γ form transformed to the β_1 form at 120°C, and then to the α_2 form at 190°C.

CHAPTER 4.

The thermoreversible gelation of SPS was investigated by means of infrared spectroscopy and thermal analysis. The gelation of this polymer is the formation of crystallite, and the junction points consists of a molecular aggregates having TTGG conformation. The phase diagram and the enthalpy of gel-formation in o-dichlorobenzene solution were obtained. It was suggested that SPS molecules construct a stoichiometric complex with solvent molecules, as in the case of IPS and APS. The average number of solvent molecules per monomeric unit was estimated as 0.87. The SPS/o-dichlorobenzene and SPS/chloroform systems yield transparent gel, whereas the SPS/decalin system gives crystalline precipitates in two crystallization regimes below and above 70°C. The infrared spectral measurements showed that the crystals deposited at low temperature were the

TTGG from and those at high temperature were of the all trans (TT) form. The factors that control two competitive self-organization processes of gelation and crystallization were considered.

A preliminary result of small angle neutron scattering (SANS) of SPS/D-o-dichlorobenzene was presented concerning with the dimension of the gel forming structure.

CHAPTER 5.

Stable conformation and their sequential order in IPS gel have been investigated by infrared spectroscopy. The process of the conformational change during the gelation of the IPS/CS_2 system has been followed by infrared spectroscopy, and it was demonstrated that the partially ordered skeletal conformation existing in gel was of a (3/1) helix (TG) type having the pendant phenyl groups oriented in a disordered fashion, rather than the near-TT [(12/1) helix] form proposed previously for IPS/decalin gels. The temperature dependence of the absorption intensities has been interpreted quantitatively by a simple statistical model. The TG regular sequence formed in gel was estimated as long as 5 turns of 3/1 helix.

CHAPTER 6.

Gelation of non-crystalline APS sample was investigated by infrared spectroscopy. It was clarified that gelation of APS with diad syndiotacticity (Pr) of 0.65 was accompanied with the conformational ordering (TTGG) in the syndiotactic portion of the molecules. In order to elucidate the relation between gel

structure and tacticity, epimerized samples (EPS) were prepared (Pr=0.13, 0.2, 0.43 and 0.6). In isotactic-rich samples, the infrared bands due to the TG sequences of IPS increased in intensity on gelation. With increasing syndiotacticity, the bands characteristic of the TTGG sequences of SPS appeared. This result indicates that the physical gelation of non-crystallizable polymer is accompanied by the formation of locally ordered conformation in particular stereoregular sequences. The analysis of critical sequence length lead to the conclusion that at least two turns in helical unit required to form cross-links.

CHAPTER 7.

Local and long-range conformational structures of SPS, IPS and APS molecules in the glassy state were investigated by means of infrared and low-frequency Raman spectroscopy. The content of trans skeletal C-C bonds, estimated from the infrared absorption intensities, was found to be richer in SPS than in IPS glass. The trans-richest structure of SPS was established by CP/MAS ^{13}C-NMR spectroscopy by the consideration of γ-gauche effect as well. The stiffness of disordered chain segments estimated from the "disordered longitudinal acoustic mode (D-LAM) frequency, as well as the specific volume of glassy samples, was found to increase in the order of IPS<APS<SPS. The local conformational structure lead to the differences of chain dimension ; the lowest value of density and the largest means square radius gyration for SPS.

The present work was dealt with the structure of crystal, gel and amorphous of various stereoregular polystyrenes (SPS, IPS and APS). Together with the analysis of crystal modifications of newly synthesized SPS, the gel structure of cross-linking point and amorphous structure were clarified in relation to stereoregularity.

List of Publications

The contents of this thesis have been published in the following papers.

1. Vibrational spectroscopic study of isotactic and syndiotactic polystyrenes.
   M. Kobayashi, T. Nakaoki, M. Uoi,. Rep. Prog. Polym. Phys. Jpn., **31**, 481 (1988).
2. Polymorphic Structures and Molecular Vibrations of Syndiotactic Polystyrene.
   M. Kobayashi, T. Nakaoki, N. Ishihara, Macromolecules, **22**, 4377 (1989).
3. Molecular Vibrations of Two Forms of Syndiotactic Polystyrene.
   M. Kobayashi, T. Nakaoki, N. Ishihara, Rep. Prog. Polym. Phys. Jpn., **32**, 125 (1989).
4. Molecular Structure in Syndiotactic Polystyrene Gel : Comparison with Isotactic Polystyrene Gels.
   M. Kobayashi, T. Nakaoki, N. Ishihara, Rep. Prog. Polym. Phys. Jpn., **32**, 427 (1989).
5. Molecular Conformation in Glasses and Gels of Syndiotactic and Isotactic Polystyrenes.
   M. Kobayashi, T. Nakaoki, N. Ishihara, Macromolecules, **23**, 78 (1990).
6. Thermoreversible Gelation of Isotactic and Atactic Polystyrenes : Structure of Cross-links.
   T. Nakaoki, M. Kobayashi, Rep. Prog. Polym. Phys. Jpn., **33**, 91 (1990).

7. Solid-State High-Resolution Carbon-13 nuclear Magnetic Resonance of Stereoregular Polystyrenes.
T. Nakaoki, M. Kobayashi, Rep. Prog. Polym. Phys. Jpn., **33**, 521 (1990).

8. Conformational Order in Crystalline States and Gels of Isotactic, Syndiotactic and Atactic Polystyrenes Studied by Vibrational Spectroscopy.
T. Nakaoki, M. Kobayashi, J. Mol. Struct., **242**, 315 (1991).

9. Physical Gelation of Epimerized Polystyrenes.
T. Nakaoki, M. Kobayashi, Rep. Prog. Polym. Phys. Jpn., **34**, (1991).

10. Vibrational Spectra of Two Crystal Modifications of Syndiotactic Polystyrene-d_8.
T. Nakaoki, M. Kobayashi, Rep. Prog. Polym. Phys. Jpn., **34**, (1991).